

Appendix F4. Nantucket Shoals Hydrodynamic Impacts Study

Document Revision A

Issue Date June 2024





Draft Final Report

Nantucket Shoals Hydrodynamic Impacts Study

Submitted to:

SouthCoast Wind

Submitted by:

Daniel Mendelsohn, MS, IES
Craig Swanson, PhD, SE
Kathleen J. Vigness-Raposa, PhD, INSPIRE
Sarah Glancy, MS, INSPIRE
Drew Carey, PhD, INSPIRE
June 2024

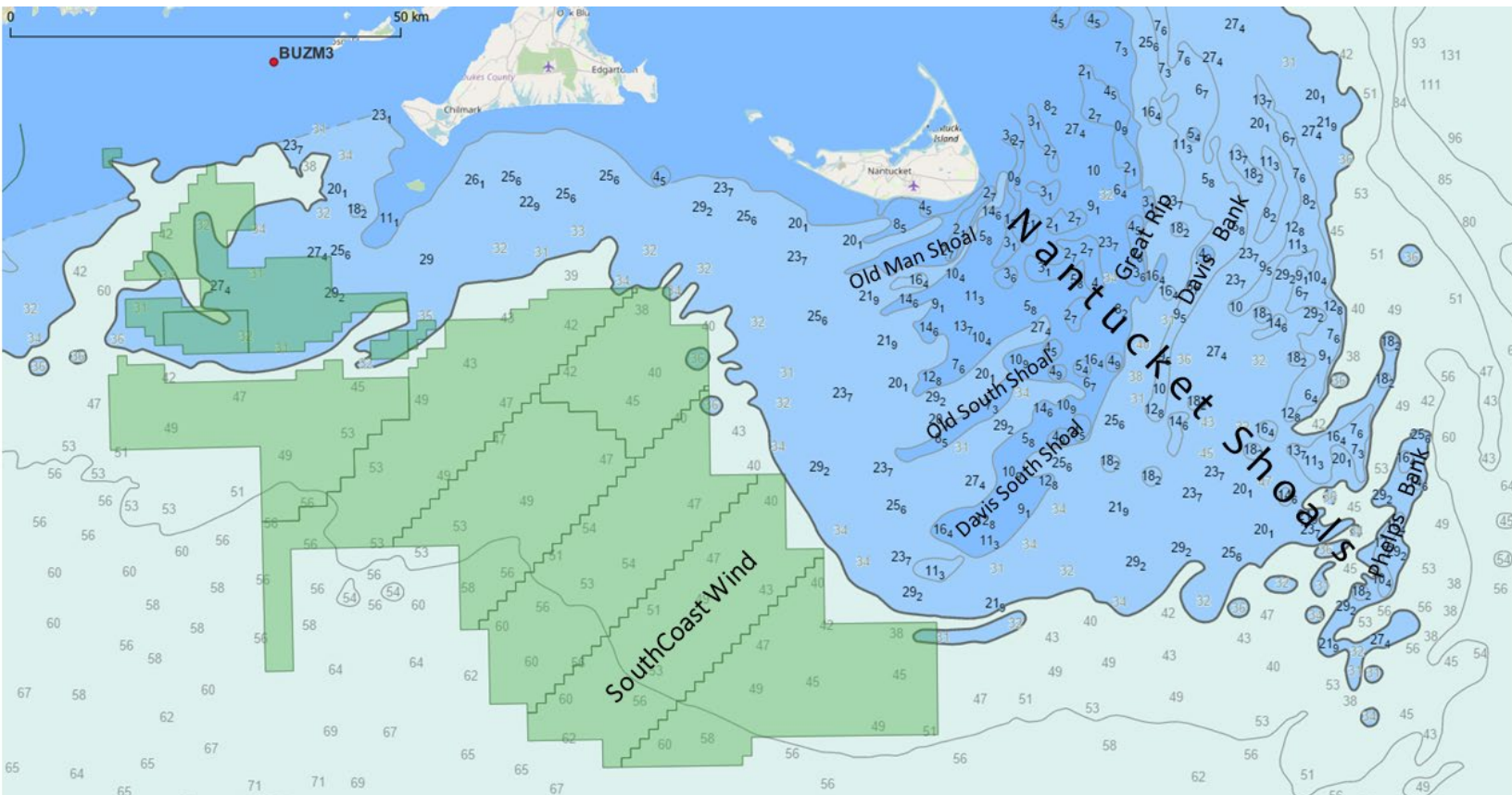




TABLE OF CONTENTS

1	Introduction	1-1
1.1	Project Objective	1-1
1.2	Project Description.....	1-2
2	Physical Oceanography of Nantucket Shoals	2-1
2.1	Large Scale Regional Circulation	2-1
2.2	Tidal Currents and Tidal Mixing Fronts	2-3
2.3	Stratification and Mixing.....	2-6
3	Biological Oceanography of Nantucket Shoals	3-1
3.1	North Atlantic Right Whales.....	3-1
3.2	Copepods.....	3-3
4	SouthCoast Wind Farm Near Field Domain	4-1
4.1	SouthCoast Wind Study Area Description.....	4-1
4.2	SouthCoast MetOcean Buoy Data Analysis.....	4-2
5	Wind Turbine Impacts on Hydrodynamics	5-1
5.1	Near Field Turbine Tower Hydrodynamic Wake Effects	5-2
5.2	Near Field/Far Field Turbine Atmospheric Wake Effects	5-10
6	Conclusions	6-1
7	References.....	7-1

LIST OF FIGURES

Figure 1-1. Overview of the Project and local bathymetry in the area and the Nantucket Shoals.	1-2
Figure 2-1. The general circulation in Gulf of Maine/Georges Bank region during stratification condition (May-September). From Beardsley et al. [1997].	2-2
Figure 2-2. Left: Depth-averaged tidal current ellipses for M_2 , plotted every 5 grid points. Right: Depth-averaged M_2 tidal residual circulation (He and Wilkin, 2006).	2-4
Figure 2-3. Tidal mixing parameter $\text{Log}_{10}(h/U^3)$ for M_2 tidal currents. The solid dark line indicates a tidal mixing parameter value of 1.9, defining the tidally induced frontal locations (He and Wilkin, 2006), with the SouthCoast Wind Energy Lease Area outlined in blue for reference.	2-5
Figure 2-4. Example cross shelf thermal stratification in the Mid-Atlantic Bight by month. The cross shelf transects are farther south than the Nantucket Shoals area but are representative of the area. (Figure from Castelao et al. 2010).	2-7
Figure 2-5. Left: across shelf thermal stratification near Nantucket Shoals at the beginning of August, 1979. Right: cross shelf salinity at the same time. The Nantucket Shoals area is represented in the upper left corner of each figure, from a depth of approximately 60 m and shallower. (Figures from Write et al. 1983, Beardsley et al. 1985).	2-7
Figure 3-1. North Atlantic right whale critical habitat. Figure courtesy of NOAA Fisheries.	3-2
Figure 3-2. Hotspot analysis of right whale distribution relative to wind farm lease areas in the Nantucket Shoals region. Figure 5 in Quintana-Rizzo et al. 2021.	3-3
Figure 3-3. Calculated densities of <i>Calanus</i> individuals sampled in the Nantucket Shoals region since 1990 shown with the 25 m (green), 30 m (blue), and 60 m (navy) bathymetry lines. Point size is scaled to <i>Calanus</i> per cubic meter, and the color indicates if the sample was above the recognized 1000 per cubic meter NARW foraging threshold.	3-5
Figure 3-4. Copepod densities and right whale sightings per unit effort in Cape Cod Bay by month. Figure 2a from Pendleton et. al., 2009	3-6
Figure 3-5. Monthly averaged <i>Calanus</i> individuals per cubic meter, calculated from ECOMON (1990-current). Showing 25 m (green), 30 m (blue), and 60 m (navy) bathymetry lines; points are sized according to number of <i>Calanus</i> per cubic meter.	3-7
Figure 4-1. IES hydrodynamic model application showing the influence of the Nantucket Shoals on current speeds (from South Coast Wind [formerly Mayflower Wind] COP, 2022).	4-2
Figure 4-2. SouthCoast Wind Project location showing local bathymetry, Nantucket Shoals and the SouthCoast Wind metocean buoy locations; the first half of 2020 at location SV1 and the remaining duration of the study at location SV2-4.	4-3
Figure 4-3. Example near surface (10 m, orange line) and near bottom (30 m, blue line) current speed (top) and direction (bottom) time series at the SouthCoast Wind metocean buoy site.	4-4
Figure 4-4. Example near surface (10 m) currents showing current vectors (left) for each hour and a progressive vector diagram (right) over a single tidal cycle, where each orange dot represents an hour. 4-5	
Figure 4-5. Current roses and directional frequencies for the 10 m and 30 m depths from the SouthCoast Wind metocean buoy observations.	4-6
Figure 4-6. Net current flow speed and direction at 10 m during summer 2020 from observations at the SV2-4 buoy deployment location. The map shows the buoy location(s) and proximity to Nantucket	

Shoals seen as shallow (more red) depths. The buoy was deployed at SV1 for the first half of 2020 and at location SV2-4 into 2022. 4-9

Figure 4-7. Wind rose and directional frequencies for the wind speed at 4 m above the sea surface. ... 4-10

Figure 4-8. SouthCoast Wind metocean buoy recorded surface (blue line) and bottom (orange line) temperature and the temperature difference (green line) for 2020 (top plot) and 2021 (bottom plot). The red ellipses indicate timing of the onset of stratification (left side) and collapse (right side) of stratification for the two years. 4-11

Figure 4-9. SouthCoast Wind metocean buoy observations time series stack plot for July – August, 2020. 4-12

Figure 4-10. IES hydrodynamic model application showing the influence of the Nantucket Shoals on current speeds overlain on the local bathymetry (from South Coast Wind COP – Appendix F3, 2023). The metocean buoy locations are also shown for reference, where the buoy was deployed at SV1 for the first half of 2020 and at SV2-4 into 2022. 4-13

Figure 4-11. Tidal mixing front location estimation based on local bathymetry, SouthCoast Wind metocean buoy measured currents, IES model predicted currents and the mixing front relationship from Dorrell, 2022. 4-14

Figure 5-1. Velocity profiles measured at different distances downstream of the pile and with no pile. Distances are specified by the number of pile diameters downstream from the center of the pile (n_D) (Miles et al., 2017). 5-3

Figure 5-2. Schematic of the potential downstream hydrodynamic effects of WTG tower (16 m diameter) and 1 nm (1852 m) WTG spacing is shown. Two potential mixing lengths are shown for the 11D and 50D cases, equating to 176 m and 800 m, respectively. 5-5

Figure 5-3. Basic sketch of the idealized setup considered. A typical density profile is illustrated where stratification (i.e., change in $\rho(z)$) is confined to a pycnocline layer with thickness, b , at height, h , from the seabed. Only a single foundation structure is shown in the sketch (Carpenter et.al. 2016). 5-5

Figure 5-4. Comparison of profiles of time-averaged mean velocity at several downstream distances (x/D_s) on the vertical central plane (Xie and Archer, 2015). 5-11

Figure 5-5. Comparison of the hub height downwind speed deficit predictions for the minimum and maximum SouthCoast Wind WTG design parameters. 5-13

Figure 5-6. Cross-wind wake wind speed deficit at $x=0$ (upper) and $x=2,000$ m (lower) for $D=220$ m (left) and $D=280$ m (right). The color bar indicates the fraction of deficit from an undisturbed field where yellow colors indicate high deficit and blue colors indicate low deficit. 5-14

Figure 5-7. Downwind centerline wake wind speed deficit for the $D=220$ m (upper) and $D=280$ m (lower) cases. The color bar indicates the fraction of deficit from an undisturbed field where yellow colors indicate high deficit and blue colors indicate low deficit. 5-15

Figure 5-8. Sea surface wake effect wind speed deficit for the $D=220$ m (upper) and $D=280$ m (lower) cases. The color bar indicates the fraction of deficit from an undisturbed field where yellow colors indicate high deficit and blue colors indicate low deficit. 5-16

Figure 5-9. Comparison of the sea surface downwind speed deficit predictions for the minimum and maximum SouthCoast Wind WTG design parameters. 5-17

Figure 5-10. Comparison of the sea surface cross wake speed deficit predictions for the minimum and maximum SouthCoast Wind WTG design parameters at the 1st and 4th WTG locations. 5-17



Figure 5-11. Wind speed changes due to wind farms in the mid-Atlantic Bight, averaged over 3 summer months: (a) at hub height (~120 m AMSL) and (b) at the surface. The red-dashed line shows the contour of 0.5 m/s wind speed deficit, which is considered as the edge of the wake (Golbazi et.al., 2022).5-19



LIST OF TABLES

Table 1. Current speed statistics for the SouthCoast Wind MetOcean buoy 1/23/20 – 10/8/21	4-5
Table 2. Harmonic Analysis of the SouthCoast Wind buoy water surface elevation and current speeds showing the 5 largest constituents.	4-7
Table 3. Long term net current speeds and directions by season and year for the SouthCoast Wind ADCP data. Note that current speed data is presented in cm/s.	4-8
Table 4. Wind speed statistics from the SouthCoast Wind metocean buoy 1/23/20 – 1/22/22	4-10
Table 5. Relationship between power extracted by the wind turbine towers and that extracted by the bottom mixing.	5-7
Table 6. Mixing time estimate for the constant thermocline thickness model	5-9
Table 7. Mixing time estimates for the variable thermocline thickness model	5-10
Table 8. WTG Design Parameters Used in the wake effect modeling (SouthCoast Wind COP, 2022).	5-12
Table 9. WTG layout parameters (SouthCoast Wind COP, 2023).	5-18
Table 10. Estimated area coverage by wind speed deficit at the sea surface for the two cases.	5-18
Table 11. Estimated wind speed deficit at the sea surface for the 25th, 50th and 75th percentiles of the free stream speed.	5-19



Abbreviations and Acronyms

ac	Acre(s)
BOEM	Bureau of Ocean Energy Management
CFR	Code of Federal Regulations
COP	Construction and Operations Plan
ECC	Export Cable Corridor
ft	Foot/feet
GB	Georges Bank
GSC	Great South Channel
km	Kilometer(s)
kts	Knots
LES	Large Eddy Simulation
LiDAR	Light Detection and Ranging
m	Meter(s)
mi	Statute mile(s)
MLLW	Mean Lower Low Water
m ³ /hr	Cubic meters per hour
mm	Millimeter
mi/hr	Miles per hour
m/s	Meters per second
mg/L	Milligrams per liter
µm	Micrometers
NARW	North Atlantic Right Whale
NOAA	National Oceanic and Atmospheric Administration
nm	Nautical mile(s)
N/m ²	Newtons per meter squared
NS/the Shoals	Nantucket Shoals
OCS	Outer Continental Shelf
OSP(s)	Offshore Substation Platform(s)
SCW	SouthCoast wind
WTG	Wind Turbine Generator



1 INTRODUCTION

SouthCoast Wind is in the process of developing an offshore wind renewable energy generation project (Project) located in federal waters off the southern coast of Massachusetts in the Outer Continental Shelf (OCS) Lease Area OCS-A 0521 (Lease Area). Innovative Environmental Science (IES) along with Swanson Environmental (SE) and Inspire Environmental, have been contracted by SouthCoast Wind to provide an evaluation of the potential for the operational phase of the Project to affect hydrodynamics in the Nantucket Shoals area of coastal southern New England. It has been postulated that the wind turbine generator (WTG) rotor induced wake effect in the atmosphere and the subsurface turbine tower/foundation effects on the local water column might alter the current circulation and mixing in local and regional waters. The concern lies primarily in the potential for any alteration of the hydrodynamics in the area to affect the aggregation and local population density of copepods which are the favored prey species of the endangered North Atlantic right whale.

To address that potential IES, an ocean and coastal, environmental engineering and modeling consulting firm, put together a team of experts in the field to evaluate the physical and biological characteristics of the wind energy and Nantucket Shoals areas, and the SouthCoast Wind offshore wind farm and its components. The team working with IES consists of Inspire Environmental (Inspire), an integrated team of skilled marine environmental scientists and analysts trained to characterize, interpret and contextualize water column and seafloor health and Swanson Environmental Associates (SE), a strategic technical advisor to clients on solutions to marine related environmental issues.

1.1 PROJECT OBJECTIVE

The SouthCoast Wind Nantucket Shoals Hydrodynamics Study was performed in two connected tasks:

- Task 1. Prepare a synthesis of relevant information and recommendations for a scope of work to complete an evaluation of the potential impacts of the SouthCoast Wind Project on the Nantucket Shoals system.
- Task 2. Complete the agreed upon scope of work developed under Task 1, to include an assessment of near-field hydrodynamic effects of turbines and an evaluation of the potential for combined effects from the wind farm and far-field effects that could influence Nantucket Shoals.

This report provides a description of the studies performed and the results and findings of the Task 2 scope of work.

There are five basic areas that need to be understood to address the issues described above and to quantify the potential for impacts from the wind farm on local and remote resources, i.e., Nantucket Shoals. The five areas include the local biology, the physical domain, the meteorological and oceanographic conditions present, the direct water column impacts from the turbine tower and the indirect water column impacts from the turbine wake effect. Each will be addressed in the following report.

1.2 PROJECT DESCRIPTION

The SouthCoast Wind Lease Area is located offshore of the southern coast of Massachusetts, approximately 49 kilometers (km) [26 nautical miles (nm)] south of Martha’s Vineyard and 37 km (20 nm) south of Nantucket, shown in Figure 1-1.

The Project WTG layout will align to a 1 nm x 1 nm (1.85 km x 1.85 km) grid with an east-west and north-south orientation, as agreed upon across the entire Massachusetts/Rhode Island (MA/RI) Wind Energy Areas. The Project will consist of up to 149 positions within the Lease Area, to be occupied by WTGs and Offshore Substation Platforms (OSPs), connected with inter-array cables. Power will be transmitted to shore via submarine offshore export cables installed within two export cable corridors (ECC), the Brayton Point ECC and the Falmouth ECC.

Additional details regarding the Project description and details of the wind turbines and their layout in the offshore energy area are available in Section 3 of the Construction and Operations Plan (COP) (SouthCoast Wind, 2022).

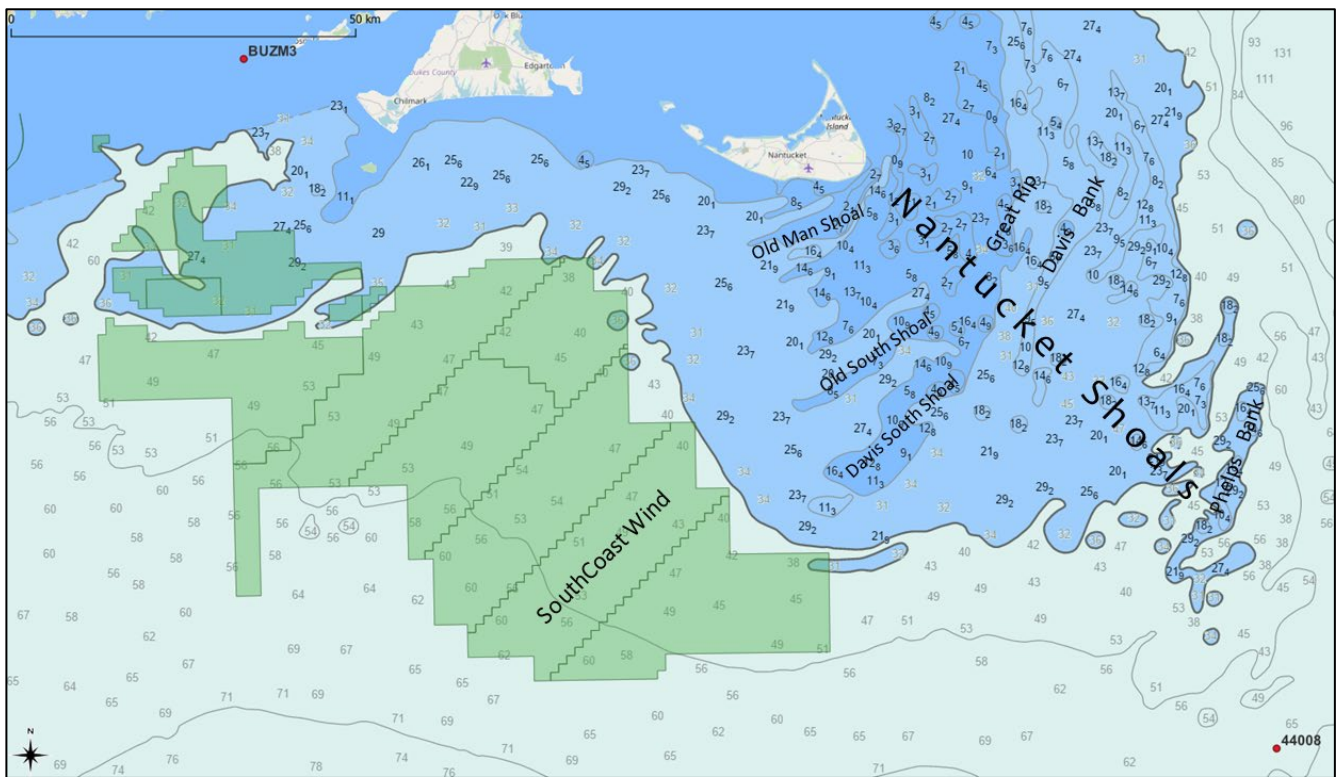


Figure 1-1. Overview of the Project and local bathymetry in the area and the Nantucket Shoals.



2 PHYSICAL OCEANOGRAPHY OF NANTUCKET SHOALS

Nantucket Shoals refers to a group of shoals and sandbars located in the Atlantic Ocean off the southeastern coast of Nantucket Island, Massachusetts, United States. These shoals extend approximately 75 km (41 nm) to the southeast from the southeast corner of Nantucket Island to Phelps Bank, 50 km (27 nm) to the south, 45 km (24 nm) to the east and are approximately 75 km (41 nm) across in an east-west direction. The SouthCoast Wind Lease Area lies to the south and west of the Nantucket Shoals area.

The Nantucket Shoals area is known for its complex underwater topography, which consists of sand ridges, channels, and shifting sands. These features pose a significant navigational challenge for vessels, particularly due to the strong currents and shallow depths in the region. Over the years, many ships have run aground or suffered damage in this area, earning it a reputation as a treacherous passage for mariners.

The geographical significance of Nantucket Shoals extends beyond navigation. The Shoals serve as a vital habitat for marine life, making it a popular location for fishing enthusiasts. The area is home to a diverse range of fish species, including cod, flounder, bluefish, and striped bass, among others.

Furthermore, Nantucket Shoals plays a crucial role in the ecology of the region. The mixing of warm Gulf Stream waters and cooler waters from the north creates a nutrient-rich environment, supporting a productive marine ecosystem. The Shoals also contribute to the formation of dynamic currents and eddies, influencing the movement of water and affecting the distribution of plankton and other marine organisms.

In recent years, there have been efforts to study and understand the ecological significance of Nantucket Shoals. Scientists and researchers have conducted surveys and collected data to assess the impact of human activities, climate change, and other factors on the region's marine life and environment.

2.1 LARGE SCALE REGIONAL CIRCULATION

The physical oceanography of Nantucket Shoals is influenced by the large-scale circulation patterns in the region. Research conducted by the Provincetown Center for Coastal Studies and other studies indicate a consistent southwestward flow along Nantucket Shoals (PCCS, 2005). Understanding the large-scale circulation patterns is crucial for comprehending the overall movement of water masses and the associated currents in the area.

The Nantucket Shoals hydrodynamic system is part of a larger regional circulation pattern. From a large-scale point of view, Georges Bank and Nantucket Shoals waters are part of a coastal current system, originating from the Newfoundland Shelf and the Labrador Current. This contributes to the transport of cold, nutrient-rich water southward along the coast. This can affect the water temperature and nutrient availability in the region, influencing the marine ecosystem around Nantucket Shoals. Flowing along the Scotian Shelf, the current diverges to flow west through the Northeast Channel into the Gulf of Maine then out to the Great South Channel (on the east flank of Nantucket Shoals) and Nantucket Shoals, and south along the southern slope of Georges Bank to the New England Shelf (Chapman and Beardsley, 1989; Beardsley et al., 1997, Beardsley et al. 1985) and shown in Figure 2-1.

Brooks (1992) found that flow around the edge of Georges Bank is clockwise and diverges from the main Gulf of Maine counterclockwise circulation to follow the edge of the Nantucket Shelf heading west. The divergence is in

an area where upwelling of deeper nutrient-rich water occurs in response to the diverging water masses and is thus an area where production should be higher. The contour-hugging current flows clockwise around Nantucket Shoals, along depth contours of 20 meters (m) (66 ft) or greater, bending around the Shoals (Brooks, 1992).

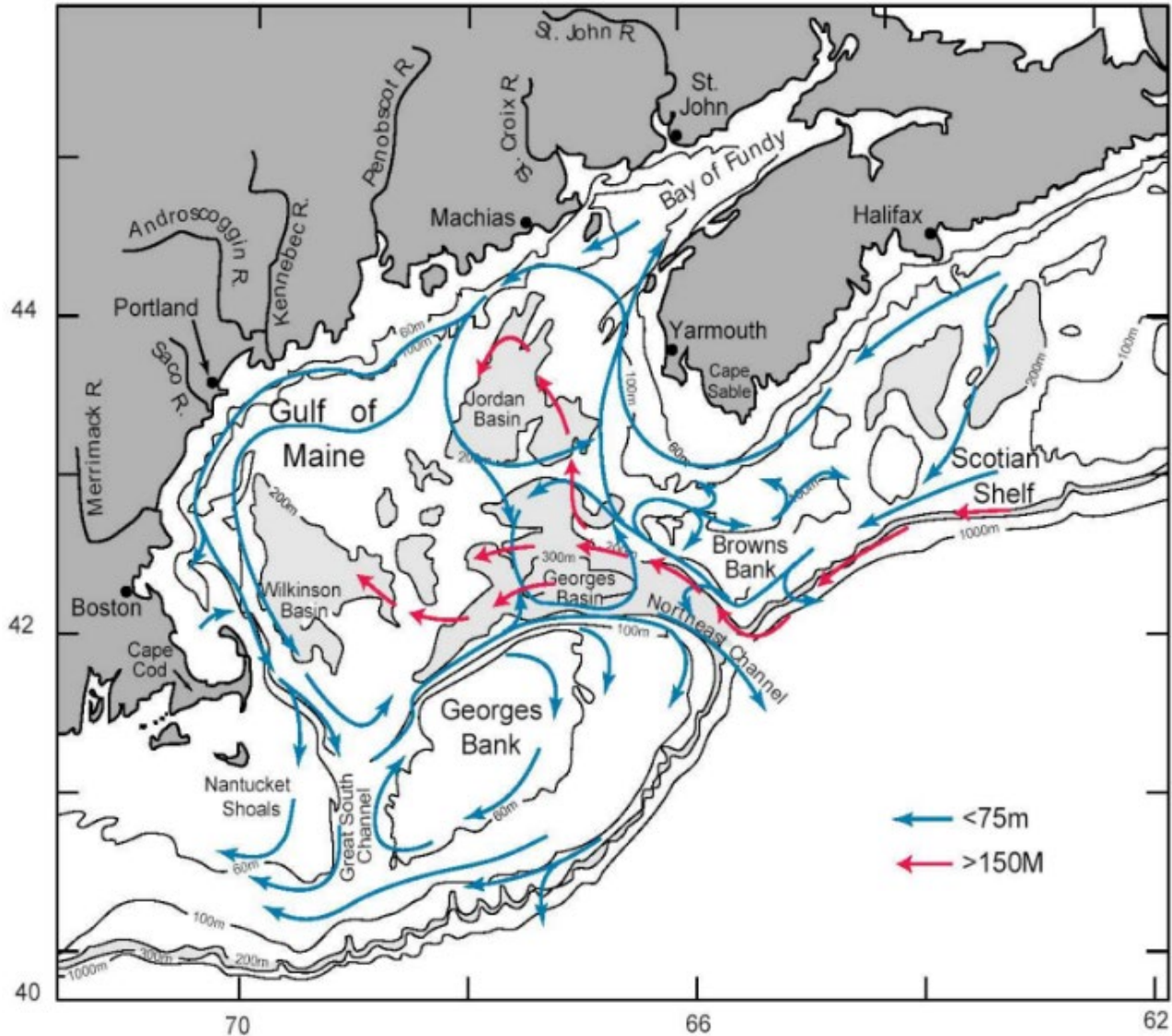


Figure 2-1. The general circulation in Gulf of Maine/Georges Bank region during stratification condition (May-September). From Beardsley et al. [1997].

In a field and analytical study of current time series (200+ days) over 33 sites over the Middle Atlantic Bight, Lentz (2008) found consistent mean circulation with southwestward flow along southern Georges Bank and Nantucket Shoals, similar to earlier measurements by Butman et al. (1982).

The net flow over Nantucket Shoals is influenced by various factors, including tidal currents, winds, and the interaction between warm and cold water masses in the region. The currents in the area are highly variable and



can change depending on the time of year and prevailing weather patterns. Therefore, it is challenging to provide an exact or constant value for the net flow.

2.2 TIDAL CURRENTS AND TIDAL MIXING FRONTS

Tidal currents play a significant role in driving water movement and mixing in Nantucket Shoals. The gravitational interactions of the moon, sun, and Earth create tidal forces that influence the direction, speed, and intensity of currents in the region. The unique bathymetry of Nantucket Shoals contributes to the development of tidal fronts, where the interaction between tidal currents and topographic features leads to localized variability in currents.

The Provincetown Center for Coastal Studies identified the following factors controlling currents in the Shelf area:

- Advection (mixing of different water masses)
- Stratification (formation of layers of water with different properties)
- Buoyancy (tendency of a less dense body of water to rise relative to a denser body of water)
- Tides (created by the constantly changing gravitational attractions of moon, sun, and earth as these move relative to each other)
- Gradient-driven flow (water flows down to a lower area due to gravity)
- Coriolis force (the earth's daily rotation under a body of water causes that water body to slowly spin clockwise or counterclockwise)
- Interactions among some, or all, of the above processes

He and Wilkin (2006) developed a high-resolution hybrid data assimilative modeling system to study tides and tidal dynamics on the southeast New England shelf using in-situ observations of harmonics of tidal constituents. Analysis revealed complex tidal variability in this transition region between the tidally amplified Gulf of Maine and the less energetic Middle Atlantic Bight. Detailed examination of the residual circulation, energetics, and momentum balances of the M_2 tide revealed the influence of the unique bottom bathymetry of Nantucket Shoals and the complex coastal geometry in affecting the regional tidal dynamics.

presents their model predicted M_2 component of the tidal currents for the region as tidal ellipses (left plot) and residual currents (right plot). Note that the ellipses show a more rectilinear (back and forth) and faster flow over Nantucket Shoals but more elliptical (rotary) and slower at the SouthCoast Wind Lease Area. The M_2 residual plot shows bathymetrically generated currents heading southward from the Gulf of Maine through the Great South Channel, bending south westward around Nantucket Shoals meeting with the westward flow from Georges Bank joining to flow west and northwest at the SouthCoast Wind Lease Area.

He and Wilkin (2006) predicted that the maximum tidal current speeds over Nantucket Shoals were in excess of 1 m/s and up to 1.5 m/s near the southeastern edge of the island. Further offshore in a study of sand waves on Nantucket Shoals, it was found that tidal currents dominate water movement and surface tidal currents exceed 0.6 m/s (Twichell et al., 1987).

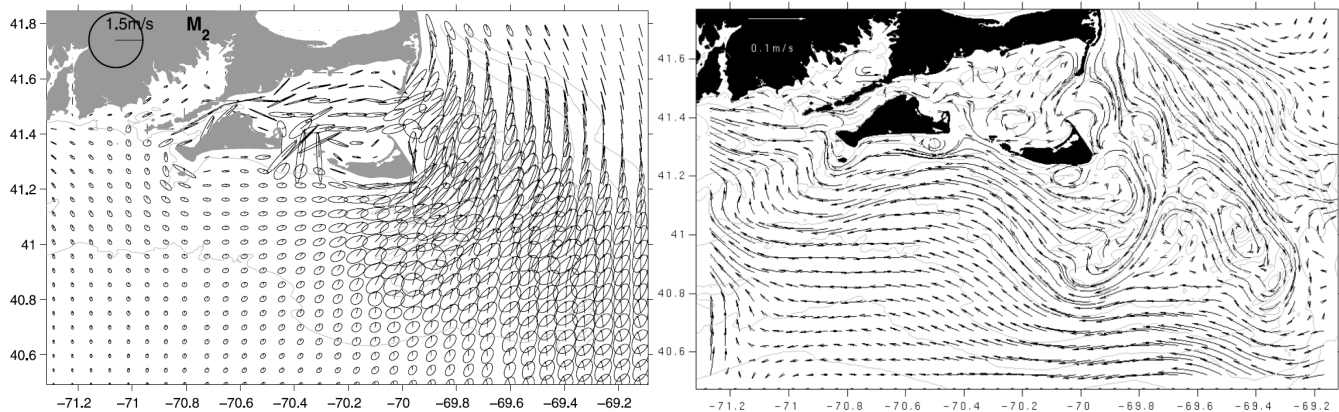


Figure 2-2. Left: Depth-averaged tidal current ellipses for M_2 , plotted every 5 grid points. Right: Depth-averaged M_2 tidal residual circulation (He and Wilkin, 2006).

The Nantucket Shoals tidal front refers to a dynamic and complex transition zone where tidal currents converge and interact with each other in the vicinity of Nantucket Shoals. This front is formed due to the interaction between the tidal flows and the underwater topography of the region, creating distinct features and characteristics. The specific characteristics of the tidal front can vary depending on factors such as the phase of the tide (spring/neap cycle), the alignment of the shoals, and the prevailing weather conditions (Simpson & Sharples, 2012; He & Wilkin, 2006; Loder & Greenberg, 1986; Simpson & Hunter, 1974).

The Nantucket Shoals tidal front plays a significant role in the distribution and movement of marine organisms and sediments in the area. It serves as a transition zone between different water masses, where the mixing of warm and cold waters can create favorable conditions for the growth and abundance of plankton and other marine life. This, in turn, attracts larger marine species, making it an important feeding and breeding ground (White & Veit, 2020; Simpson & Sharples, 2012).

The tidal front can also have implications for navigation and maritime activities. The convergence of tidal currents can create strong currents, which may pose challenges for vessels navigating through the area. The presence of eddies and turbulent waters can affect the stability and maneuverability of ships, requiring careful navigation and awareness of these conditions.

Simpson and Hunter (1974) found that the location of a tidal front in the Irish Sea could be specified by the balance between the potential energy due to surface heating and the turbulence kinetic energy due to the tidal current on the bottom and suggested that the front should be defined by a value of h/u^3 , where h (m) is the local depth and u (m/s) is proportional to tidal current velocity. Data and modeling showed that the front could be found between $h/u^3 = 65$ and 100 , which is often represented as the \log_{10} values (i.e. 1.81 and 2.0 with an average of 1.9).

Loder and Greenberg, (1986) performed an extensive modeling analysis on the tidal mixing parameter in the Gulf of Maine, where a portion of the model domain covered the Nantucket Shoals area. Following Garrett et al. (1978) who found that the transition from well-mixed to stratified conditions in the Bay of Fundy in July and

August occurs at $\log_{10}(h/D_t) = 1.9$, where h/D_t is approximately equal to U^3 . They also found that the same h/D_t contour lay near the observed frontal positions around Georges Bank and Nantucket Shoals.

He and Wilkin (2006) calculated the tidal mixing parameter h/u^3 using the M_2 component from their model predictions (

) for the Nantucket Shoals region as presented in Figure 2-3. The value for $\log_{10}(h/u^3) = 1.9$, equivalent to the average of the Simpson and Hunter findings, is highlighted on the map and appears to roughly follow the 20 m bathymetric contour.

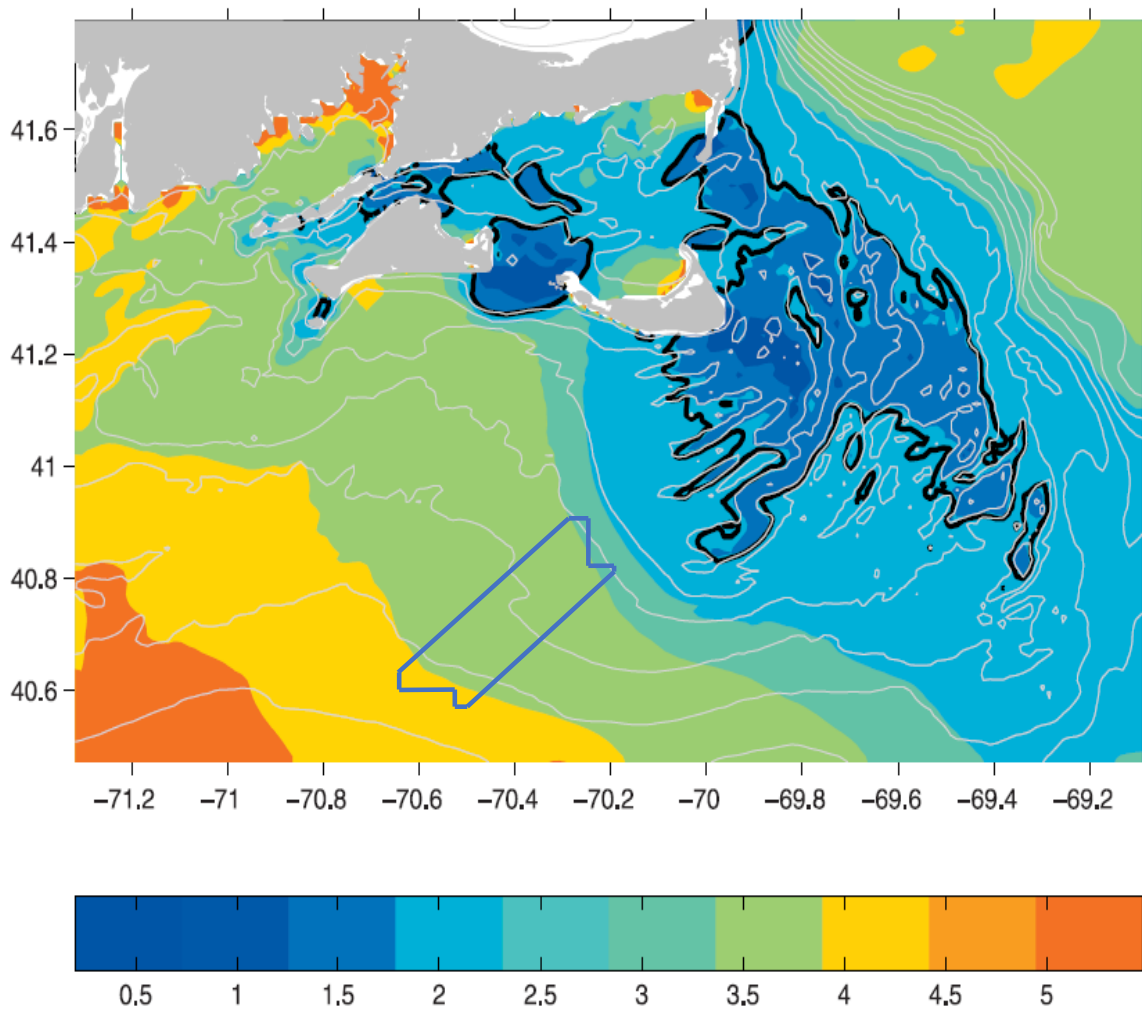


Figure 2-3. Tidal mixing parameter $\text{Log}_{10}(h/U^3)$ for M_2 tidal currents. The solid dark line indicates a tidal mixing parameter value of 1.9, defining the tidally induced frontal locations (He and Wilkin, 2006), with the SouthCoast Wind Energy Lease Area outlined in blue for reference.

In their evaluation of the potential impacts of offshore wind infrastructure on mixing in stratified seas, Dorrell et. al. applied the Simpson and Hunter (1974) ratio to shelf seas around the globe using bathymetry and M_2 tide data

taken from TPX09 global tidal atlas (Egbert and Erofeeva, 2002). Findings included that model resolution limits precise location of stratified fronts from global data but noted that in terms of area, regions of seasonal stratification dominate the continental shelf seas. They concluded that while the critical value for the ratio characterizing the position of tidal mixing fronts was initially estimated for the Irish Sea, (Simpson and Hunter, 1974), consistent values have continued to be estimated for a range of shelf seas globally, including for example the Gulf of Maine and Bay of Fundy, (Garrett et al., 1978 and Loder and Greenberg, 1986) and half a dozen addition locations around the world. The robustness of the critical value highlights the key role of the tides in determining the position of shelf sea fronts and provides the first quantitative link between the dissipation of tidal energy and ocean mixing. Citing Simpson and Sharples, (2012) Dorrell et.al. (2022) used a value of $h/u_{M_2}^3 = 220$, (i.e. $\text{Log}_{10}(h/u_{M_2}^3) = 2.34$) for their analysis of the coastal North Sea areas.

2.3 STRATIFICATION AND MIXING

Stratification refers to the formation of layers of water with different properties such as density or temperature. On Nantucket Shoals, stratification plays a role in shaping the current dynamics. The interaction between stratified water masses and tidal currents can lead to enhanced mixing, affecting the vertical exchange of heat, nutrients, and other properties. Understanding stratification and mixing processes is crucial for assessing the distribution of biological productivity and the transport of materials in the region.

Shelf waters of the Mid-Atlantic Bight and Georges Bank exhibit a large seasonal variation in both temperature and stratification (Lentz, 2008; Beardsley, 1989). During the summer months, surface waters warm and the coastal areas thermally stratify due to strong surface heating and weak wind stresses. During the fall and winter months, as the air cools and stronger wind flows prevail, the surface waters cool and overturn destroying the stratification, mixing the water column from weakly stratified to well mixed. An example seasonal progression of the formation and buildup of stratification, through well stratified to final decomposition of stratification in the winter is presented in Figure 2-4 for a site farther south along the shelf, off the coast of New Jersey that exhibits similar trends as the Nantucket Shoals area.

A slightly older cross-shelf study, the Nantucket Shoals Flux Experiment, (Wright, 1983), conducted south of Nantucket Shoals, shows similar stratification buildup during the spring and summer months. An example of the level of stratification attained by the beginning of August, 1979, is presented in Figure 2-5, along with the observed salinity at that time.

In summary, the physical oceanography of Nantucket Shoals is influenced by various factors, including large-scale circulation, tidal currents and fronts, as well as stratification and mixing. The consistent southwestward flow along Nantucket Shoals, driven by large-scale circulation patterns, highlights the predominant movement of water masses in the region. Tidal currents and fronts contribute to the complexity of currents, while stratification and mixing processes play a crucial role in vertical exchanges and the distribution of biological productivity. Understanding these factors is essential for managing and conserving the marine environment and assessing the potential impacts of human activities. Further research and monitoring efforts are necessary to deepen our understanding of the physical oceanography of Nantucket Shoals and its implications for coastal management and conservation.

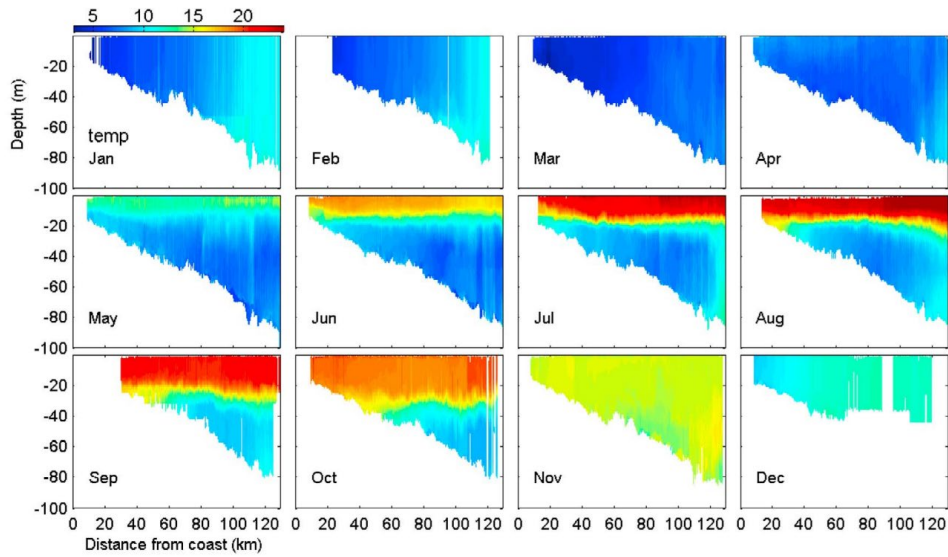


Figure 2-4. Example cross shelf thermal stratification in the Mid-Atlantic Bight by month. The cross shelf transects are farther south than the Nantucket Shoals area but are representative of the area. (Figure from Castelao et al. 2010).

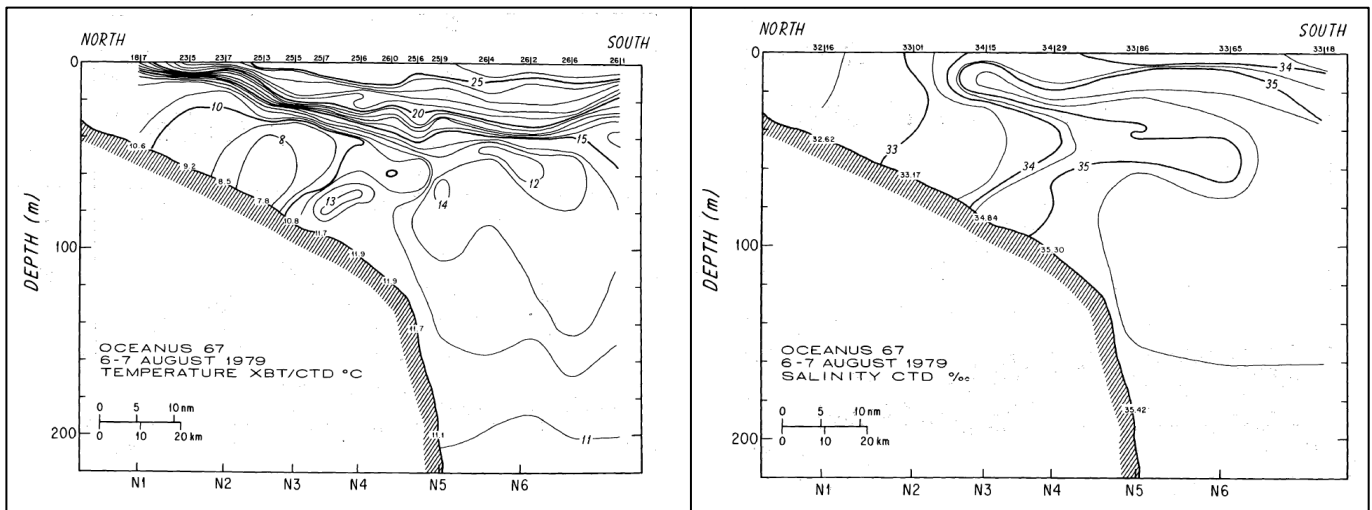


Figure 2-5. Left: cross shelf thermal stratification near Nantucket Shoals at the beginning of August, 1979. Right: cross shelf salinity at the same time. The Nantucket Shoals area is represented in the upper left corner of each figure, from a depth of approximately 60 m and shallower. (Figures from Write et al. 1983, Beardsley et al. 1985).



3 BIOLOGICAL OCEANOGRAPHY OF NANTUCKET SHOALS

3.1 NORTH ATLANTIC RIGHT WHALES

North Atlantic right whales (*Eubalaena glacialis*) range from Florida to Canada, with some degree of seasonal migration between calving and wintering grounds off the southeastern United States and summer socializing and foraging grounds off New England and Canada. A portion of the population remains north of Cape Hatteras, North Carolina year-round, though there is limited knowledge of their winter distributions. Classified as an endangered species under the U.S. Endangered Species Act, critical habitat has been identified to include a Northeastern U.S. Foraging Area (Unit 1) and a Southeastern U.S. Calving Area (Unit 2) (50 CFR 226; NMFS 2016) (Figure 3-1).

Within the Northeastern U.S. Foraging Area, there were traditional regions where right whales aggregated. During summer months, right whales have traditionally been found in high densities in eastern Cape Cod Bay and Massachusetts Bay; the Great South Channel and the northern portion of Georges Bank; the Bay of Fundy; and the southeastern Scotian Shelf (Quintana-Rizzo et al., 2021; O'Brien et al., 2022). More recently (e.g., since 2010), the distribution of North Atlantic right whales has been more unpredictable, with animals migrating as far north as the Gulf of St. Lawrence during summer months (Davies and Brillant, 2019; O'Brien et al., 2022).

Recent studies show that right whales are increasing their use of the Nantucket Shoals region, in particular, the shallow water Shoals themselves, slightly northeast of the MA/RI Wind Energy Area (Quintana-Rizzo et al., 2021). Right whales have been observed in this location during all times of the year, with peak occurrences in the winter and spring (Figure 3-2 courtesy of Quintana-Rizzo et al., 2021; Meyer-Gutbrod et al., 2022; O'Brien et al., 2022). Quintana-Rizzo et al. (2021) suggest that 23% of the right whale population is present in the region at some point between December and May, with a mean residence time of 13 days. Right whales have been observed foraging in this region year-round, and social behaviors associated with mating have been observed in the winter and spring seasons (Quintana-Rizzo et al., 2021). Southern New England is not a new habitat for right whales; this reflects a return to historically important shelf waters known to have been a whaling ground (O'Brien et al., 2022). It is hypothesized that these shifts are occurring throughout New England as climate change affects the distribution and abundance of the plankton species on which right whales feed.

Right whales are specialized foragers, focusing on zooplankton prey, primarily late-stage copepods (*Calanus finmarchicus*) in high density layers (Baumgartner and Mate, 2003). The diving behavior of foraging right whales has been shown to be highly correlated with the distribution and density of copepods, which appear to be concentrated into discrete, high-density layers directly above the bottom mixed layer (Baumgartner and Mate, 2003; Baumgartner et al. 2003). In Grand Manan Basin of the lower Bay of Fundy, right whale sightings and copepod abundance at water depths of 90 to 140 m were highly correlated, with variability in both parameters correlated with changing tidal fluxes (Baumgartner et al., 2003). Tides within the Bay of Fundy do not produce fronts, but instead advect particles into and out of the Bay. It is hypothesized that the correlation with tidal cycles observed at the stationary locations in the Bay of Fundy demonstrated advection of both predator and prey by the tides and small scale (100s of meters or less) movements by the right whales to continue feeding on the *Calanus* patches (Baumgartner et al., 2003).

For effective foraging, right whales must target high-density patches of prey, requiring densities of at least 3,600 copepods per cubic meter (m^3) to meet daily metabolic requirements (Baumgartner and Mate, 2003), with densities reaching levels of 15,000 copepods m^{-3} or more in some instances (Wishner et al., 1988; Baumgartner

and Mate, 2003). Studies of plankton patches show that aggregating processes vary across regions, depending on circulation, bathymetry, and water mass structure (Sorochan et al., 2021).

Studies specific to the wind lease areas near Nantucket Shoals, or even the broader Nantucket Shoals region, are limited. At a broad spatial scale, it is believed that zooplankton are advected onto Nantucket Shoals from the Gulf of Maine. On a smaller spatial scale on the Shoals, aggregated patches of zooplankton are believed to occur due to a tidal front (Ganju et al., 2011). With the complex bathymetry of Nantucket Shoals, these tidal currents, and the resulting tidal front, can create high-density aggregations of copepods within which right whales can forage effectively (Davies et al., 2013).

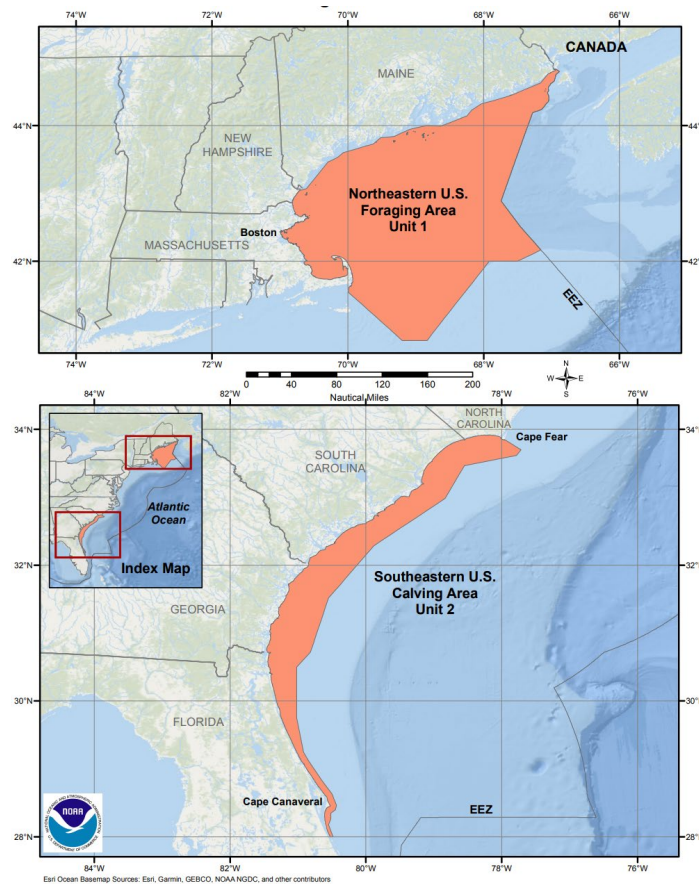


Figure 3-1. North Atlantic right whale critical habitat. Figure courtesy of NOAA Fisheries.

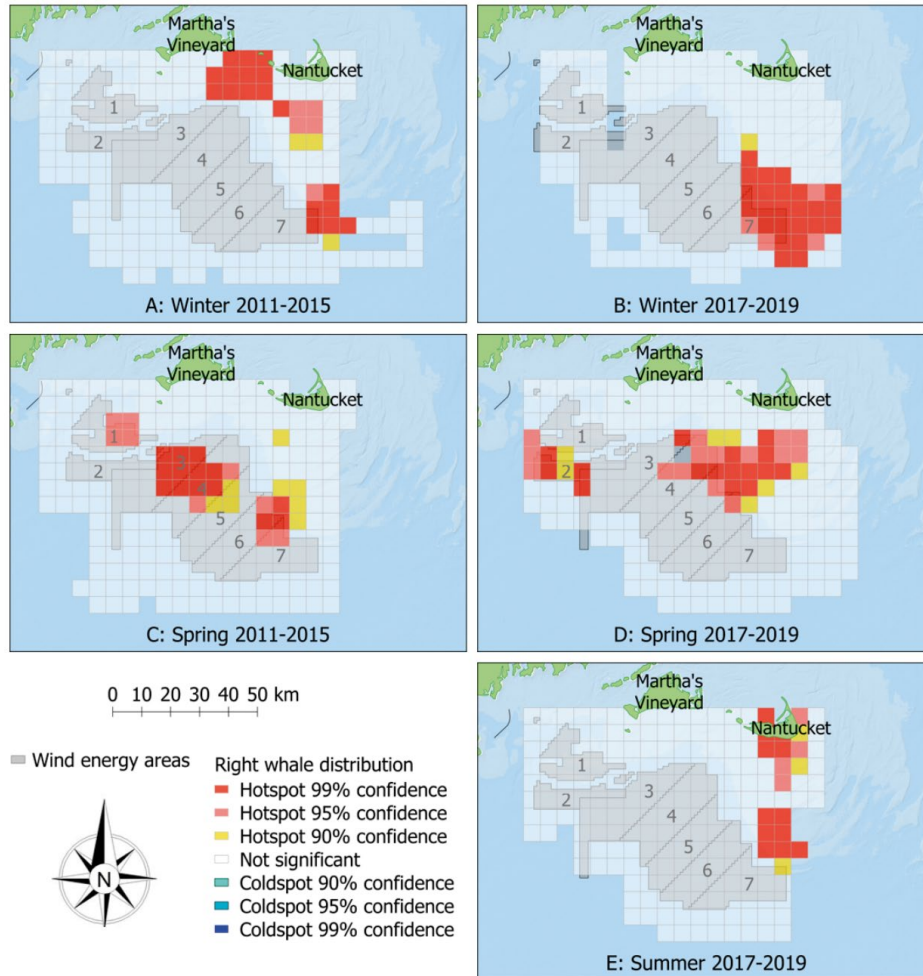


Figure 3-2. Hotspot analysis of right whale distribution relative to wind farm lease areas in the Nantucket Shoals region. Figure 5 in Quintana-Rizzo et al. 2021.

3.2 COPEPODS

The presence of North Atlantic right whales is highly dependent on its food supply, with the large calanoid copepod, *Calanus finmarchicus*, representing the most desirable and nutritious food source in the Northeast US Foraging area. The biology of *C. finmarchicus* (life stage, depth occupancy, and activity) is greatly influenced by external environmental drivers resulting in variable availability and caloric value of this desirable prey. NOAA’s Ecological Monitoring program (ECOMON) takes oblique bongo samples for plankton in a stratified pattern at stations across the Northeast continental shelf, multiple times each year. Samples are taken of the whole water column using a 333 µm mesh net designed to target large calanoid copepods and ichthyoplankton. EcoMon data are available publicly online (Hare, 2021), and a subset (from 1990 to 2015 for the unstaged *Calanus spp*) has been used below to help visualize the potential aggregations of zooplankton on Nantucket Shoals. 333 µm sized mesh is comparable to the estimated filtering efficiency of the North Atlantic right whale (Mayo et al. 2020).



Calanus stages C2 through Adult are large enough to be captured by this sampling method; the smaller stages (<C4) have the lower catch efficiencies.

In the Gulf of Maine and Bay of Fundy, the seasonal patterns of *C. finmarchicus* availability have been well described (Baumgartner, 2003; Baumgartner and Mate 2003; Meyer-Gutbrod et al., 2015; Hayes et al., 2022; Ross et al., 2023). In the small region of Nantucket Shoals, there is a dearth of information on *Calanus* stage, depth occupancy, and level of activity. Of the *Calanus* developmental stages C5 is the most energetically dense. At this stage, *Calanus* have oil-filled sacks intended to be used for overwintering (diapause). Adult and C4 *Calanus* are also nutritious and targeted prey by North Atlantic right whale, although to a lesser degree. Whales have been documented targeting dense patches of *Calanus* at varying depths, over other species of copepods, indicating that foraging is driven by prey selectivity, rather than a set feeding depth or random water sampling to locate patches (Baumgartner 2003). North Atlantic right whales begin feeding when *Calanus* become densely concentrated, or are aggregated, to levels greater than 1,000 individuals per cubic meter (Baumgartner and Mate 2003, Hayes et al. 2022)

Across the Gulf of Maine and Bay of Fundy, the presence of sufficiently dense copepod aggregations for the growth and reproduction of right whales (Ross et al., 2023) is the product of several factors.. There are varying scales for each area of interest discussed with the SouthCoast Wind Lease Area representing a local area, and Nantucket Shoals representing a regional area. At the regional scale, the supply of copepods coming onto the Shoals from the Gulf of Maine must be sufficient enough to create aggregations when combined with local factors. Once near Nantucket Shoals, the local factors influencing the lifecycle and stage of *Calanus* are temperature, tidal mixing and front dynamics, phytoplankton availability, and stratification. Each of these are important to ensure that once advected, the copepods are found in densities and conditions that will entice North Atlantic right whale feeding. Changes in the locations of sufficient prey concentrations would directly affect the successful feeding of North Atlantic right whales (Meyer-Gutbrod et al., 2015). Ross et al., (2023) points out the necessity of not only identifying where whales are feeding, but predicting which areas may become or have the potential to become important feeding grounds.

While the Nantucket Shoals region remains understudied, zooplankton reports show that aggregation potential is dependent on a number of physical parameters of the region and local environment (Sorochan et al., 2021, Ross et al., 2023). On a spatial scale similar to the wind lease area mentioned above, *Calanus* aggregations are believed to occur because of, and along, the tidal front (Ganju et al., 2011), which remains quasi-static (Belkin et al., 2009) between the 20 m and 25 m bathymetric lines (He & Wilkin, 2006, Garrett et al., 1978 and Loder & Greenberg, 1986)(Figure 2-3). Davies et al. (2013) identified that the complex bathymetry of Nantucket Shoals and resultant tidal front are capable of creating aggregations where North Atlantic right whales can forage effectively. Figures 3-3 and 3-5 support higher *Calanus* densities along the tidal front, but there is a lack of samples upon Nantucket Shoals to validate that the density at the front is greater than upon the Shoals themselves (Figure 3-3).

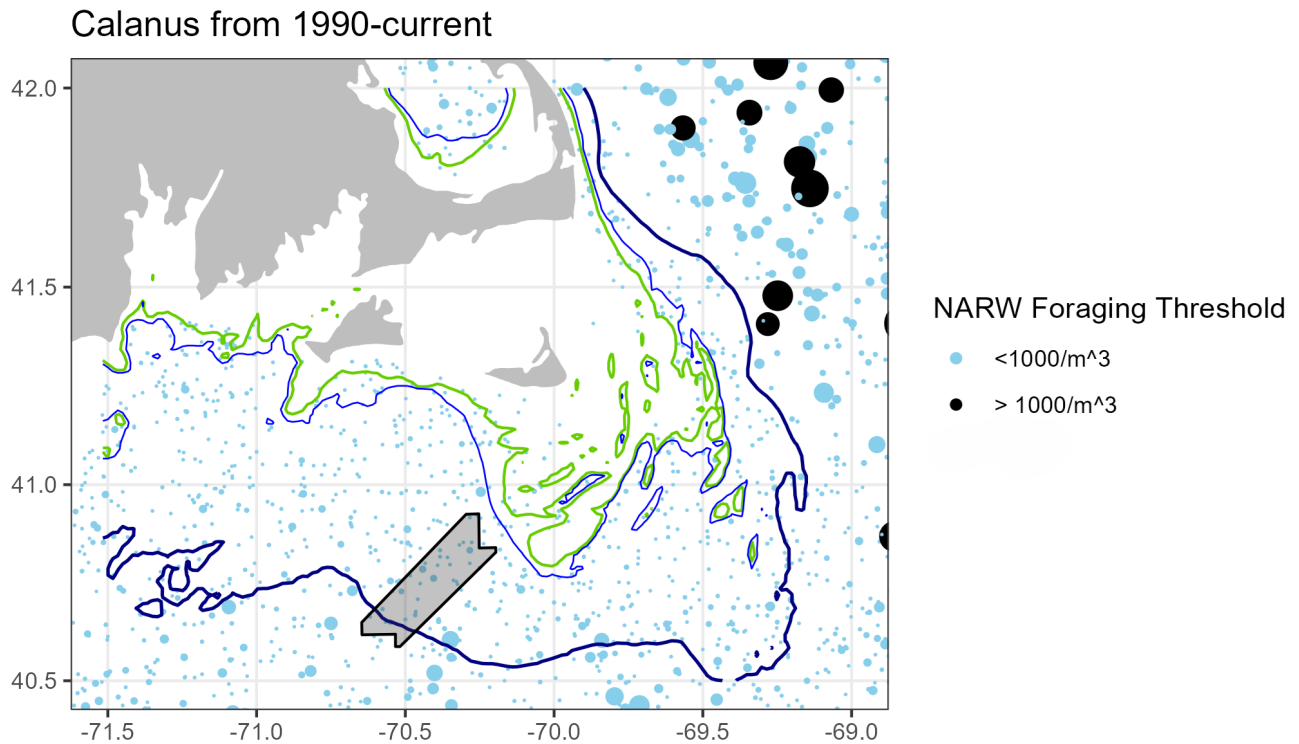


Figure 3-3. Calculated densities of *Calanus* individuals sampled in the Nantucket Shoals region since 1990 shown with the 25 m (green), 30 m (blue), and 60 m (navy) bathymetry lines. Point size is scaled to *Calanus* per cubic meter, and the color indicates if the sample was above the recognized 1000 per cubic meter NARW foraging threshold.

Seasonal fluctuations dominate the relative abundance of plankton assemblages in the western North Atlantic, and the occupancy of whales and other planktivores. North Atlantic right whales were observed feeding below a depth of 75 m during the summer in the Bay of Fundy and late fall on Jeffreys Ledge, on targeted layers of copepods. These non-migratory copepods were confirmed to be in diapause (i.e., C5) (Baumgartner et al. 2017). C5 *Calanus* diapausing in the cold pool north of Cape Cod and, in the fall and late summer, have the highest concentrations of fatty lipids. During periods when *C. finmarchicus* are largely unavailable to right whales, right whales have been observed feeding on other smaller and less nutritious, but more numerous species (e.g. *Pseudocalanus* complex, *Centropages* spp; Mayo & Marx 1990, Record et al., 2009).

In the Great South Channel, the seasonal pattern of *Calanus* and other copepods is inverted. *Calanus* slowly increase in density and then peak quickly in mid-May, and then slowly decline with other copepods persisting over winter (Figure 3-4) (Pendleton et al., 2009). Pendleton et. al. (2009) also demonstrated that there would be more aggregations forming in areas with potential like the Great South Channel and Nantucket Shoals, with an increasing regional mean. Record et. al. (2019) support the idea that favorable prey are being advected onto Nantucket shoals, indicated by the temporal delay in the peak of *Calanus* as compared to source populations.

Peaks in *Calanus* in the Bay of Fundy occurred in February and March, while *Calanus* presence is only detectable in Cape Cod Bay in April and May (Record et al., 2019). Support to the hypothesis of advection is also given by EcoMon data, plotted by month (Figure 3-5).

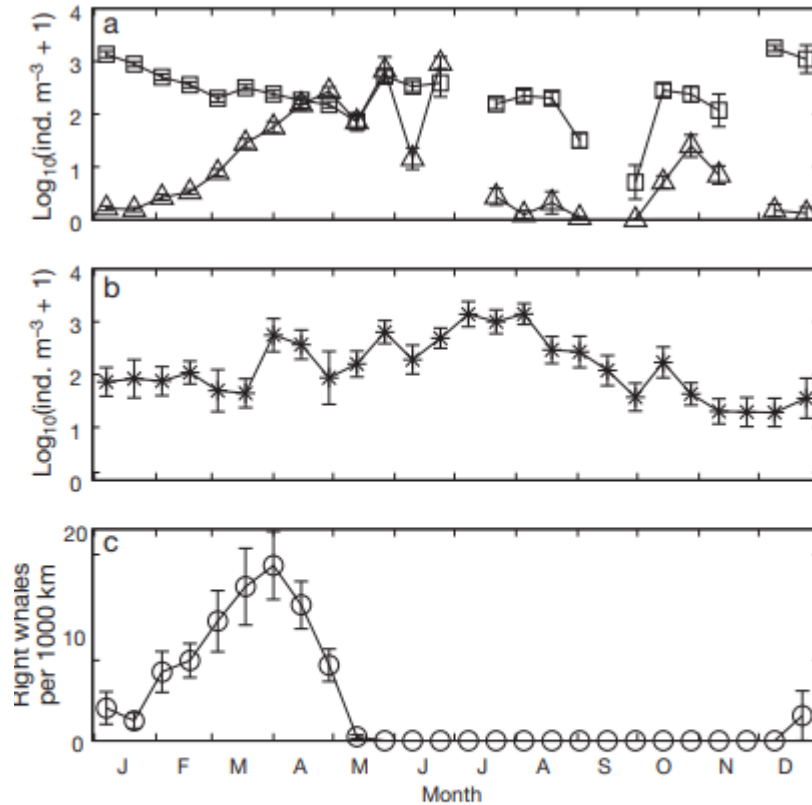


Fig. 2. *Calanus finmarchicus*, other copepods (*Pseudocalanus* spp. and *Centropages* spp.) and *Eubalaena glacialis*. Climatological time series of (a) *C. finmarchicus* (Δ) and other copepods (\square) from surface tows in Cape Cod Bay (1999–2006), (b) *C. finmarchicus* ($*$) from the Massachusetts Bay tract of the CPR (1961–2006), and (c) right whale SPUE (whales per 1000 km of survey effort) (\circ) in Cape Cod Bay (1999–2006). Each point represents the mean \pm 1 SE for a 14 d period

Figure 3-4. Copepod densities and right whale sightings per unit effort in Cape Cod Bay by month. Figure 2a from Pendleton et. al., 2009

Calanus from 1990-current

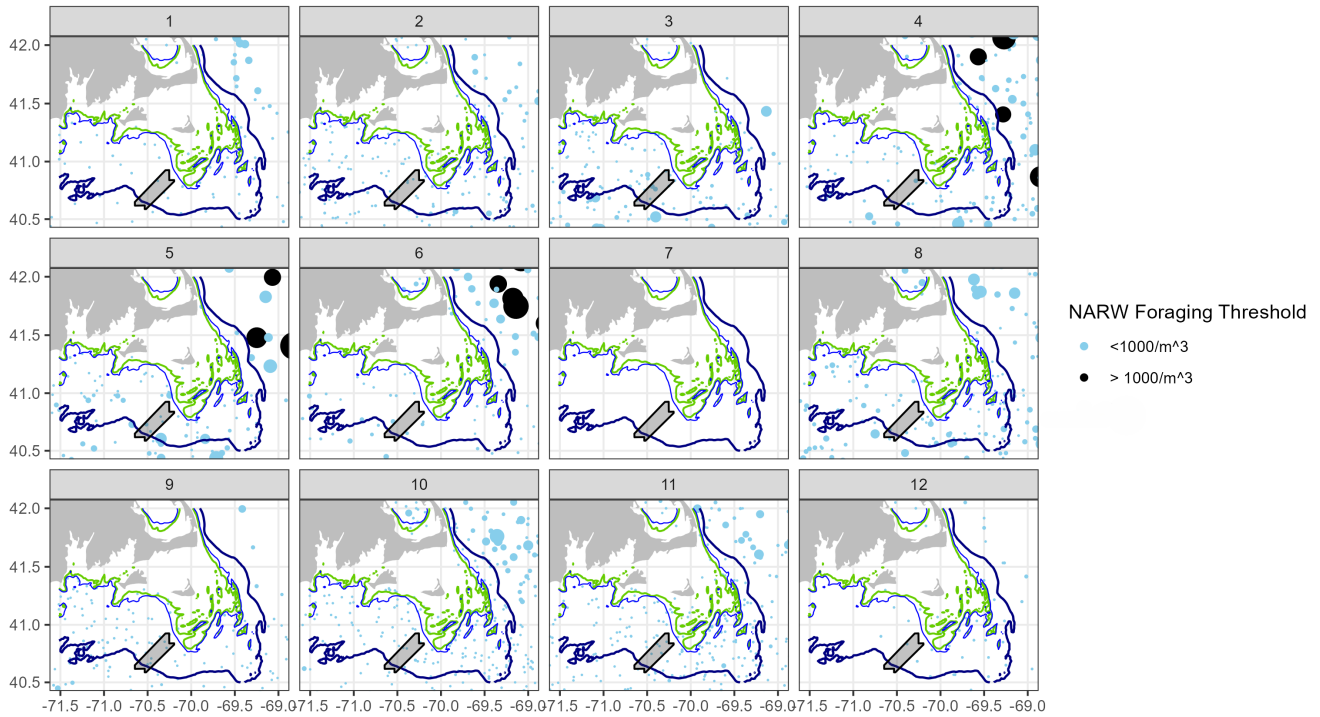


Figure 3-5. Monthly averaged *Calanus* individuals per cubic meter, calculated from ECOMON (1990-current). Showing 25 m (green), 30 m (blue), and 60 m (navy) bathymetry lines; points are sized according to number of *Calanus* per cubic meter.

To understand the dynamics of the preferred prey at Nantucket Shoals, the tidal front location and density of source copepod populations have been considered. The lack of site-specific information on the area surrounding Nantucket Shoals hinders firm conclusions. Information presented here on stratification, currents, and tidal mixing front location above begins to supply the oceanographic information that will help predict if and where aggregations will form. Sampling at discrete depths is needed to understand where copepods are in the water column and what stages of *Calanus* are being advected as well as what effects will be from environmental drivers.



4 SOUTHCOAST WIND FARM NEAR FIELD DOMAIN

4.1 SOUTHCOAST WIND STUDY AREA DESCRIPTION

The SouthCoast Wind Lease Area lies roughly 49 km (26 nm) south of Martha’s Vineyard (Figure 1-1). The Lease Area is oriented in a northeast to southwest direction, straddling a gradual deepening across the shelf from approximately the 40 m to 60 m (131 ft to 197 ft) bathymetry contours.

Physical Environment

Detailed bathymetry for the analyses performed was obtained from the National Geophysical Data Center’s U.S. Coastal Relief Model (CRM) which provides a comprehensive view of the U.S. coastal zone, integrating offshore bathymetry with land topography into a seamless representation of the coast. The CRM spans the U.S. East and West Coasts, the northern coast of the Gulf of Mexico, Puerto Rico, and Hawaii, to beyond the continental slope.

Meteorological and Oceanographic Conditions

Understanding the hydrodynamic circulation and wind speed and directional characteristics in the study is extremely important in determining both the near field effects of the wind field, the potential for any of those effects to reach the Nantucket Shoals region and at what strength they might have upon arrival. SouthCoast Wind deployed a meteorological and oceanographic (metocean) observation buoy in the Lease Area from 2020 to 2022. The SouthCoast Wind metocean buoy has a detailed 2-year data set including time series of wind speed and direction, meteorological data, wave height, period and direction, water surface elevation, current speed and direction profiles, and surface and bottom water temperatures and salinity. On-site observations are invaluable in local characterization and thus the analyses to follow relied mainly on the SouthCoast Wind metocean buoy data. These will be discussed in greater detail in the following section.

A regional scale hydrodynamic model was previously calibrated and run by IES for an export cable burial study in support of the SouthCoast Wind Project (Mendelsohn and Swanson, 2022). The model was calibrated to the SouthCoast Wind buoy data (among other sources) prior to its application in a sediment transport study; this allows for greater understanding of the current speeds, directions and circulation patterns in the areas not only within the wind farm but in the surrounding area as well, including Nantucket Shoals. The model predictions clearly show the rotary tides also seen in the modeling of Codiga and Ullman (2010), He and Wilkin, (2006), and noted early on in Embert (1924). The current speeds in the lower right corner of Figure 4-1 demonstrate the influence of Nantucket Shoals.

MetOcean Data Analysis and Forcing Data Set Development

The metocean data sets identified were analyzed to develop a more detailed understanding/characterization of the metocean climate in the region, and the necessary data for use in the near field impact models. Two particular metocean characteristics are well known in the region and those are the predominance of the SW winds in the warmer months and the rotary tidal current regime in the area of Nantucket Island. The SW winds are likely to transport impacts to the surface waters from the SouthCoast Wind Lease Area towards the northeast and the Nantucket Shoals area. The nature of the rotary tidal currents suggests that the downstream direction is

constantly changing and the duration in any one direction is therefore limited, similarly limiting the extent of any WTG tower impacts to the water column.

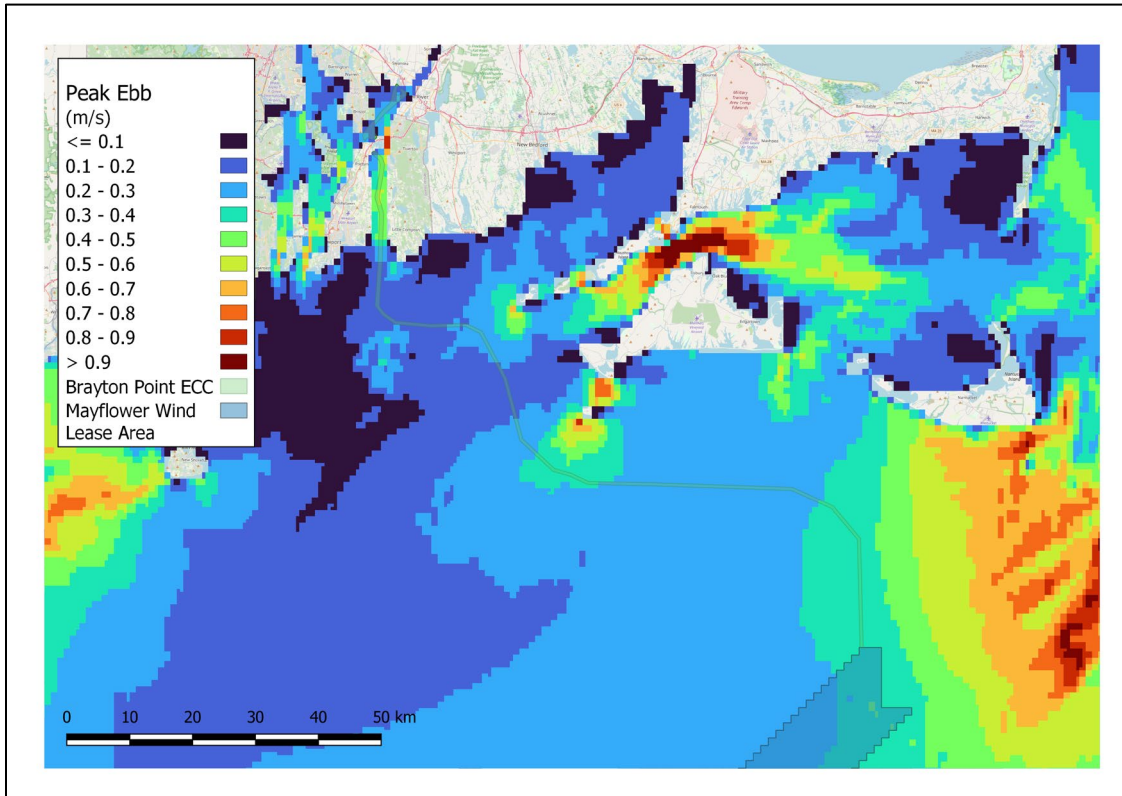


Figure 4-1. IES hydrodynamic model application showing the influence of the Nantucket Shoals on current speeds (from South Coast Wind [formerly Mayflower Wind] COP, 2022).

4.2 SOUTHCOAST METOCEAN BUOY DATA ANALYSIS

As a part of their site assessment work for the Project, SouthCoast Wind deployed a metocean observation buoy in the SouthCoast Wind Lease Area for two years from 1/23/20 to 1/22/22. The buoy deployed a floating Light Detection and Ranging (Lidar) system for measurement of the vertical profile of wind speed and direction, used for wind resource assessment. In addition to the Lidar, the buoy hosted a series of additional meteorological and oceanographic measurement systems for air temperature and wind speed and direction near the surface (i.e., on the buoy); wave height, period and direction; surface and bottom water temperature, salinity, and tides; and an acoustic doppler current profiler (ADCP) for measurement of the vertical profile of current speed and direction. This metocean data set constitutes one of the first long term time series in close proximity to Nantucket Shoals.

The location(s) of the metocean buoy is shown in Figure 4-2 along with the local bathymetry. The buoy was first deployed just outside the Lease Area's northeast boundary (identified as SV1 in subsequent figures), for half a year, pending final deployment permit acceptance, then moved to a more central location (identified by SV2-4 in subsequent figures) for the remaining year and a half. The “SV” in the buoy location name refers to “Service Visit”

so SV2-4 implies that for service visits 2, 3 and 4 the buoy was re-deployed in the same location. Only the first deployment was in a different location. The bathymetry shown in the figure is from the NOAA NGDC US Coastal Relief Model.

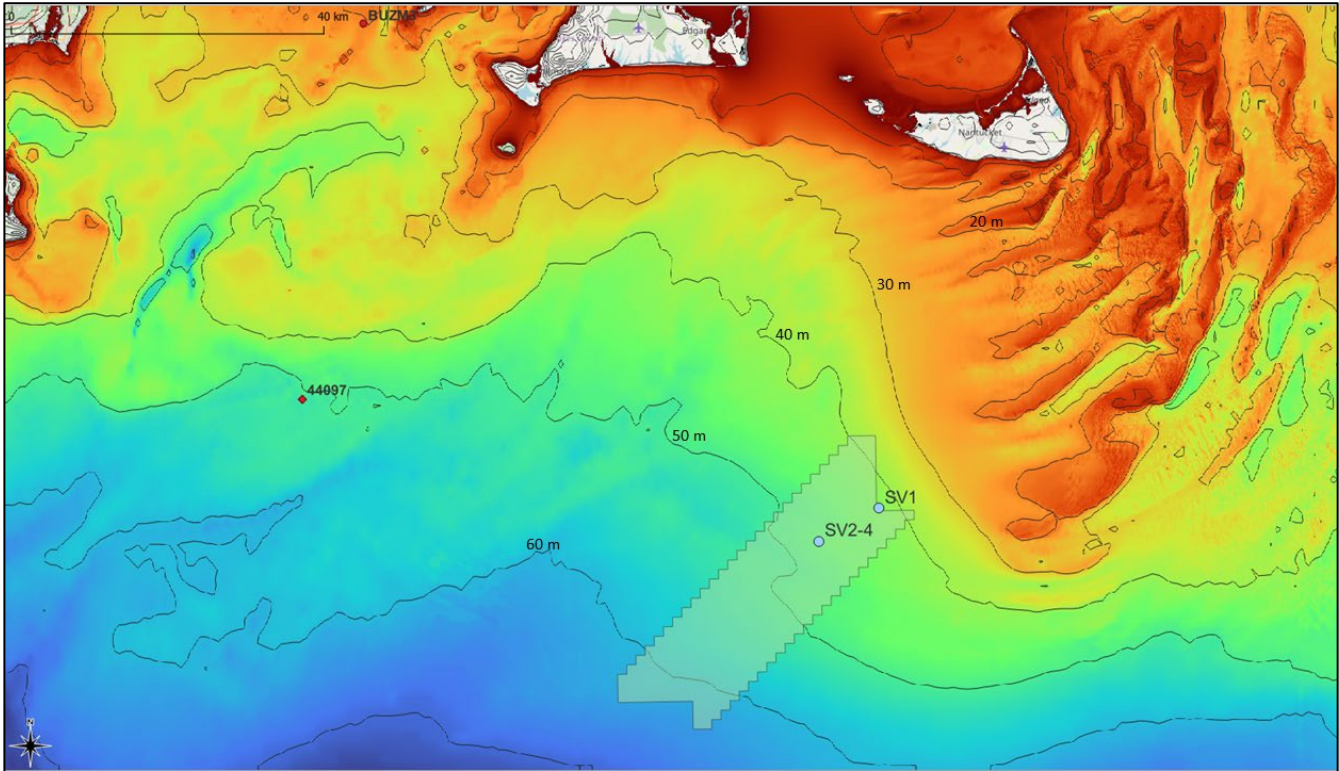


Figure 4-2. SouthCoast Wind Project location showing local bathymetry, Nantucket Shoals and the SouthCoast Wind metocean buoy locations; the first half of 2020 at location SV1 and the remaining duration of the study at location SV2-4.

Each of the SouthCoast Wind metocean buoy data sets were processed and statistically analyzed to develop a characterization of the area. The analyses primarily focused on the current profile, the wind speed and direction, and the surface and bottom temperature series, which are the fundamental drivers of the potential impacts.

The two-year current data set from the Acoustic Data Current Profiler (ADCP) was statistically analyzed to determine prevailing speed and direction at various depths in the water column. In light of the regional assessment described in Section 2, the data set was also evaluated to detect the influence of controlling factors for currents in the SouthCoast Wind Lease Area and Nantucket Shoals such as net flow indicative of: the large scale circulation as part of the shelf flow from the Scotian Shelf, Georges Bank and the Gulf of Maine to the Nantucket Shoals and on to the Mid-Atlantic Bight; bathymetric steering effects on current speeds; tidal forces producing rotary currents; and tidal mixing fronts; wind speed, direction and duration affecting surface currents, enhancing or slowing speeds and increasing mixing of the upper water column.

SouthCoast Wind Buoy Current Observations

After review of the ADCP time series at all levels, it was found that the near surface bin with the most consistent record was at a water depth of 10 m and for the near bottom, the record at 30 m was selected. Data nearer to the extremes on both ends of the depth range were found to have large gaps in the coverage and missing critical time periods.

The currents observed at the SouthCoast Wind metocean buoy site clearly showed the rotary tidal nature described in Section 2. Figure 4-3 shows an example current time series comparison at 10 m and 30 m during January 2020. The time series of speeds (top plot) and directions (bottom plot) for currents at 10 m (orange line) and 30 m (blue line) at the buoy location for the eight-day period are shown. Referring to the figure, the speed time series visually displays the two tides a day (semi-diurnal) frequency, though uneven, at both the surface and the bottom. The semi-diurnal rotary currents aspect can be seen in the direction time series, where twice a day the direction slowly migrates through all 360 degrees of the compass at both the near surface and near bottom. The consistency of currents at surface and at depth indicates that the water column primarily acts as a unit.

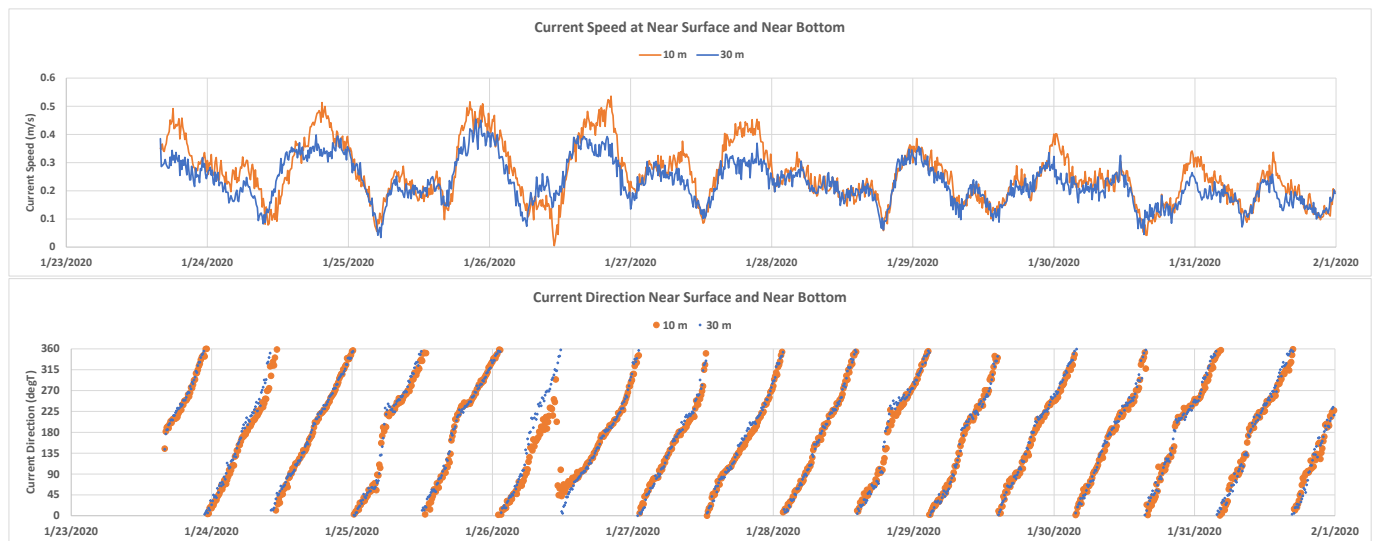


Figure 4-3. Example near surface (10 m, orange line) and near bottom (30 m, blue line) current speed (top) and direction (bottom) time series at the SouthCoast Wind metocean buoy site.

Another way to look at the rotary currents is through a tidal ellipse (left plot) and a progressive vector diagram (PVD) (right plot) as shown in Figure 4-4 for a single 12-hour tidal cycle. In the ellipse plot, each current vector represents one hour (although the actual currents progress more smoothly around the compass) of the tidal cycle towards which the current is flowing. Using the currents in the ellipse to drive a parcel of water, the PVD plot shows the path that the parcel would follow over that tidal cycle giving an indication of the complexity of tidal currents in the domain.

Current roses and directional frequency charts for the 10 m and 30 m depth are presented in Figure 4-5 for the two-year data set from the SouthCoast Wind metocean buoy. Current roses show the percentage of current speeds for each direction of the compass as a summary of all observations. The directional frequency shows the percentage that the currents flow at each of the 16 points of the compass. The roses and the frequency diagrams indicate that there is a slight preference for southwestern and northwestern current flows. Both of those

directions are potentially indicative of the clockwise flow around Nantucket Shoals. Greater southwestern flow is potentially indicative of the strong regional ebb tide currents off the Shoals. The relatively even spread of directions is consistent with the time series showing the rotary nature of tidal currents.

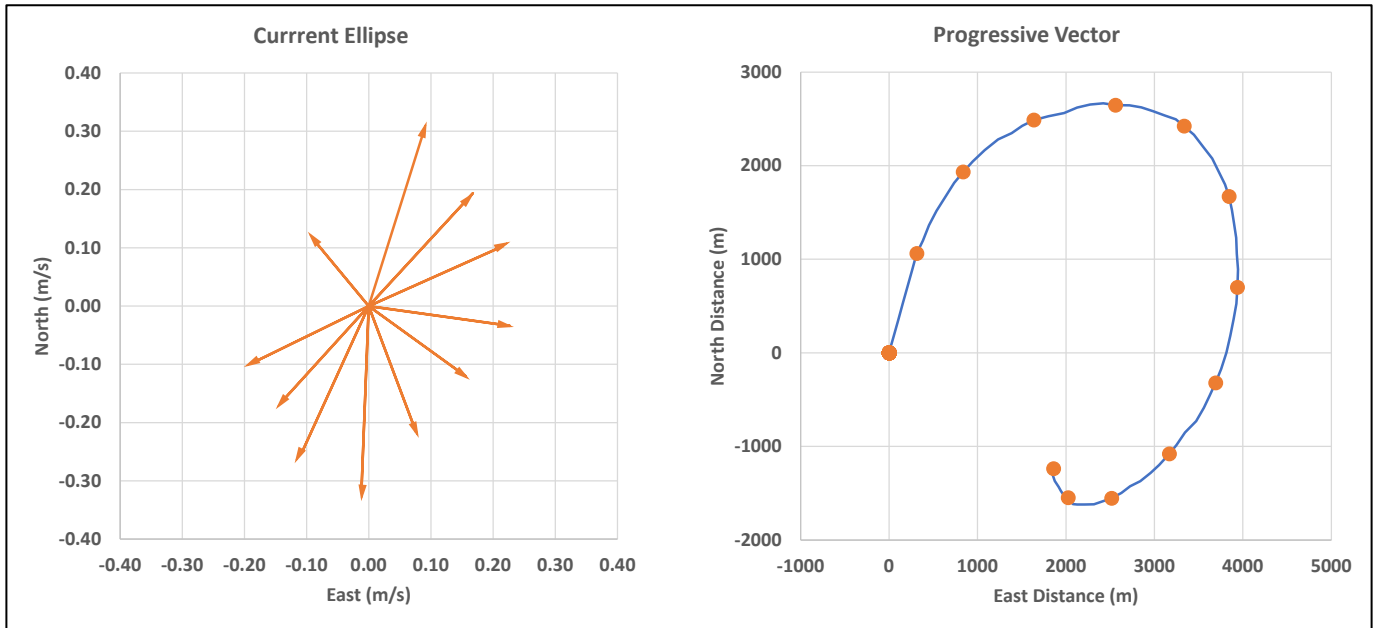


Figure 4-4. Example near surface (10 m) currents showing current vectors (left) for each hour and a progressive vector diagram (right) over a single tidal cycle, where each orange dot represents an hour.

Speeds are generally less than 0.5 m/s and often slightly larger at the surface than at the bottom with an average of 0.246 m/s at 10 m and 2.39 m/s at 30 m. The min, mean, max and percentile speeds are summarized in **Table 1** (a) and (b), respectively at the 10 m and 30 m depths.

Table 1. Current speed statistics for the SouthCoast Wind MetOcean buoy 1/23/20 – 10/8/21

(a) Current Speed Statistics		
	10 m	30 m
count	88790	84400
min =	0.001	0.002
mean =	0.246	0.239
max =	0.913	0.783

(b) Percentiles		
	10 m	30 m
5%	0.079	0.084
10%	0.109	0.114
25%	0.166	0.169
50%	0.234	0.233
75%	0.316	0.299
90%	0.392	0.366
95%	0.443	0.413
99%	0.572	0.528

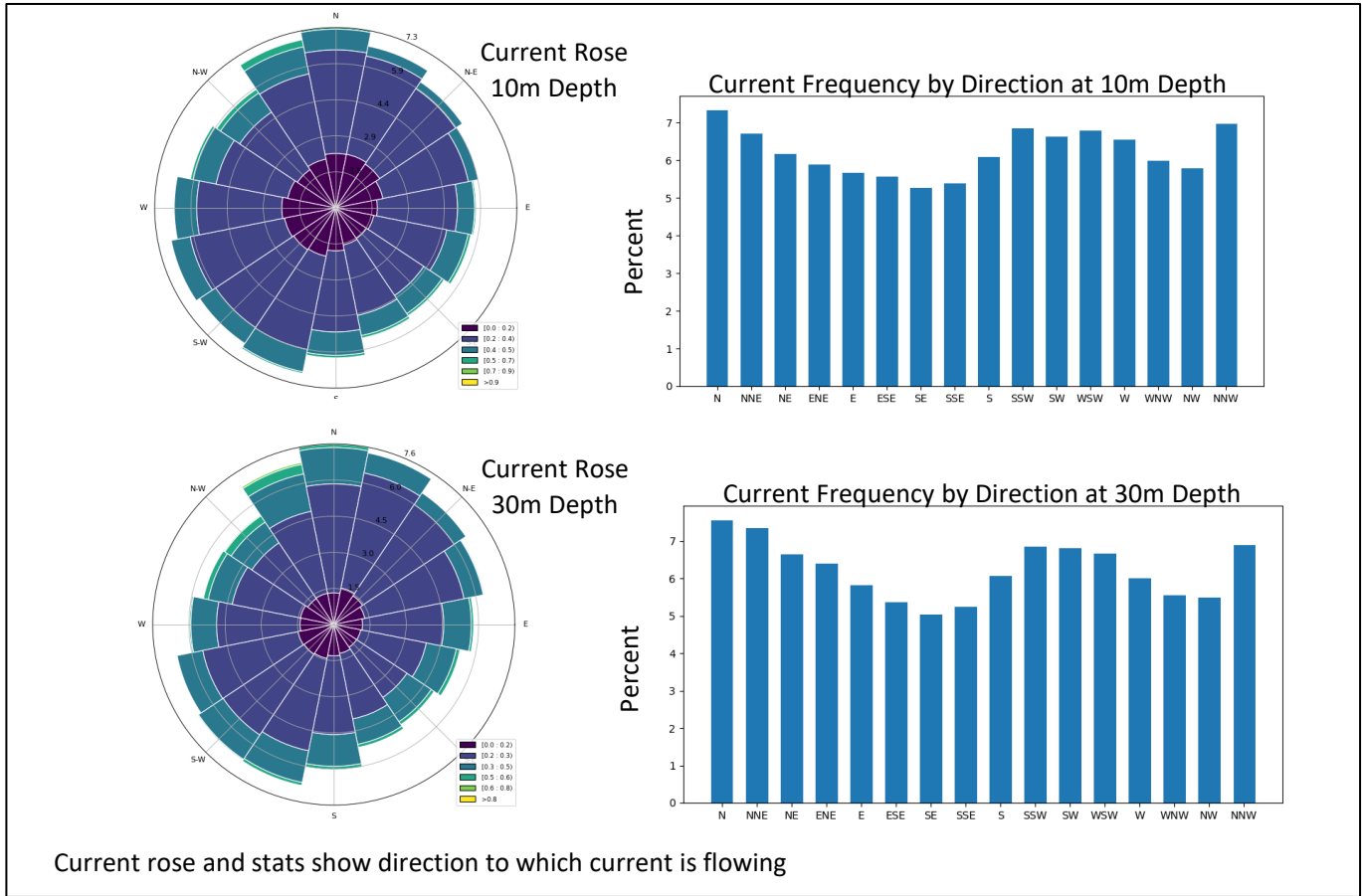


Figure 4-5. Current roses and directional frequencies for the 10 m and 30 m depths from the SouthCoast Wind metocean buoy observations.

A tidal harmonic analysis was also performed on both the currents and the water surface elevation which can be found in Table 2. Tidal harmonics refer to the cyclical variations in water levels caused by gravitational forces exerted primarily by the moon and the sun, as well as the rotation of the Earth. These variations occur in predictable patterns, forming the basis of tidal predictions and analyses. Tidal harmonics are composed of various tidal constituents, each representing a specific tidal cycle or frequency. The five most significant constituents include:

- Principal Lunar (M2): The primary lunar tidal constituent, responsible for the dominant semidiurnal (twice-daily high and low tides) tidal cycle.
- Principal Solar (S2): The primary solar tidal constituent, also associated with the semidiurnal tidal cycle and in conjunction with the M2 in primarily responsible for the spring-neap cycle of the tides.
- Larger lunar elliptic semidiurnal constituent (N2): Modulates the amplitude and frequency of M2 for the effect of variation in the Moon's orbital speed due to its elliptical orbit.
- Lunar Diurnal (O1): The diurnal (once daily) tidal constituent primarily influenced by the moon.



- Solar Diurnal (K1): The diurnal tidal constituent primarily influenced by the sun.

Tidal harmonics result from the interactions between various tidal constituents, as well as other factors such as coastline geometry, bathymetry, and resonance effects. These interactions can lead to complex tidal patterns observed in different regions. Each tidal constituent has a specific amplitude (magnitude) and phase (timing) that determine its contribution to the overall tidal pattern. These parameters are derived from tidal analysis and are used to better understand the tidal forces that generate the surface elevation variation and tidal currents and to predict tidal behavior more accurately. When running a hydrodynamic model of a particular area, comparison of the model predicted tidal harmonic constituents to the observed data derived constituents is very instructive in determining whether the model is predicting the tidal dynamics (magnitudes and timing) of the area appropriately.

Table 2. Harmonic Analysis of the SouthCoast Wind buoy water surface elevation and current speeds showing the 5 largest constituents.

Water Surface Elevation			Current Speeds			Description
	Amp (m)	Phs (deg)		@10 m	@30 m	
M2	0.385	98.57	M2	0.200	0.202	Principal lunar semidiurnal constituent
S2	0.089	21.77	S2	0.033	0.035	Principal solar semidiurnal constituent
N2	0.100	202.42	N2	0.047	0.047	Larger lunar elliptic semidiurnal constituent
K1	0.077	197.25	K1	0.061	0.057	Lunar diurnal constituent
O1	0.059	253.50	O1	0.039	0.036	Lunar diurnal constituent

A long-term analysis was run to determine the net currents at the buoy site by season, to match the seasonal assessments of the copepod distributions in the area. Each year was broken down into four seasons with:

- Winter – Dec, January, February
- Spring – March, April, May
- Summer – June, July, August
- Fall – September, October, November

The results of the analysis are presented in

Table 3. with year, season, depth, speed (in cm/s) and direction (in degrees True, towards). The accompanying figure for Seasonal Net Currents represents the speed and directions in the table on an x-y grid with east-west along the x-axis and north-south along the y-axis.

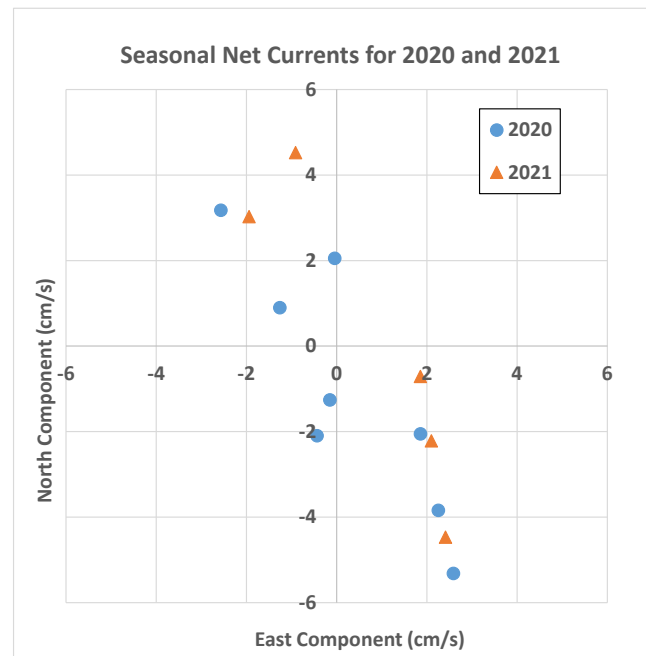
Reviewing the plot, it appears that the net currents over each season are aligned with the Nantucket Shoals bathymetry in a NNW – SSE axis and implies orographic steering of the currents in the net. Net flow directions and



speeds indicate that water mass traversal time from one side to the other of SouthCoast Wind Lease Area would be an average of 4 – 6 days. An example of the net flow speed and direction is presented in Figure 4-6 showing the net current for the summer seasons, 2020 on the map, in proximity to the Nantucket Shoals bathymetry, highlighting the net direction.

Table 3. Long term net current speeds and directions by season and year for the SouthCoast Wind ADCP data. Note that current speed data is presented in cm/s.

Year	Season	Depth (m)	Speed (cm/s)	Dir (degT)
2020	Winter	10	4.45	149.6
2020	Spring	10	2.14	191.8
2020	Summer	10	4.08	321.1
2020	Fall	10	1.27	186.9
2021	Winter	10	5.91	154.0
2021	Spring	10	2.77	137.9
2021	Summer	10	2.06	358.7
2021	Fall	10	1.55	305.5
2020	Winter	30	3.85	135.8
2020	Spring	30	2.42	156.1
2020	Summer	30	3.59	327.3
2020	Fall	30	3.05	136.6
2021	Winter	30	5.08	151.6
2021	Spring	30	1.99	110.9
2021	Summer	30	4.61	348.6
2021	Fall	30	-	-



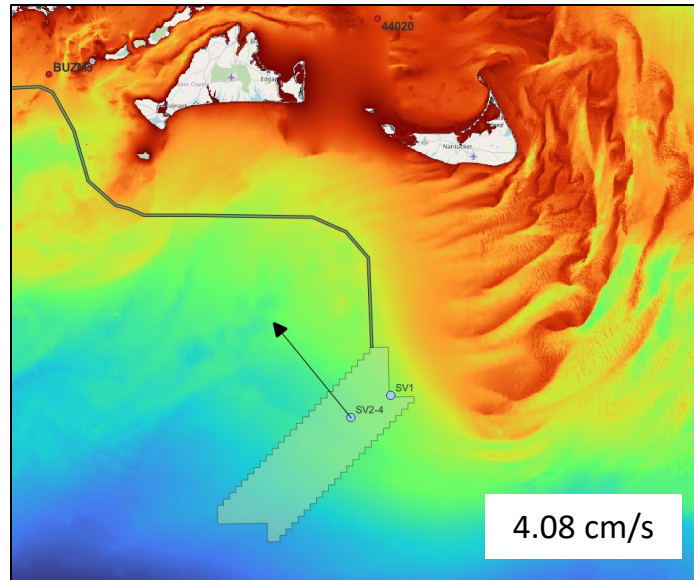


Figure 4-6. Net current flow speed and direction at 10 m during summer 2020 from observations at the SV2-4 buoy deployment location. The map shows the buoy location(s) and proximity to Nantucket Shoals seen as shallow (more red) depths. The buoy was deployed at SV1 for the first half of 2020 and at location SV2-4 into 2022.

SouthCoast Wind Buoy Surface Wind Observations

A statistical analysis of the wind speed and direction from the SouthCoast Wind metocean buoy data was also performed to characterize the meteorological environment for the wake effect assessment. The anemometer height was 4 m above the sea surface. The meteorology in the southeast coastal New England area has been studied for many years and is relatively well understood. Winds are often strongest from the NE to NW directions, but winds from the SW are predominant and in this case are predisposed to potentially have impacts from the offshore wind areas directed towards the Nantucket Shoals. In addition, wind is one of the drivers of currents, second to tides, and a mixing generator, from the surface water down.

A statistical analysis was performed to better understand and characterize the wind regimes present near the surface at the SouthCoast Wind metocean buoy location. The statistical analysis of the wind data showed that the prevailing winds were southwesterly $\approx 30\%$ of the time. That included 30% – 40% directed towards Nantucket Shoals and 60% - 70% away from Nantucket Shoals. A wind rose for the two-year deployment and a directional frequency histogram a presented in Figure 4-7 and the accompanying statistics are presented in **Table 4**. The plots show the SW wind predominance quite clearly and indicate that the stronger W and NW winds are also frequent. The wind strength is indicated by the color bands on each of the sectors, with the lighter colors indicating stronger winds and the ends of each sector arc. The wind speed statistics show an average wind speed of about 6.5 m/s at the 4-m height over the two-year period.

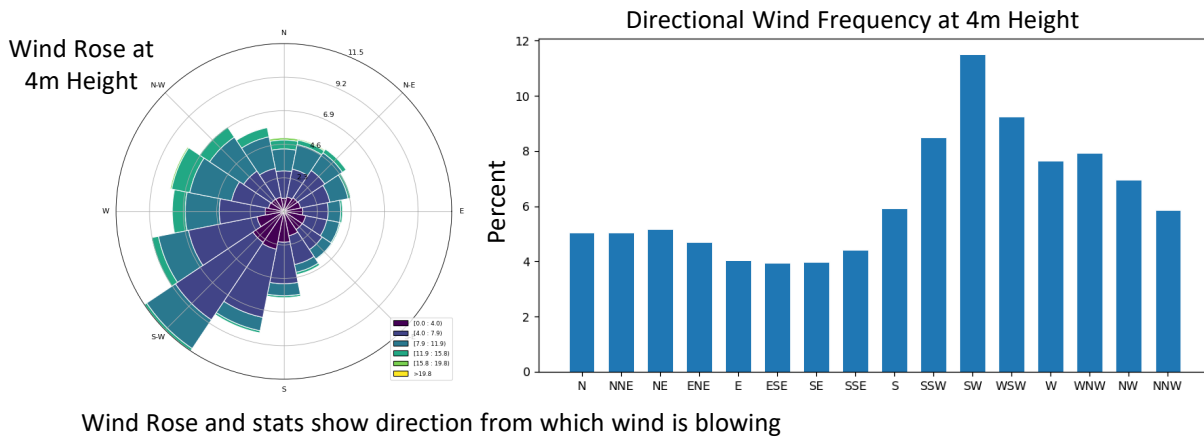


Figure 4-7. Wind rose and directional frequencies for the wind speed at 4 m above the sea surface.

Table 4. Wind speed statistics from the SouthCoast Wind metocean buoy 1/23/20 – 1/22/22

	Wind Speed (m/s)
Min	0.08
Mean	6.58
Max	18.97
Percentiles	
5%	1.86
10%	2.56
25%	4.06
50%	6.14
75%	8.81
90%	11.20
95%	12.43
99%	14.85

SouthCoast Wind Buoy Surface and Bottom Water Temperatures and Salinity Observations

One of the more important aspects of this study concerns the water column stratification in the Nantucket Shoals area. Studies of the biological activities in the area found that the North Atlantic right whale’s preferred prey primarily inhabit the lower water column of stratified waters (Plourde et a., 2019). Stratification of a water

column is a function of the salinity and primarily water temperature in this area (Castelao et al. 2010; Lentz, 2008; Beardsley, 1989; Wright, 1983) as the salinity is fairly constant (see Figure 4-9).

The SouthCoast Wind metocean buoy system was equipped with temperature sensors both at the surface and the bottom of the water column making the presence of stratification, and its strength measurable, although not its depth, as there is no profile data. A time series plot of temperatures over the two-year deployment is presented in Figure 4-8 where the upper plot is 2020 and the lower plot is 2021. The surface water temperatures are represented with the blue lines, the bottom waters with the orange lines and the difference between the two are the green lines. The red ovals mark the approximate times of stratification onset in the late spring, to the left of each plot, and the breakdown in the mid fall, to the right of the plots. The time series indicates that the water column is stratified for approximately 5 months from May to October over both years. The stratification appears to be the strongest during the months of July and August, reaching 10°C with weaker stratification during the months of June and September, where it is often 5°C.

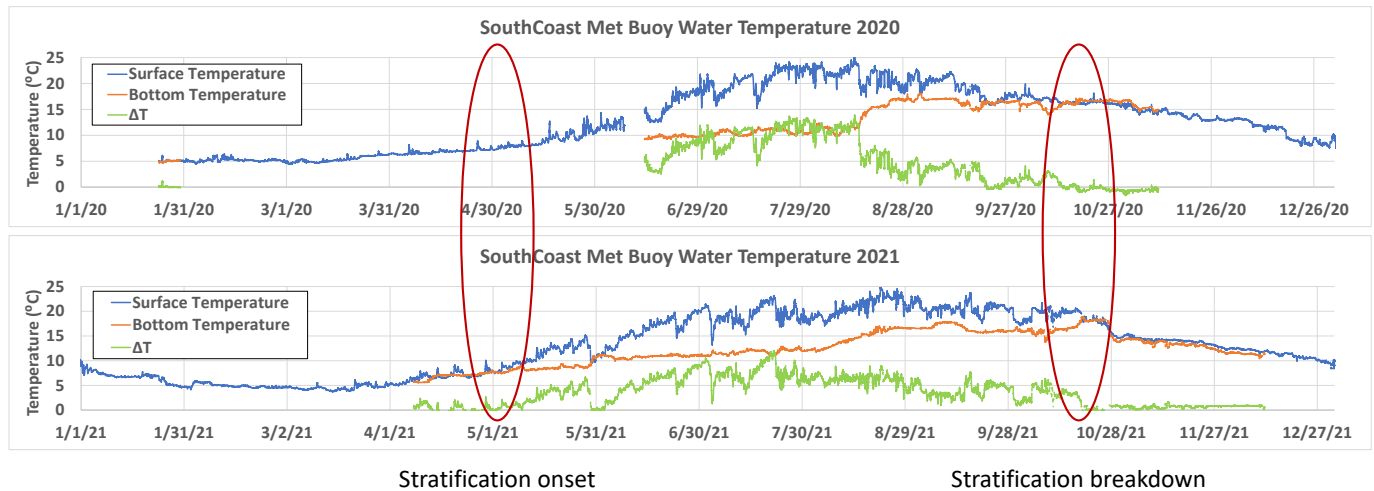


Figure 4-8. SouthCoast Wind metocean buoy recorded surface (blue line) and bottom (orange line) temperature and the temperature difference (green line) for 2020 (top plot) and 2021 (bottom plot). The red ellipses indicate timing of the onset of stratification (left side) and collapse (right side) of stratification for the two years.

It is useful at this point to review a time series comparison of the major parameters being evaluated to characterize the system at Nantucket Shoals. Figure 4-9 presents a time series stack plot of, from top to bottom, wind speed, wind direction, significant wave height, air temperature, surface and bottom water temperature and salinity. The plot covers a time period between July and August, 2020. The water temperature indicates an essentially stable, stratified water column until August 15th, 2020 when a clear decline in surface temperature can be seen, along with an increase in the bottom temperature, around 40 m below the surface, while the salinity at the near surface increases. Not surprisingly, in reviewing the wind speed and direction and the air temperature, a cold front/storm can be postulated as moving through the area. The wave heights add to the storm hypothesis. The result appears to be a dynamic mixing of almost the entire water column, nearly collapsing the stratification in a matter of a day. These data indicate that there is a clear influence on temperature and salinity from storms, even at depths on the order of 50 m.

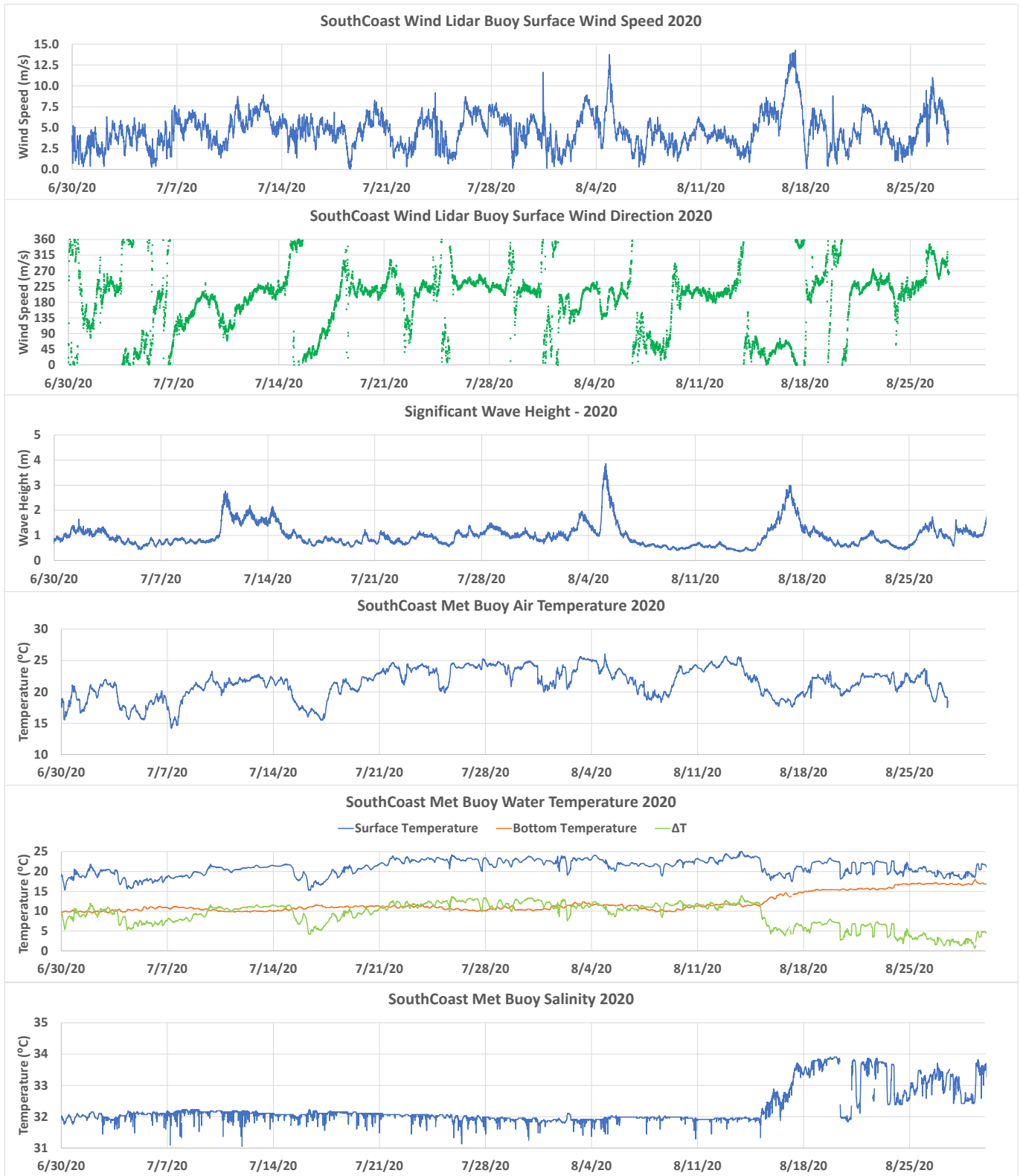


Figure 4-9. SouthCoast Wind metocean buoy observations time series stack plot for July – August, 2020.

Nantucket Shoals Tidal Mixing Front

Tidal mixing fronts separate regions of seasonal stratification from well mixed regions and as discussed in Section 2.2 are of biological interest. Simpson and Hunter (1974) used an energetics argument to derive a single parameter to predict the positions of these fronts. By considering only vertical exchange processes and assuming the surface input of heat was the only stratifying influence, and that tidal currents are the only source of energy driving mixing, they showed that the first order determinate for the position of shelf sea fronts is given by the ratio (Dorrell et.al. 2022):

$$h/u_{M_2}^3$$

where u_{M_2} is the amplitude of the principal lunar tidal harmonic component M_2 and h is water depth. To estimate the location of the tidal mixing front on the west side of Nantucket Shoals a series of mixing ratio were calculated based on the $u_{M_2} = 0.2$ m/s, calculated for the ADCP data at 10 m and the depth at the buoy site for the SV2 - SV4 period, of $h = 47$ m, yielding $\text{Log}_{10}(h/u_{M_2}^3) = 3.77$. In order to estimate the tidal front location at Nantucket Shoals additional depth and current ratios needed to be assessed. For those estimates values from the previously verified hydrodynamic model application described briefly in Section 4.1 were used to scale the M_2 component, where an example model output can be seen in Figure 4-1. The model predictions clearly show the influence of Nantucket Shoals on the current speeds.

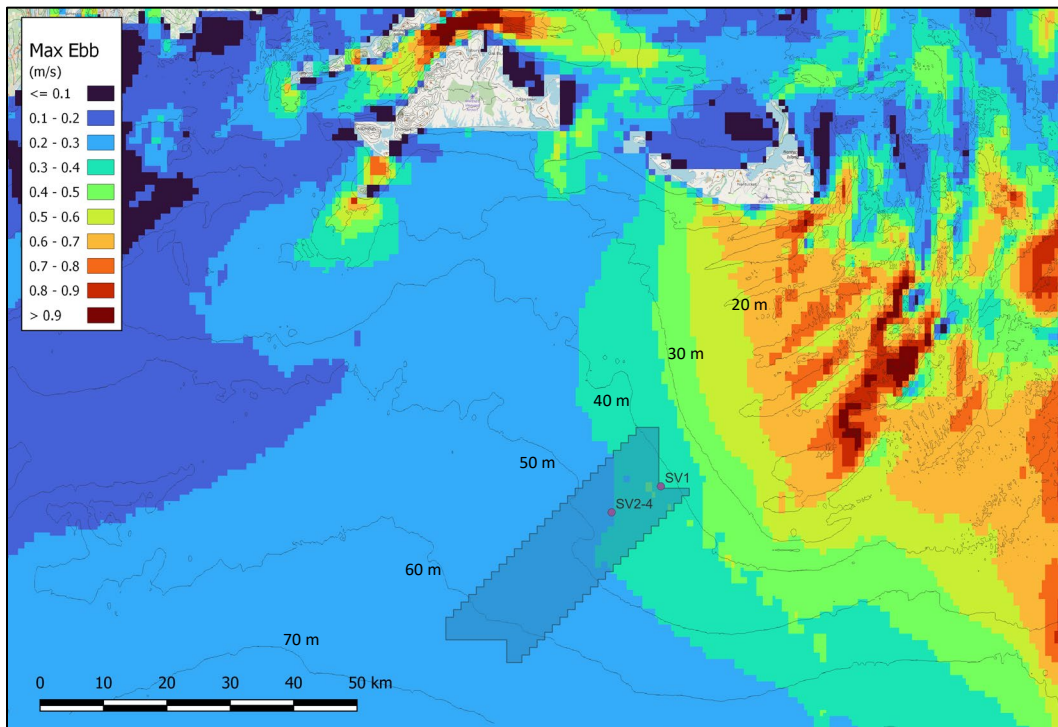


Figure 4-10. IES hydrodynamic model application showing the influence of the Nantucket Shoals on current speeds overlain on the local bathymetry (from South Coast Wind COP – Appendix F3, 2023). The metocean buoy locations are also shown for reference, where the buoy was deployed at SV1 for the first half of 2020 and at SV2-4 into 2022.

Using the ratios calculated at various depths, a relationship between the bathymetry and mixing ratio was developed, which is plotted in Figure 4-11. The figure presents a map of the Nantucket Shoals bathymetry with contour lines of key depths, the locations of the SouthCoast Wind Lease Area and the metocean buoy, and an estimate of the tidal mixing front location on the Shoals. The mixing front ratios estimated were compared to the value used by Dorrell et.al. (2022) who estimated the mixing front based on the M_2 tidal component to be at $h/u_{M_2}^3 = 220 \text{ s}^3/\text{m}^2$, which is $\text{Log}_{10}(h/u_{M_2}^3) = 2.34$. The depth of the mixing front was selected based on the intersection of the line of ratios and the $\text{Log}_{10}(220) = 2.34$ line, yielding approximately 20 - 25 m. The dashed line on the map represents the tidal mixing front location on the Shoals.

The location of the tidal mixing front presented in Figure 4-11 can be compared favorably with the location of the front predicted by He and Wilkin (2006) (Figure 2-3) and Loder and Greenberg (1986), though the equation and criteria used by the two are slightly different than that used here. The estimated location of the tidal mixing front is approximately 10 km (5.4 nm) from the nearest WTG location in the SouthCoast Wind Lease Area.

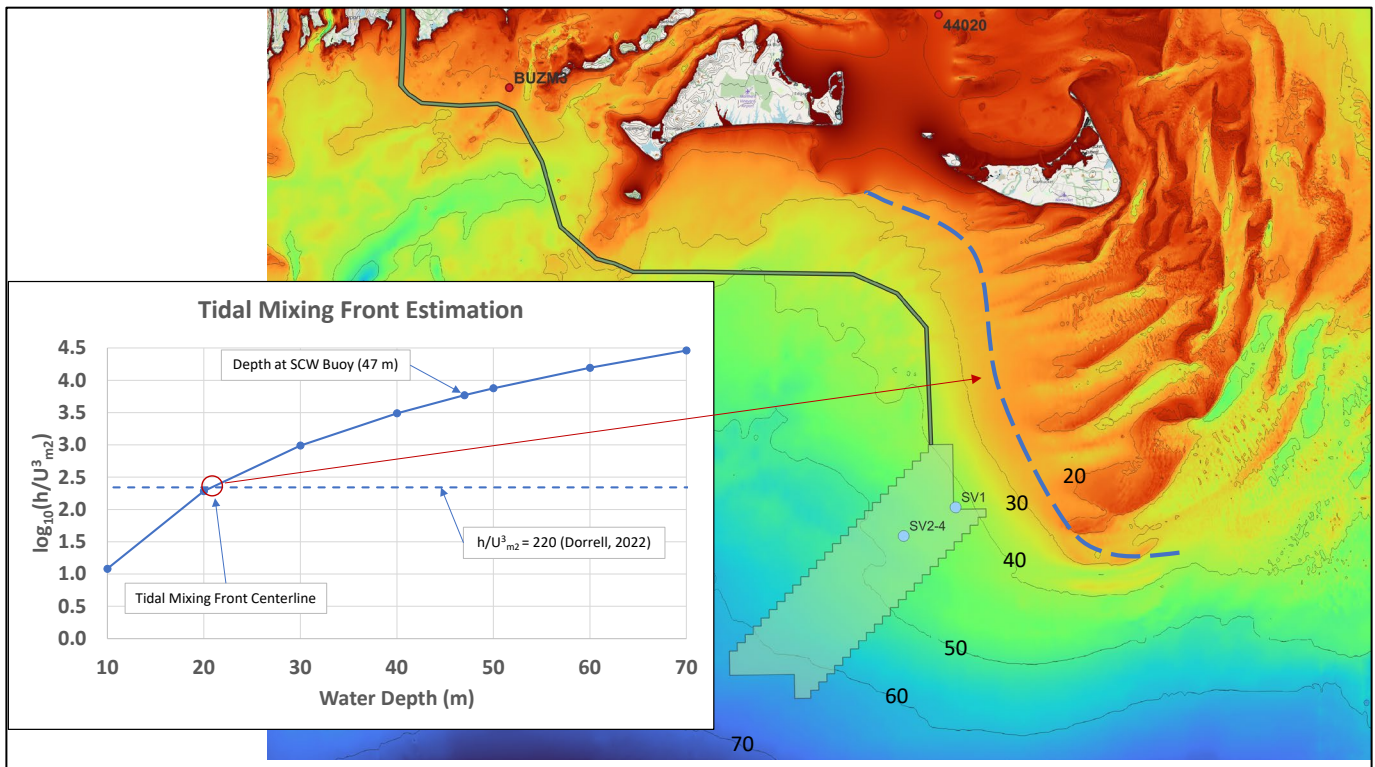


Figure 4-11. Tidal mixing front location estimation based on local bathymetry, SouthCoast Wind metocean buoy measured currents, IES model predicted currents and the mixing front relationship from Dorrell, 2022.



5 WIND TURBINE IMPACTS ON HYDRODYNAMICS

Various states in the European Union have been pursuing offshore wind energy for over two decades and performed numerous environmental studies in the process. Many of those studies have focused on the specific issues of concern in the present study. Van Berkel et.al. (2020) provide a high-level summary of the issues at hand and the recent state of studies in Europe. Their summary is presented in bullet form below.

Local

- Increased turbulence at and downstream of the foundation of the wind turbine
- Changes in the remobilization of sediments, or areas of erosions and accretion
- Increased water residence time inside the offshore wind farm due to reduced flow
- Increased vertical turbulent exchange of matter in stratified flow leading to downstream reduction in stratification
- Reduction in near-bottom salinity in estuarine systems
- Vertical redistribution of water temperatures
- Changes in nutrient upwelling and related primary productivity

Regional

- Losses in tidal energy and changes in tidal dynamics, [including the rotary tides seen in the vicinity of the Shoals (Embert, 1924)]
- Decreased stratification downstream of the offshore wind farm, with reduced bottom salinity in estuarine systems
- Wind wake effects leading to reduced wind stress and wave energy downwind of an OWF and upwelling/downwelling dipoles at the edge of the wake, leading to increased vertical exchange and nutrient supply to the euphotic zone
- Theoretical island effects (i.e., where turbine spacing is sufficiently close to create a cumulative effect) with mixing behind the offshore wind farm destratification and upwelling effects impacting on primary production (i.e., an effect seemingly negligible compared to wind-wake effects)

There are five basic areas that need to be understood to address the issues bulleted above and to quantify the potential for impacts from the wind farm on remote resources, i.e., Nantucket Shoals. The five areas include the local biology, the physical domain, the meteorological and oceanographic conditions present, the direct water column impacts from the turbine tower and the indirect water column impacts from the turbine wind wake effect.

For this study, the literature was reviewed to understand and appropriately evaluate the potential near field impacts of the offshore wind farm and whether they are sufficient to affect the Nantucket Shoals area. Once those impacts were better understood and quantified, the next step was to determine whether they are sufficient to reach another WTG location and therefore cumulate and whether they are strong enough to impact the hydrodynamics in the near field and ultimately in the Nantucket Shoals region generally.



5.1 NEAR FIELD TURBINE TOWER HYDRODYNAMIC WAKE EFFECTS

The impacts described in the upper bullet list are near field effects, in the immediate surroundings of the WTG. The literature is extensively populated with efforts to determine the best approach to quantifying the potential impacts to the water column of the two major near field impacts, wind wake and WTG tower subsurface wake.

Some data are available on the turbine near-field physical impacts, primarily through lab studies, (Miles et al., 2017; Carey, 1983). In the absence of in-situ data, one method for better understanding the potential for impacts from an offshore wind farm is through analytical and computer modelling. The first of the two main causes of potential impacts that a WTG might have on the local water column stratification and mixing in the near field is the direct influence of the subsurface portion of the WTG tower causing passing currents to flow around the obstruction (essentially flow around a cylinder) generating turbulence in its wake.

Flow around a vertical cylinder has been investigated extensively, with specific relevance to the flow and scour around pile foundations in marine and coastal engineering, and around bridge piers in river engineering. Offshore wind farms have a potential of tidal energy loss to turbulence in the range of 4% - 20% of the bottom friction energy loss (Carpenter et al., 2016). Observations show locally enhanced levels of turbulence in the wake of the cylinder (Grashorn and Stanev, 2016) and increased sediment erosion and turbidity in the water column as a result.

Monopile foundations can obstruct the flow and induce vertical and horizontal mixing in the water column and could impact the formation and maintenance of stratification in the water column (Dorrell, 2022; Rennau et al., 2012). Observations of flow properties in stratified water collected downstream of a bridge in Denmark found strong vertical mixing and internal wave generation close to the bridge pylons (Lass et al., 2008). Depending on the sizes of the wakes, Floeter et al. (2017) suggest there could be a joint blocking effect involving an entire offshore wind farm though little evidence exists for that conclusion.

An assessment of the tidal regime and stratification was made based on observations from the SouthCoast Wind metocean data set. Water depths from the two ends of the SouthCoast Wind Lease Area near field domain were selected to create a matrix of turbine tower impact calculations. Several model applications based on literature developments were evaluated and used to focus on the downstream impacts of the turbine tower to the water column, over the range of conditions, gauging the downstream extent and strength of the impacts for each of the cases.

Downstream Wake and Turbulence Excursion

Miles et al. (2017) performed a series of laboratory experiments to determine the downstream impacts of a vertical cylinder in the flow field, aimed at understanding this influence in the wake of the subsurface portion of offshore wind turbine towers. They noted that the flow behind a subsurface turbine tower is affected through the generation of vortices, or turbulence in the wake region, including lee wake vortices, horseshoe vortices and (vertical) counter-rotating vortices. The present study will focus on the lee wake vortices as they can be transported far downstream whereas the horseshoe and vertical vortices are primarily near field effects.

The results from Miles et al. experiments found that the velocity profile behind the turbine towers had recovered to within 5% of free stream values in an average of $8.3D$ and to full flow by approximately $11D$, where D is the tower diameter (Figure 5-1). For the maximum foundation diameters within the SouthCoast Wind Project Design Envelope of $D=16$ m, $11D$ downstream equates to $11 \times 16\text{m} = 176$ m. Miles et al. also found that turbulence

peaked at 1.5D behind the tower and decreased with distance downstream and approaches but did not return to within 5% of background within their observational domain of 15.5D. Recovery distance was also seen to be loosely related to the free stream speeds, decreasing with increasing speed.

Schultz et al. (2020) performed measurements in the wake of existing piles in the North Sea during the summers of 2015 and 2017. They found for the weakly stratified conditions in 2015, with a 0.5°C difference between the sea surface and the bottom mixed layer which reached to approximately 10 m depth in a shallow area of approximately 24 m depth, that with a mean current speed 0.3 m/s “...the disruption of background stratification by the wake is observed within a narrow region of up to 70 m width that reaches at least 300 m downstream of the monopile.” A vertical profile measured at approximately 500 m downstream showed a stronger temperature gradient than profiles closer to the monopile, indicating re-stratification. They confirmed this trend by comparing the North Sea results to data collected at the platform FINO3 where, within the wake of the monopile, stratification decreased by up to 35 % at 250 m, after which the strength of stratification increased again. For weak stratification Schultz et al. also found that wake behind the tower was reached up to 10D, consistent with Miles et al. observations. The ultimate disturbance of the vertical structure of the water column under weak stratification reached 450 m downstream, after which re-stratification of the wake region began, differentiating between downstream disturbance and the initial wake behind the tower. While they did not explicitly state the pile diameter, based on further analyses it is assumed that $D = 7$ m for their observations.

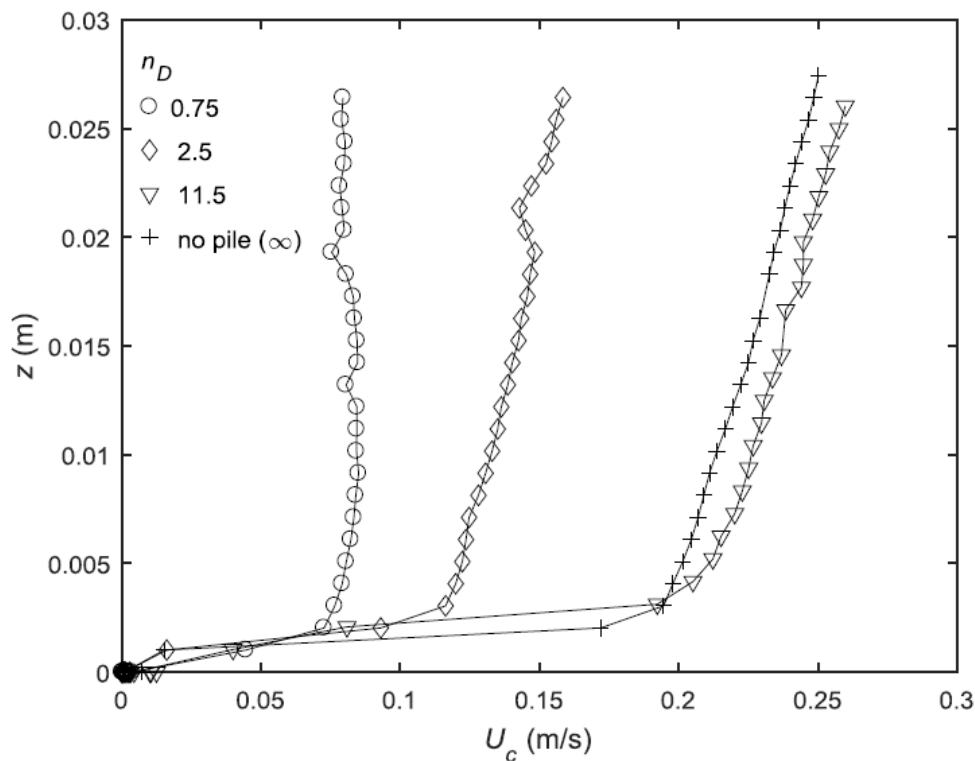


Figure 5-1. Velocity profiles measured at different distances downstream of the pile and with no pile. Distances are specified by the number of pile diameters downstream from the center of the pile (n_D) (Miles et al., 2017).



Using measurement results from 2017, Schultz et al. (2020) performed a similar study on an ocean that was now more strongly stratified; 2°C surface to bottom difference in a 27–30 m depth region and average current speeds of 0.3 m/s. Their measurements found no clear influence of the monopile at 400 m, or at 200 m downstream.

To better quantify the observations in the field Schultz et al. developed a Large Eddy Simulation (LES) model of the system observed. The resulting wakes were characterized by a narrow region of strong turbulence within the first 50–100 m downstream, (7–14 monopile diameters) and dissipation of turbulent kinetic energy an order of magnitude greater than background, which dissipated within 300 m (42D) past the monopile, after which dissipation becomes comparable to background levels.

While the field observations and model simulations found that the impacts are identifiable hundreds of meters downstream, they are strongly dependent on stratification and dissipation. Observations and modeling showed that the thermal stratification is strongly affected under weak stratification (upper to lower water column density difference) ($\Delta T \sim 0.5^\circ\text{C}$); under stronger stratification ($\Delta T \sim 1.5^\circ\text{C}$) the impacts are less pronounced and temperature anomalies could be masked by other mixing mechanisms or variability. In addition, the greater the temperature gradient, the stronger the forcing toward the stabilization of the wake, limiting the range of influence of the wake downstream. It should be noted that the temperature difference in the stratified summer conditions off the coast of southern New England build to $>10^\circ\text{C}$, roughly 10 times the stratification strength of the North Sea conditions. The implication here is that the force for re-stratification would similarly be on the order of a magnitude greater as well.

An analysis of the downstream tower wake was performed by Dorrell et al. (2022) to assess the potential for direct mixing of a stratified water column with the installation of wind turbines. In their analysis they review wake effect literature for both stratified and unstratified conditions citing the Reynolds number dependence of the wake development. The references with downstream wake lengths of $x/D > 50$ were for relatively low Reynolds numbers (i.e. $Re_D = 300\text{--}2,000$ to 1×10^5 for a typical North Sea example). The SouthCoast Wind environmental conditions and WTG tower diameter give a Reynolds number of 3.36×10^6 , (see eqn. 6.2 below) an order of magnitude larger and well above the laminar to turbulent transition in the cylinder boundary layer, altering the downstream wake formation (Lienhard, 1966).

As an example of turbulent mixing zone downstream excursion, mixing zone lengths as reported above for 11D (Miles et al., 2017) and a far wake distance of 50D (Dorrell et al., 2022) are presented visually for the SouthCoast Wind specifications. For a 16 m diameter tower the 11D and 50D mixing zone lengths for the two cases are 176 and 800 m, respectively which can be seen graphically in Figure 5-2. Another interesting exercise is to compare the noted potential wake excursions of 176 m and 800 m to the PVD in Figure 4-4, where it can be determined that both lengths lie within the first hour (between the first two orange dots).

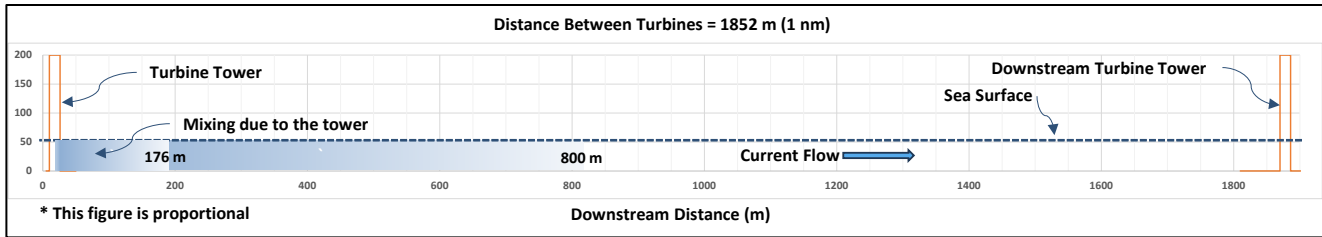


Figure 5-2. Schematic of the potential downstream hydrodynamic effects of WTG tower (16 m diameter) and 1 nm (1852 m) WTG spacing is shown. Two potential mixing lengths are shown for the 11D and 50D cases, equating to 176 m and 800 m, respectively.

Stratification and Mixing

As shown in the SouthCoast Wind buoy data analysis in Section 4, each summer the region to the west of Nantucket Shoals stratifies due to rising temperatures in the water surface layer from heat generated by solar radiation and rising air temperatures (see Figure 4-8). The temperature difference between the surface and bottom can rise to $>10^{\circ}\text{C}$. This seasonal stratification cycle with development in the spring and destruction in the fall affects the region's productivity. During the stratified months, mixing of the surface water affects the strength of the stratification in terms of temperature difference, thickness of the warmer surface layer, and the depth of the transition zone between the surface and bottom layers. Surface wind mixing increases the average temperature and thickness of the surface layer in the heating months. Tidal currents tend to disturb the interface of the upper and lower layers increasing the thickness of the thermocline, the area of dramatic temperature change, without breaking the stratification. It has been postulated that the introduction of WTG towers in the water column could increase the mixing enough to throw off the existing balance and potentially destroy the thermocline, a schematic of which is presented in Figure 5-3.

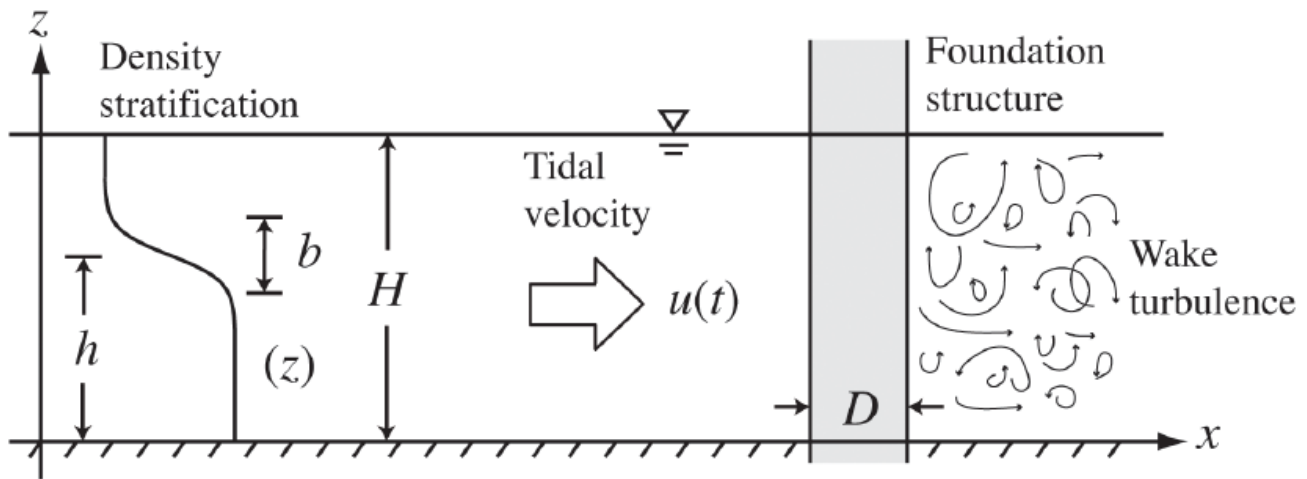


Figure 5-3. Basic sketch of the idealized setup considered. A typical density profile is illustrated where stratification (i.e., change in $\rho(z)$) is confined to a pycnocline layer with thickness, b , at height, h , from the seabed. Only a single foundation structure is shown in the sketch (Carpenter et.al. 2016).

To address this question Carpenter et al. (2016) first looked at the drag on the water column exerted by the tower (a cylinder in a cross flow) subject to the local tidal currents:

$$F = -\frac{1}{2}\rho_0 C_D A |u|u \quad (5.1)$$

where ρ_0 is the seawater density, C_D is the drag coefficient, A is the tower cylinder frontal area and u is the free stream velocity.

To understand the potential for the towers to impact the flow and stratification in local seas, we will look at a matrix of cases spanning the depths of the SouthCoast Wind Lease Area ($H = 40 - 60$ m), free stream velocities and a range of the drag coefficient. Noting that C_D has been found to be a function of the Reynolds number, roughness and the cylinder length (see also F.M. White, 1979) Carpenter used a range of C_D from 0.35 to 1.0 which is in line with the high Reynolds number expected in the SouthCoast Wind Lease Area,

$$Re_D = \frac{\bar{u} D}{\nu} = 3.358 \times 10^6 \quad (5.2)$$

where $\bar{u} = 0.25$ m/s, $D = 16$ m and $\nu = 1.19135 \times 10^{-6}$ m²/s for seawater at an average salinity of 32.5 PSU and temperature of 15C as recorded at the SouthCoast Wind metocean buoy during the stratified months of 2020 and 2021. The drag experienced in the water column can be converted to power removal for the individual towers as:

$$Power\ removed = -\frac{1}{2}\rho_0 C_D A \langle |u^3| \rangle \quad (5.3)$$

Carpenter then used the specifics of the wind farm layout to develop a power removal per unit area which could then be summed over the entire wind farm:

$$P_{str} = \frac{\rho_0 C_D A \langle |u^3| \rangle}{2l^2} = 0.0015\ to\ 0.0022 \frac{W}{m^2} \quad (5.4)$$

where l is the distance between the individual turbines and the $\langle |u^3| \rangle$ is the cube of the average currents over a time period much longer than the dominant tidal period and $A = D \times H = 640 - 960$ m². This power extracted by the tower structures of the wind farm can then be equated to the power introduced into the generation of turbulence, used to determine mixing rates. To evaluating P_{str} we use the distance between turbines of 1 nm (1852 m). Finally, to understand the relative strength of the tower induced mixing in relation the bottom friction induced mixing the power extracted by the bottom can be calculated as:

$$P_{bot} = \rho_0 C_{Dbot} |u^3| \quad (5.5)$$

The bottom drag coefficient C_{Dbot} is basically a function of the bottom roughness and is usually in the range of $2 - 4 \times 10^{-3}$ (Kowalik, 1993) and was taken to be $\sim 2.5 \times 10^{-3}$ by Carpenter et.al. The power extracted by the turbine towers can be related to the bottom drag power extraction by taking the ratio of the two which yields:

$$\frac{P_{str}}{P_{bot}} = \frac{C_D A}{2C_{Dbot} l^2} \quad (5.6)$$

It is instructive to look at the several components of the ratio, in particular the difference between the area of the turbine towers and the wind farm bottom area, i.e. A/l^2 , which for SouthCoast Wind is between $1.8 \times 10^{-4} - 2.8 \times 10^{-4}$, which indicates just how small an area the turbine towers cover when compared to the bottom area

surrounding them. These numbers are also an order of magnitude less than the ratio provided in the analysis performed by Carpenter et al. (2016) for two North Sea wind farms.

Table 5 presents the results of the comparison for the range of coefficients and depths associated with the SouthCoast Wind Lease Area. It can be seen from the table that the maximum power extracted by the WTG towers is only 6% of that extracted by the bottom drag.

Table 5. Relationship between power extracted by the wind turbine towers and that extracted by the bottom mixing.

u (m/s)	Tower Diam. (m)	Depth (m)	l (m)	C_D	C_{Dbot}	ρ_0 (kg/m ³)	P_{str} (Wm ²)	P_{bot} (W/m ²)	P_{str} / P_{bot}
0.25	16	40	1852	0.35	0.0025	1025	0.000523	0.040039	1%
0.25	16	60	1852	0.35	0.0025	1025	0.000784	0.040039	2%
0.25	16	40	1852	1	0.0025	1025	0.001494	0.040039	4%
0.25	16	60	1852	1	0.0025	1025	0.002241	0.040039	6%

With an understanding of the power extracted from the water column due to the presence of the WTG towers, we can now evaluate what impact that will have on the summer stratification. The basic premise centers on the transformation of energy taken from tidal currents into turbulence in the water column. This energy is dissipated through two primary mechanisms: internal friction (viscous dissipation) and mixing of the different layers of the water column (i.e., the stratification).

To get an understanding of the stratification present, an analysis of the buoy data for the stratified period of July and August 2020 was performed. The range of thermal stratification during that period is from a 25th percentile of 9.24 °C, a 50th percentile of 10.97 °C and a 75th percentile of 11.81 °C, (see also Figure 4-8).

Carpenter et al. provide a set of simplified estimates for the mixing process using various methods. The primary objective is to determine specific time scales related to the stratification of the water column. These time scales are used to compare how long it takes for the water to return to its natural state after seasonal stratification and to assess how long water remains within an offshore wind farm. These estimates assume that no other turbulent mixing processes are occurring simultaneously.

An equation for a measure of the potential energy of the water column, $\varphi(t)$, called the stratification parameter can be written as,

$$\varphi(t) = \int_0^H [\rho_{mix} - \rho(z, t)]gz dz \tag{5.7}$$

where ρ_{mix} is the density if the entire water column were completely mixed and φ really represents the amount of energy required to mix the water column.

No information on the vertical profile of the temperature in the water column was collected at the SouthCoast Wind metocean buoy past the surface and bottom temperature time series so the historical data presented in Section 2 was used to develop a vertical profile of temperature. Referring to Figure 2-4 and Figure 2-5 for the observed vertical temperature during the summer months of July and August there is a surface warm layer of

about 5 - 10 m, a thermocline between 5 – 10 m thick and a lower cool layer to the bottom with a surface to bottom temperature delta of about 10 °C. Coordinating that with the observed temperatures at the SouthCoast Wind metocean buoy a vertical profile of the temperature was developed. Based on the nearly constant observed salinity average of 32.5 PSU an effective density profile was estimated and the stratification parameter calculated.

The connection between stratification and turbulence can be developed through a conservation equation for the kinetic energy of turbulence. This equation, often referred to as the "local equilibrium hypothesis", can be written as:

$$P + B - \varepsilon = 0 \tag{5.8}$$

where the three factors are (i) the production of turbulent kinetic energy (P), (ii) the work done by this energy on the buoyancy field, which relates to the mixing of the stratification (B), and (iii) the energy loss due to viscous dissipation (frictional losses, ε). In this general equation, the production term (P) can have multiple contributions, where for this study it is from the turbulence generated by the towers. Specifically, $P = P_{str}/(\rho_{mix}H)$, which is considered constant over time and independent of z. Using this basic equation, Carpenter et.al. describe three idealized mixing models (i.e., parameterizations) of increasing complexity in order to estimate a characteristic residence time for the stratification, τ_{mix} .

They begin by forming an equation for the time dependent evolution of the mean density profile and develop an equation for the evolution of stratification parameter through solution with the stratification parameter definition (eqn. 6.7), and using the vertical buoyancy flux due to turbulent mixing acting on the density field solve for the rate of decrease in the stratification due to mixing,

$$\frac{d\varphi}{dt} = -R_f \frac{b}{H} P_{str} \tag{5.9}$$

where b is the stratification thickness and R_f is the flux Richardson number defined as $R_f \equiv B/P = 0.17$ as a constant often used in oceanographic studies. The rate of change in the stratification parameter is then used to estimate the residence time of stratification,

$$\tau = \frac{\varphi}{d\varphi/dt} \Rightarrow \tau_{mix} = \frac{\varphi_{max}H}{R_f P_{str} b} \tag{5.10}$$

The details of this derivation can be found in Carpenter et al. (2016). The equation for τ_{mix} is Model 1, which assumes a constant thermocline thickness (b). Inserting the parameters given in Table 6.1 and assuming a constant stratification thickness of 10 m to 20 m based on the observations discussed above, results for the time to mix the stratification range from a high of 1941 days to a low of 340 days. Clearly these times are much longer than the annual stratification time period.

The results given can be considered as a lower bound on the mixing time (slowest) in that they are based on a constant thermocline (b) thickness that does not change in time. As an upper bound (fastest), a thermocline thickness equal to the depth (b = H) can be evaluated giving 485 and 113 days for cases described above, respectively. The results are presented in **Table 6** below.

Table 6. Mixing time estimate for the constant thermocline thickness model

Depth (m)	C _D	P _{str} (Wm ²)	b = constant		b = constant = H	
			b (m)	τ _{mix} (days)	b (m)	τ _{mix} (days)
40	0.35	0.000523	10	1941	40	485
60	0.35	0.000784	10	1941	60	323
40	1	0.001494	10	679	40	170
60	1	0.002241	10	679	60	113
40	0.35	0.000523	15	1294	40	485
60	0.35	0.000784	15	1294	60	323
40	1	0.001494	15	453	40	170
60	1	0.002241	15	453	60	113
40	0.35	0.000523	20	970	40	485
60	0.35	0.000784	20	970	60	323
40	1	0.001494	20	340	40	170
60	1	0.002241	20	340	60	113

It should be noted that in the first set of τ_{mix} calculations (b=const.) the number of days is depth independent, as a result of the depth appearing both in the numerator and in the P_{str} term in the denominator of eqn. 6.10.

Similarly, in the second set (b = H) the calculation of τ_{mix} is independent of the thermocline thickness but depth dependent which makes sense based on the assumptions.

Carpenter et al. present a second model containing a time varying thermocline thickness, where they equate the rate of change of φ in Eq (6.9) with the amount of power that is put into mixing to derive a relationship for the (constant) rate of increase in interface thickness.

$$\frac{db}{dt} = \frac{2\pi R_f P_{str}}{g\Delta\rho H} \tag{5.11}$$

The value for Δρ can be obtained from the SouthCoast Wind metocean buoy. Using the average observed salinity S = 32.5 PSU, a surface temperature of 20 °C and a bottom temperature of 10 °C yield densities of 1022.89 and 1024.98 kg/m³ for the surface and bottom, respectively and a Δρ = 2.092 kg/m³.

The results for the same set of inputs used in the prior analyses show that the rate of change of the interface thickness is dependent on the friction factor, with the higher rate under the high turbulence case of 0.17 m/day and 0.06 m/day for the low turbulence case. Using those numbers, the time to mix the given thermocline thickness to the full water depth can be estimated as shown in **Table 7**.

Based on the forgoing analyses it appears that there are no circumstances under which there is enough turbulent energy input to the water column from currents flowing past the turbine towers to mix and collapse the stratification before the cooling weather causes the annual thermal stratification collapse beginning in October. Although the turbine tower does cause some mixing of the water column, even with the more conservative assumptions, that mixing is not enough to significantly impact the stratification.

Table 7. Mixing time estimates for the variable thermocline thickness model

Depth (m)	C_D	P_{str} (Wm ²)	b (m)	db/dt (m/day)	τ_{mix} (days)
40	0.35	0.000523	10	0.06	510
60	0.35	0.000784	10	0.06	850
40	1	0.001494	10	0.17	179
60	1	0.002241	10	0.17	298
40	0.35	0.000523	15	0.06	425
60	0.35	0.000784	15	0.06	765
40	1	0.001494	15	0.17	149
60	1	0.002241	15	0.17	268
40	0.35	0.000523	20	0.06	340
60	0.35	0.000784	20	0.06	680
40	1	0.001494	20	0.17	119
60	1	0.002241	20	0.17	238

5.2 NEAR FIELD/FAR FIELD TURBINE ATMOSPHERIC WAKE EFFECTS

The second potential impact is the turbulence created in the wake of the spinning WTG blades (wake effect) and the potential for it to alter (likely decrease) the stress on the water surface and thereby decrease turbulence and mixing in the water column generated at the surface. Such wakes can extend 5–20 km in the downwind direction, depending on weather conditions (Wu et al., 2023; Christiansen and Hasager, 2005). There are several types of wake effect models using varying levels of complexity from simple analytical studies to 3D CFD (computational fluid dynamics) modeling (Johnson et al., 2021; Porté-Agel et al., 2020).

The primary focus of many of the wake models has been on the speed deficit at downwind turbines and the potential impacts on power production. More recently the impacts on the wind stress on the ocean surface has become a focus due to potential impacts on wind mixing of the water column, as in the present study. The wake effect impacts effort will focus on determining the change in wind stress at the ocean surface downwind of the WTG(s), the magnitude of that change (deficit) and the impact that might have on the vertical mixing in the water column. It will be assumed that the WTG height above sea level is similar for all turbines in the Lease Area and not affected by the bathymetry.

To evaluate wake effects or develop wake models, it is important to study how the wake develops with distance. Xi and Archer (2020) developed a new large eddy simulation (LES) code, the wind turbine and turbulence simulator (WiTTS) to predict profiles of the time-averaged mean velocity downwind of a WTG and compared them to the observations of Chamorro and Porté-Agel (2010). Their comparison is shown in Figure 5-4 for various downwind locations measured in terms of the rotor diameter (x/D).

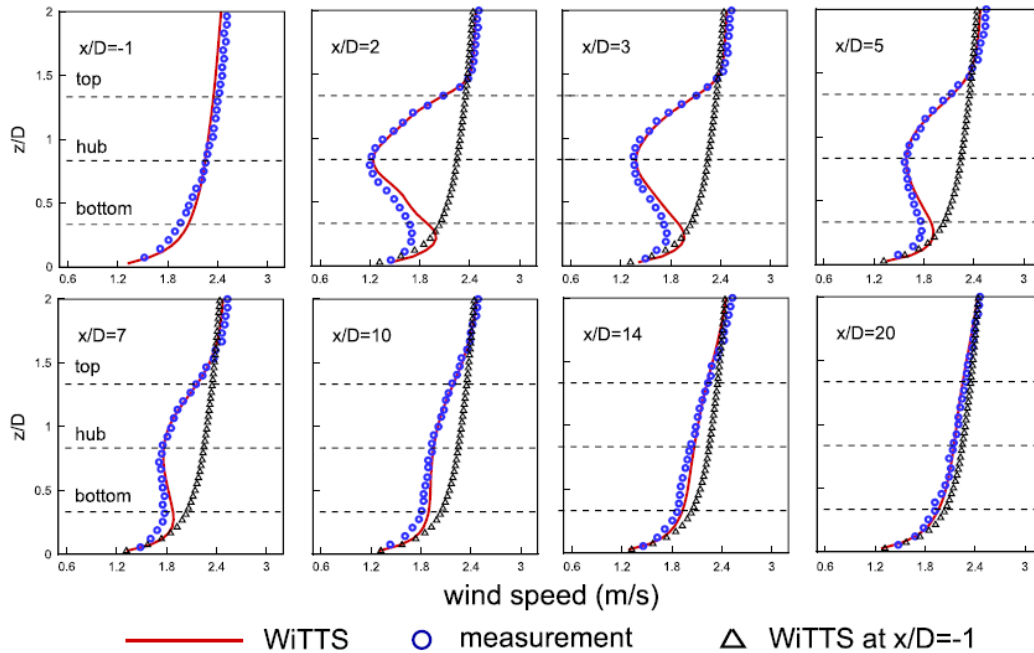


Figure 5-4. Comparison of profiles of time-averaged mean velocity at several downstream distances (x/Ds) on the vertical central plane (Xie and Archer, 2015).

The analysis shows that the velocity profile almost recovers back to its upstream speed ($x/D = -1$) after 20D downstream. Xi and Archer used the model to investigate a common assumption of self-similarity and axisymmetric behavior in the wake under neutral conditions, considering a range of wind speeds and turbine properties, finding that wind velocity deficit is generally self-similar to a Gaussian distribution in the horizontal plane; however in the vertical direction, that breaks down closer to the ground, which they attribute to factors like wind shear and interaction with the ground.

In studying wake effects, evaluation of $\delta U_{max}(x)$ is critical, and different relationships are used in different wake models. The widely used Jensen’s model (Jensen, 1983) assumes a top-hat function such that $\delta U_{max}(x/D) = \delta U(x/D)$ is constant inside the wake at $x = D$, based on a linear expansion of the wake. With similar assumptions of a top-hat profile and linear expansion of the wake, Frandsen et al. (2006) proposed an analytical model using momentum conservation in the wake, which ends up as a circular cross section. More recently Bastankhah and Porté-Agel (2014) proposed a new analytical model from the conservation of mass and momentum with the self-similarity property using a uniform Gaussian distribution of the velocity deficit based on LES results. By using the Gaussian distribution, the velocity deficit at any position $\delta U(x, y, z)$ can be found though it still underestimates the magnitude and overestimates the rate of decrease of the deficit with distance in the far wake.

Xie and Archer (2015) proposed a modification to take the anisotropic wake expansion into account. Instead of using the same σ in all directions, an elliptical Gaussian function corresponding to $\sigma_y \neq \sigma_z$ can be used in the following relationship,

$$\delta(x, y, z) = \delta_{hub}(x) \exp \left\{ - \left[\frac{(z - H)^2}{2\sigma_z^2} + \frac{y^2}{2\sigma_y^2} \right] \right\} \quad (5.12)$$



where the wind speed downwind of the WTG is $U(x, y, z) = U_{\infty}[1 - \delta(x, y, z)]$. The hub height speed deficit is determined from,

$$\delta_{hub}(x) = 1 - \sqrt{1 - \frac{C_T}{8 \frac{\sigma_y \sigma_z}{D^2}}} \quad (5.13)$$

where they used simple linear estimates of σ_y and σ_z ,

$$\frac{\sigma_y(x)}{D} = k_y \frac{x}{D} + \varepsilon, \quad \frac{\sigma_z(x)}{D} = k_z \frac{x}{D} + \varepsilon \quad (5.14)$$

where $k_y = 0.025$ and $k_z = 0.0175$ are expansion rates of the wake in the horizontal and vertical directions, respectively, $\varepsilon = 0.25\sqrt{\beta}$, $\beta = 0.5(1 + \sqrt{1 - C_T}) / \sqrt{1 - C_T}$, and $C_T = C_T(U_{in})$, is the thrust coefficient where U_{in} is the (incoming) hub-height wind speed experienced by the turbine.

The Xie and Archer (2015) model equations 5.12 through 5.14 were used to evaluate the downwind wind speed deficit based on the SouthCoast Wind WTG design parameters for the maximum and minimum range of two hub heights and two rotor diameters. The WTG design parameters as presented in **Table 8** are from the SouthCoast Wind COP (2022).

The minimum and maximum WTG heights and rotor diameters were used to bracket the potential impacts of the WTG wake effect downwind. In the following analyses rotor diameters of $D = 220$ m and 280 m, with hub heights of $H = 128$ m and 184 m, respectively, were used. Through the evaluation of Eqns. 5-13 and 5-14 the downwind speed deficit can be predicted for the two WTG cases, which are plotted in Figure 5-5. The figure presents the hub height wind speed deficit as a function of the distance downwind of the WTG. The locations of subsequent downwind WTGs are also presented for the first 5 WTGs, after which the speed deficit returns to the upwind value ($\sim <5\%$). Reviewing the figure, it can be seen that the larger rotor diameter develops a slightly larger downwind speed deficit at hub height, but the curves essentially converge down wind.

Table 8. WTG Design Parameters Used in the wake effect modeling (SouthCoast Wind COP, 2022).

	Minimum (ft)	Minimum (m)	Maximum (ft)	Maximum (m)
Rotor diameter	721.7	220	918.6	280
Rotor swept area (m ² / ft ²)	409,168.50	38,013.00	662,787.80	61,575.00
Blade length	351	107	452.8	138
Tip height above MLLW	779.5	237.6	1,066.30	325
Hub height above MLLW	418.7	127.6	605.1	184.4
Tip clearance (air gap) above highest astronomical tide	53.8	16.4	n/a	n/a

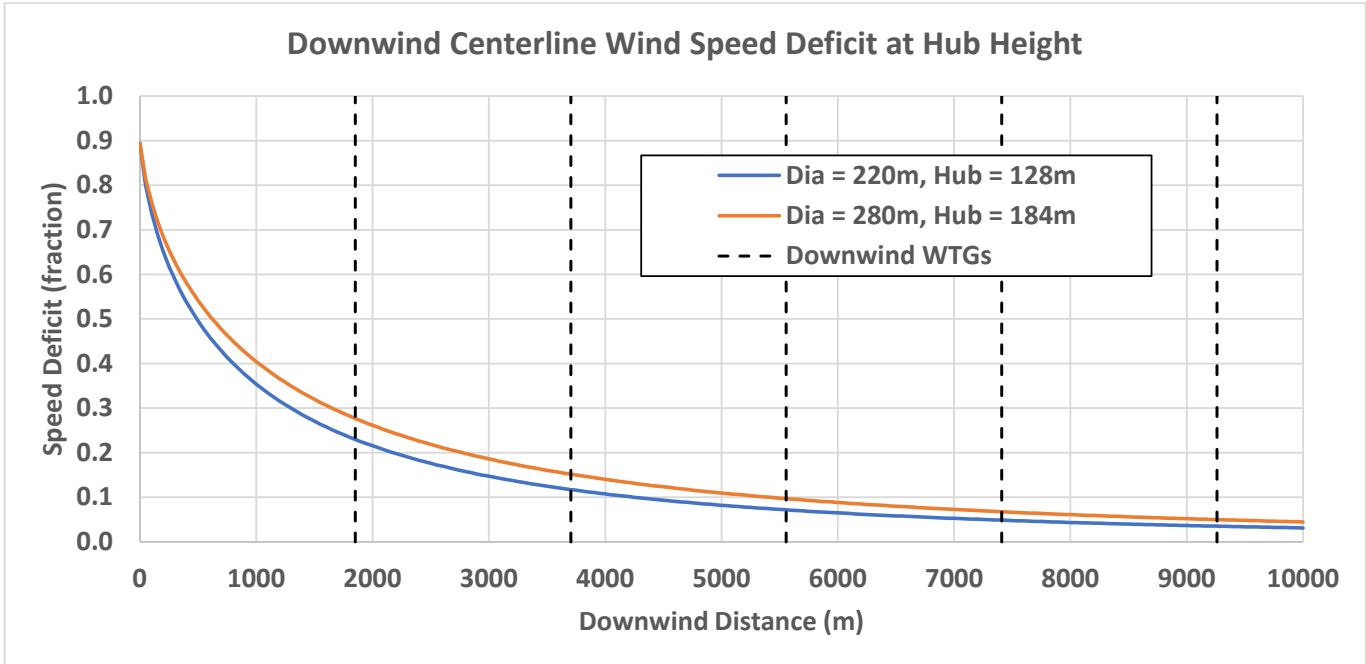


Figure 5-5. Comparison of the hub height downwind speed deficit predictions for the minimum and maximum SouthCoast Wind WTG design parameters.

The following three figures present the downwind wake predictions for the two cases, in terms of the 1) the cross-wind wake at the wake producing WTG and 2,000 m downwind (Figure 5-6), 2) the centerline wake from the WTG to 2,000 m downwind (Figure 5-7) and 3) the cross-wake water surface wake effect from the WTG to 2,000 m downwind (Figure 5-8). The color-coded contours are at 0.05 deficit intervals from 0 to 1.

Figure 5-6 through Figure 5-8 show the shape and length of the downwind wake effect and the difference between the two WTG cases. It is clear from cross-wind (Figure 5-9) and centerline (Figure 5-10) wake plots that that the area impacted the greatest is at hub height just behind the WTG whereafter the wake spreads and diffuses downwind, and that the impact is larger for the D=280 m case as would be expected. The centerline wake plots indicates that there is some interaction with the sea surface, which is shown to be fairly small in the sea surface plots (Figure 5-8). For the D=220 m case the sea surface experiences a small area of 15% deficit, a 10% deficit that extends to the 2,000 m mark and a larger 5% deficit area extending over approximately 1/3 of the domain. The D=280 m case shows only a very small 10% deficit area but a slightly larger 5% deficit area coverage.

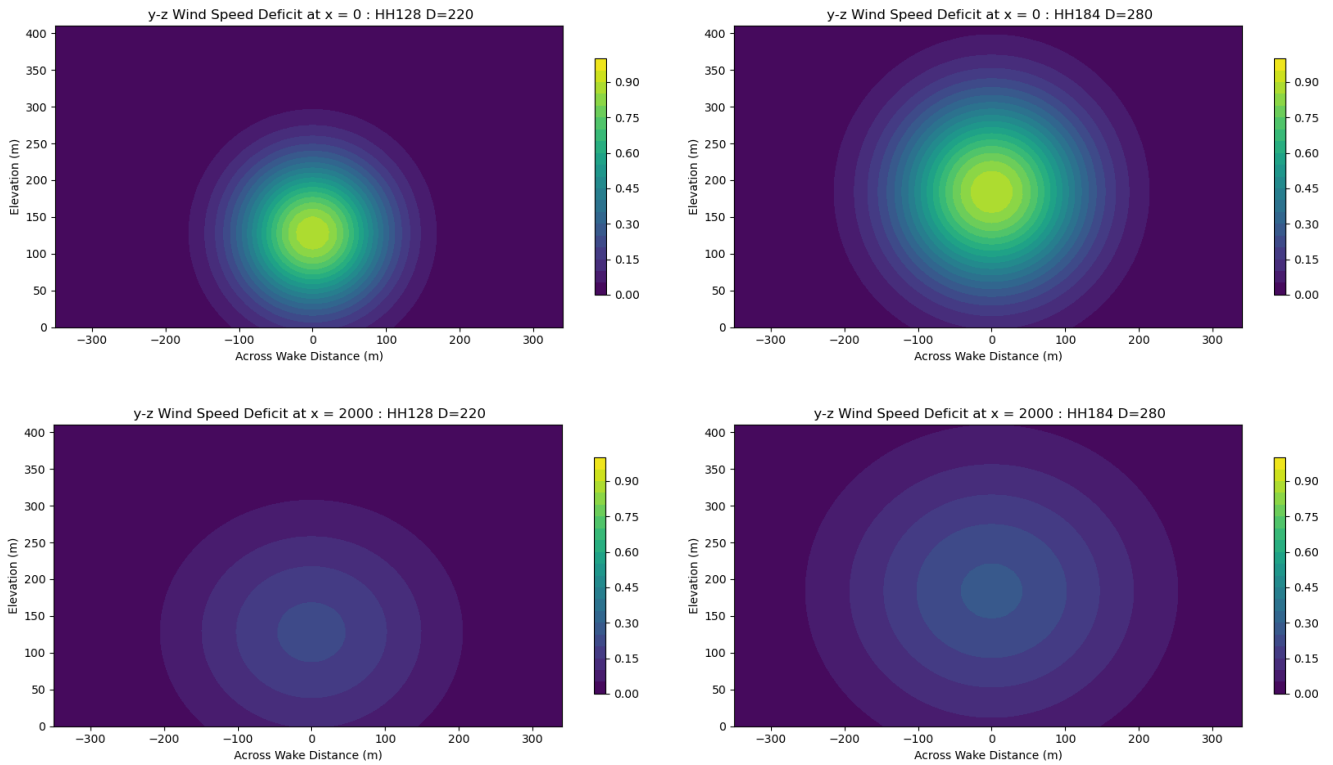


Figure 5-6. Cross-wind wake wind speed deficit at $x=0$ (upper) and $x=2,000$ m (lower) for $D=220$ m (left) and $D=280$ m (right). The color bar indicates the fraction of deficit from an undisturbed field where yellow colors indicate high deficit and blue colors indicate low deficit.

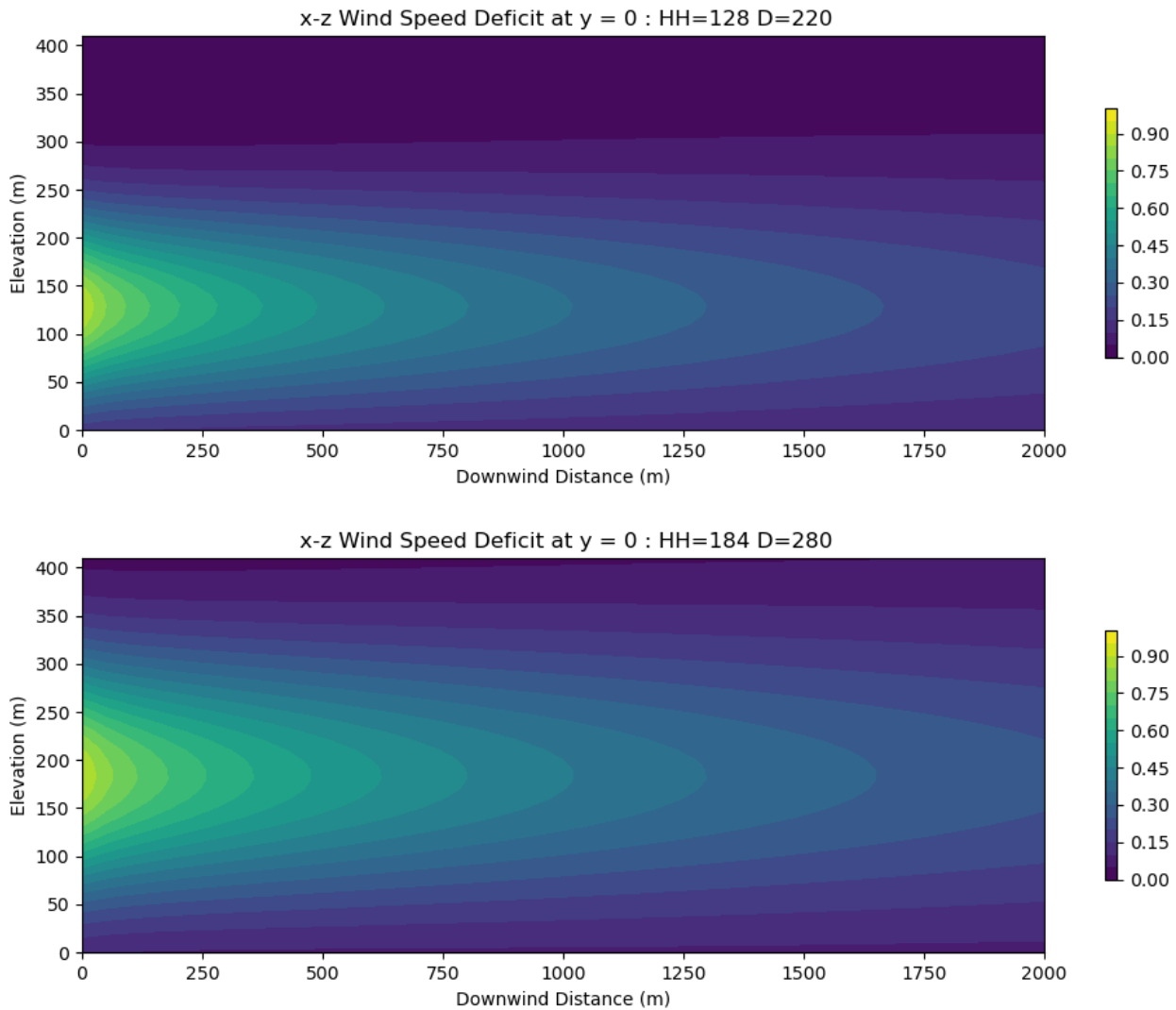


Figure 5-7. Downwind centerline wake wind speed deficit for the D=220 m (upper) and D=280 m (lower) cases. The color bar indicates the fraction of deficit from an undisturbed field where yellow colors indicate high deficit and blue colors indicate low deficit.

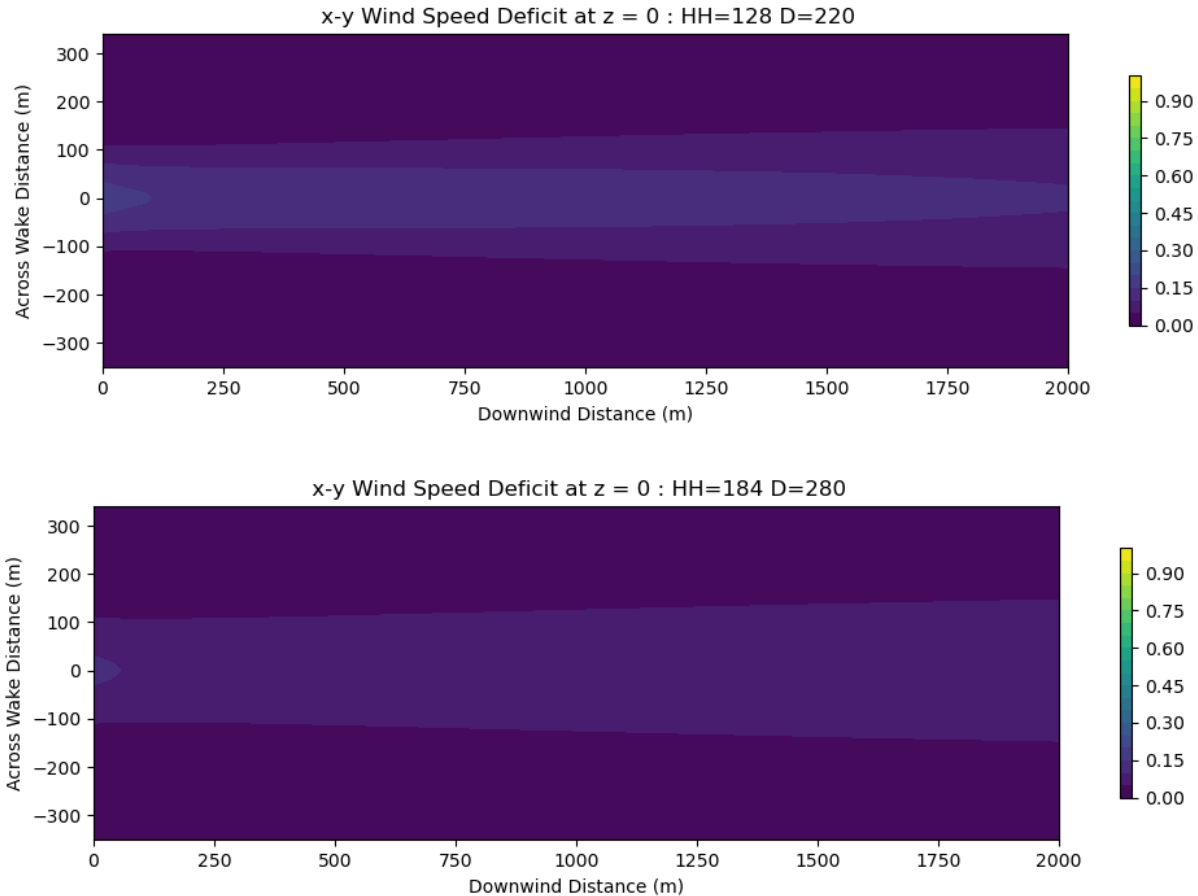


Figure 5-8. Sea surface wake effect wind speed deficit for the D=220 m (upper) and D=280 m (lower) cases. The color bar indicates the fraction of deficit from an undisturbed field where yellow colors indicate high deficit and blue colors indicate low deficit.

To better quantify the surface impacts Equation 5-12 is then evaluated to determine wind speed deficit $\delta(x, y, z)$ including the sea surface deficit. The surface deficit as a function of downwind distance is shown in Figure 5-9 along with the locations of the first 5 subsequent downwind WTGs, assuming that they are directly downwind for this comparison. At the sea surface, in opposition to the hub height speed deficit, the smaller rotor at the lower hub height presents the larger deficit, which again basically converges downwind with a slightly larger deficit from the larger rotor in the far wake.

Cross wake views of the speed deficits at the 1st and the 4th downwind WTGs are presented in Figure 5-10. There is a Gaussian distribution to the speed deficit that expands and decreases in magnitude downwind, staying within approximately 400 m of the WTG centerline. The sea surface deficit at the 4th WTG can be seen to be less than 5% for both cases. It can be seen that for the D=220 m case the 5% threshold is crossed at approximately 6,050 m and that the D=280 m case that threshold is 7,100 m.

While these wake edges are indicative of the major wake effects, based on their modeling of wind farms in the mid-Atlantic Bight, Golbazi et.al. suggest that minor wake effects, at the limit of measurement accuracy (~ 0.5 m/s)



can be used to track wake edges downwind to 50 km. In the SouthCoast Wind Lease Area the prevailing wind direction is south-southwest in the summer (i.e. blowing towards the north-northeast), therefore towards Nantucket Shoals. They also found however that wake at the surface causes at most a 0.5 m s⁻¹ reduction (~10 % reduction) in average wind speed within the wind farm areas modeled.

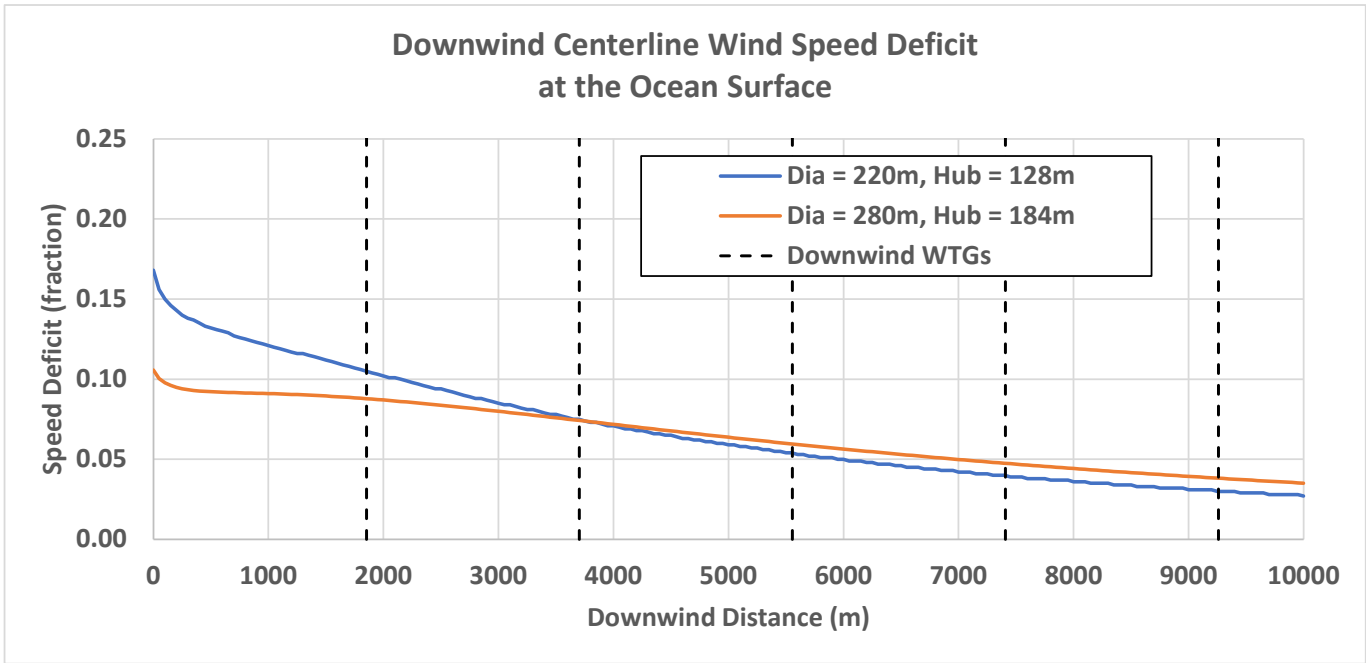


Figure 5-9. Comparison of the sea surface downwind speed deficit predictions for the minimum and maximum SouthCoast Wind WTG design parameters.

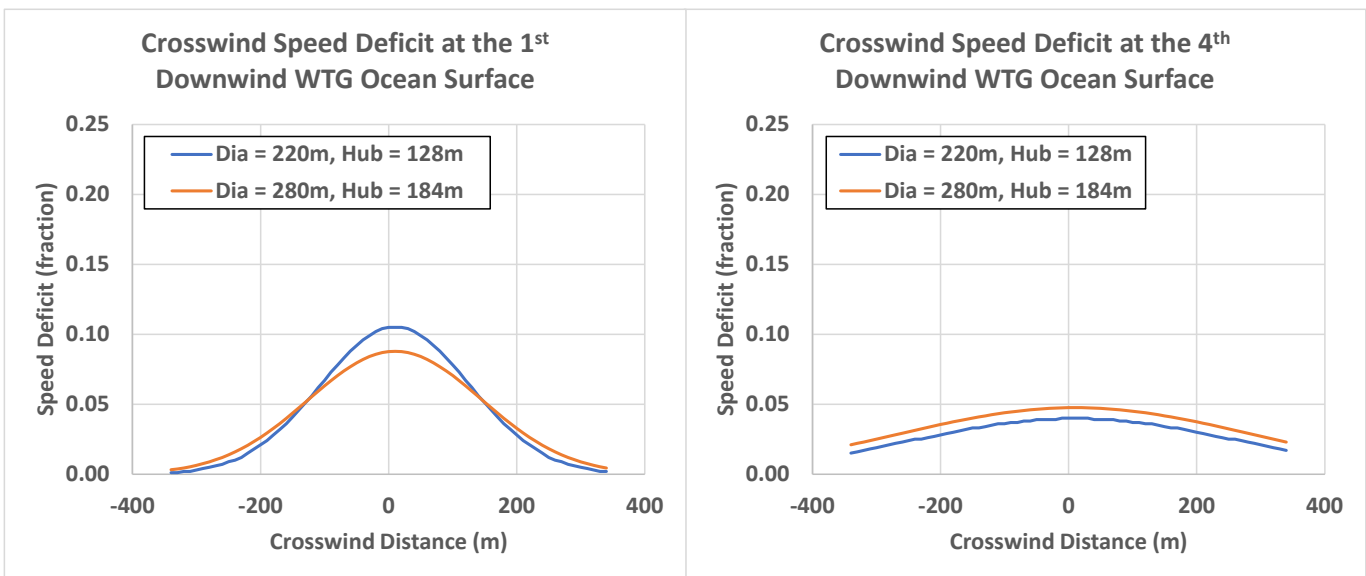


Figure 5-10. Comparison of the sea surface cross wake speed deficit predictions for the minimum and maximum SouthCoast Wind WTG design parameters at the 1st and 4th WTG locations.



From the model predictions the sea surface area coverage for a deficit > 10% and for > 5% was calculated and an estimate made of the percent of the total wind farm area coverage based on individual WTGs and the 1 nm (1852 m) separation between them. The results are presented in **Table 9** and **Table 10** below.

Table 9. WTG layout parameters (SouthCoast Wind COP, 2023).

WTG Spacing	1852 m	1.852 km (1 nm)
WTG Area	3,429,904 m ²	3.43 km ² (1 nm ²)
Number of WTGs	Up to 147	504 km ² (147 nm ²)

Table 10. Estimated area coverage by wind speed deficit at the sea surface for the two cases.

	Deficit Area per WTG (km)	Total Deficit Area for All WTGs (km)	Percent of Total WTG Coverage
D = 220 m			
Deficit > 5%	1.475	217	43%
Deficit > 10%	0.227	33.3	6.6%
D = 280 m			
Deficit > 5%	1.878	276	55%
Deficit > 10%	0.003	0.441	0.1%

The estimates presented in **Table 9** and **Table 10** are for the area coverage for the non-dimensional wind speed deficit fractions predicted at the sea surface. The actual wind speed deficit is free stream speed dependent so it is presented in **Table 11** for the 25th, 50th and 75th percentiles.

The wind speed deficits at the sea surface match well with those calculated by Golbazi et.al. (2022) who also found that the wake edge roughly corresponded to the 0.5 m/s deficit for model scenarios of wind farm in the mid-Atlantic Bight. Golbazi et.al.’s findings are presented in Figure 5-11.

Friction velocity (u_*) is directly related to surface stress (proportional to the square of the wind speed) at the sea surface decreases, which reduces air-sea friction so u_* is also reduced. Turbulence kinetic energy (TKE) is reduced at the sea surface as well in proportion to u_*^2 . Estimates of the reduction in TKE in the surface wake effect are presented in Table 5.7 for the two cases at the three wind speed percentiles as well. For the larger wind speed deficit > 5% area coverage a TKE deficit of ~13.5% is estimated which aligns very well with the Golbazi et.al findings of ~13%. Though for the deficits > 10% the TKE deficits are considerably larger, in reviewing Table 5.6 it can be seen that the area coverage of the deficits > 10% is a tiny fraction of the > 5% deficit coverage, for the D=280 m case in particular.

Table 11. Estimated wind speed deficit at the sea surface for the 25th, 50th and 75th percentiles of the free stream speed.

D=220 m	Wind Speed (m/s)	Average Wind Speed Deficit (-)		Sea Surface Wind Speed Deficit (m/s)		Average TKE Deficit (%)	
		> 5%	> 10%	> 5%	> 10%	> 5%	> 10%
Percentiles							
25%	4.06			0.31	0.46		
50%	6.14	0.075	0.115	0.46	0.70	14.5%	21.6%
75%	8.81			0.66	1.01		
D=280 m							
Percentiles							
25%	4.06			0.27	0.42		
50%	6.14	0.066	0.102	0.40	0.63	12.7%	19.4%
75%	8.81			0.58	0.90		

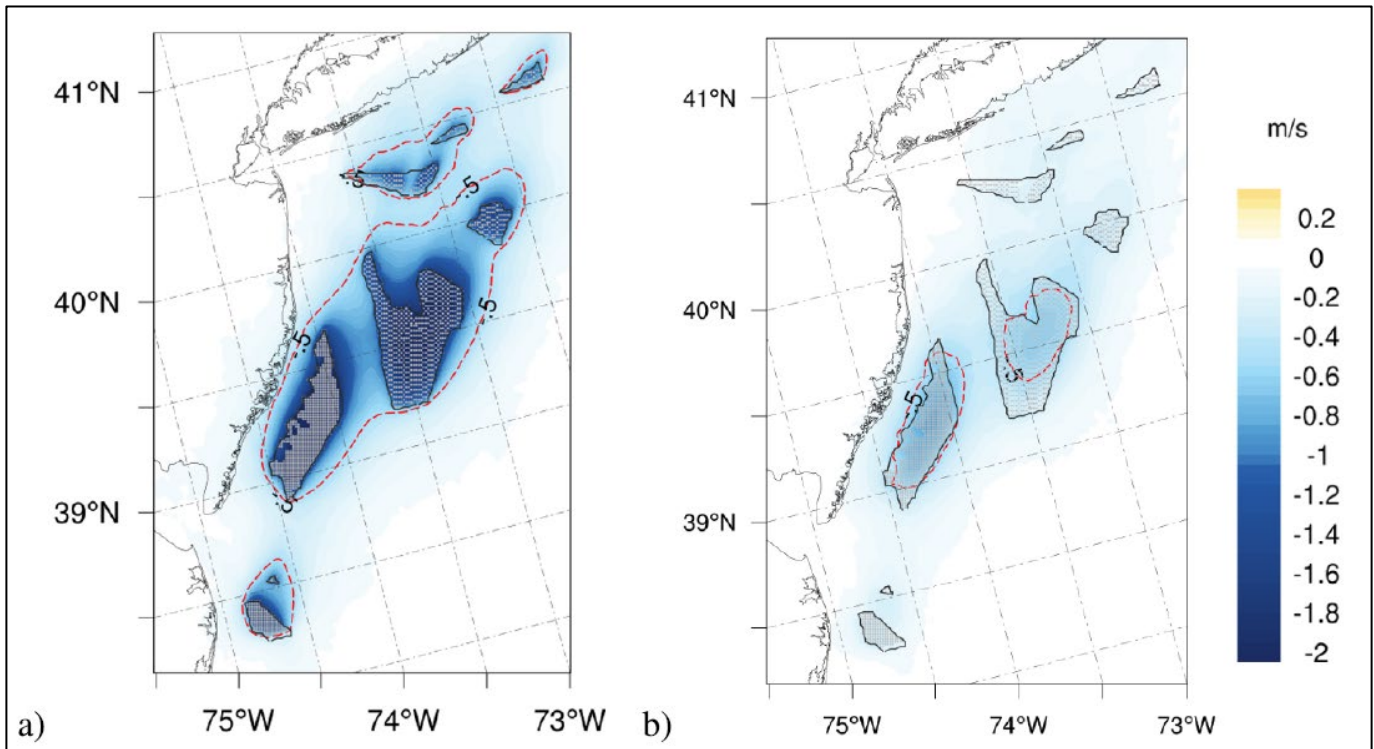


Figure 5-11. Wind speed changes due to wind farms in the mid-Atlantic Bight, averaged over 3 summer months: (a) at hub height (~120 m AMSL) and (b) at the surface. The red-dashed line shows the contour of 0.5 m/s wind speed deficit, which is considered as the edge of the wake (Golbazi et.al., 2022).



For the average wind speed in the area the wind speed deficit at the sea surface of < 0.5 m/s (Table 5.7) is well within the SouthCoast Wind metocean buoy observed wind speed variability for any given hour (0.94 m/s). Due to the low impact of the SouthCoast Wind WTGs, particularly the D=280 m WTG, it could be concluded that the impacts to mixing in the water column is likely also to be within the local variability, difficult to detect and difficult to distinguish from natural variability. The results obtained in the present study are in good agreement with the more detailed study performed by Golbazi et.al. lending support for the findings. As concluded in the Golbazi et.al. study, “on average, meteorological changes at the surface induced by next-generation extreme-scale offshore wind turbines will be nearly imperceptible in the summer.”



6 CONCLUSIONS

The goal of this project was to determine whether the operational phase of the installation of up to 147 WTGs for the SouthCoast Wind Project would impact the hydrodynamics of the Nantucket Shoals area. In turn, would any impacts to the hydrodynamics impact the copepod aggregation processes in the area that allow for effective North Atlantic right whale foraging.

The SouthCoast Wind Lease Area is south of the critical habitat of the Northeastern U.S. Foraging Area (Unit 1) of the North Atlantic right whale; classified as an endangered species under the U.S. Endangered Species Act. Since 2010, the use of protected critical habitat by North Atlantic right whales has been more unpredictable, both temporally and spatially (Davies and Brillant, 2019; O'Brien et al., 2022). Right whales are increasing their use of the Nantucket Shoals region, in particular, the shallow water shoals themselves, slightly northeast of the MA/RI wind energy lease areas (Quintana-Rizzo et al., 2021). Right whales have been observed in this location during all times of the year, with peak occurrences in the winter and spring (Quintana-Rizzo et al., 2021; Meyer-Gutbrod et al., 2022; O'Brien et al., 2022). The presence, density, life stage, and condition of the North Atlantic right whale prey, *Calanus*, determines the use of the Nantucket Shoals region by right whales. This study has evaluated publicly available zooplankton data and adapted models and equations from the literature to predict the effects that SouthCoast Wind Lease Area may have on the oceanography, zooplankton, and therefore right whales. By reviewing the available literature and data to date, analyzing the SouthCoast Wind metocean buoy data (the closest long-term data in proximity to the Shoals) and developing a site and Project specific analysis of the potential impacts, we believe that we have successfully evaluated the potential impacts.

Once those impacts were better understood and quantified, the next step was to determine whether they are sufficient to reach other WTG locations, accumulate and become strong enough to impact the hydrodynamics in the near field and ultimately in the Nantucket Shoals region generally. Each environmental driver is summarized here with the implications it may have for the biology of the area.

Regional studies indicate that the Nantucket Shoals area is not a closed system but a part of a larger circulation, transport and biological macrocosm. Net currents, strongly influenced by the northeast coastal shelf flow, transport water masses from the Gulf of Maine and Georges Bank to and past the Nantucket Shoals area, bringing with them nutrient rich waters. Strong tidal current flows on the order of 1 m/s traverse the Shoals while net currents circulate in a clockwise direction around the southern portion of the Shoals.

A relatively strong and stable stratification of 10° C forms in the SouthCoast Wind Lease Area on an annual basis as seen in the SouthCoast Wind metocean buoy data for 2020-2022. Current data from the SouthCoast Wind buoy shows a predominant diurnal forcing but significantly weaker than Shoals currents in comparison to modeling studies. Calculations based on the local bathymetry, SouthCoast Wind tidal current data and IES hydrodynamic model data predict a tidal mixing front (separating regions of seasonal stratification from well mixed areas) on the west side of the Shoals between the 20 m and 25 m depth zones, approximately 10 km from the northeast corner of the SouthCoast Wind Lease Area, corresponding well with two previous studies (He and Wilkin, 2006; Loder and Greenberg, 1986).

Stratification was evaluated because it is an important habitat feature for zooplankton. *Calanus* migrate daily between warm surface phytoplankton rich waters to feed, and cool, safe near-bottom water to preserve energy. Studies of the biological activities in the area found that the North Atlantic right whale's preferred prey, copepods, primarily inhabit the lower water column of stratified waters (Plourde et al., 2019). In mixed



environments, *Calanus* condition suffers and more of them would need to be consumed for the North Atlantic right whale to achieve sufficient energy consumption. Based on the results from this synthesis of literature, models, and observations, SouthCoast Wind WTG are unlikely to break down the thermocline within or downstream of the Lease Area.

Right whales are specialized foragers, focusing on zooplankton prey, primarily late-stage copepods (*Calanus finmarchicus*) in high density layers (Baumgartner and Mate, 2003). Studies of plankton patches show that aggregating processes vary across regions, depending on circulation, bathymetry, and water mass structure (Sorochan et al., 2021). At a broad spatial scale, it is believed that zooplankton are advected onto Nantucket Shoals from the Gulf of Maine. On a smaller spatial scale on the Shoals, aggregated patches of zooplankton are believed to occur due to the tidal front (Ganju et al., 2011). While stratification influences up and down direction in the water column, the tidal front introduces a vertical feature that may force dense aggregations.

The SouthCoast Wind buoy data clearly show that the tidal currents in the area are rotary in nature, rotating clockwise around a full circle, with a high tide and a low tide on a semi-diurnal basis (approximately twice a day), with a mean speed of 0.25 m/s. Net transport in the area is therefore also circular making large loops though with some net offset. Seasonal net currents of between 0.02 m/s and 0.06 m/s and indicate bathymetric steering from the nearby Shoals forcing it to the northwest or southeast. Net flow directions and speeds indicate that water mass excursion time from one side to the other of SouthCoast Wind Lease Area would be an average of 4 – 6 days.

Laboratory experiments (Miles et al., 2017) and field data have shown that the downstream wake generated by the submerged portion of the WTG tower (pile) has an excursion of approximately 11 times the diameter of the pile, after which the current speed profile has basically recovered. For the 16 m tower diameter in this case 11D equates to 176 m, barely 1/10th of the distance to the next downstream pile. Even if the downstream excursion is up to 50 diameters which has been suggested (Dorrell et al., 2022), (likely turbulence rather than the current speed deficit) that equates to 800 m, which still less than half the distance to the next pile. It is therefore very unlikely that there will be cumulative current speed deficit or turbulence impacts from the WTG piles.

Tidal currents tend to disturb the interface between the upper and lower layers (a thermocline in this case), increasing the thickness of the thermocline without breaking the stratification. It has been postulated that the introduction of WTG towers in the water column could increase the mixing enough to throw off the existing balance and potentially break down the thermocline.

An analysis of the potential for the WTG subsurface tower to provide enough mixing energy to break down the stratification was performed using an analytical model (Carpenter et al., 2016) for individual WTGs and the Lease Area as a whole. The calculations first compared the power generated by the force of the piles in the water column to the bottom friction generated mixing power finding the pile to generate a maximum of 6% of the bottom power using a maximum pile friction coefficient (with a best estimate of 2% - 3%). Further model calculations were used to predict time necessary to mix the water column strongly enough to break down the stratification, finding a range of 1941 days to 679 days based on friction coefficient and the observed conditions of a 10 m thermocline thickness (with a best estimate of 1096 days) with a low of 485 to 113 days for a thermocline equal to the full water depth (with a best estimate of 274 – 183 days). The estimates given do not include surface mixing due to wind stress, which was seen to significantly mix the water column in the August 2020 observations from the SouthCoast Wind buoy.



North Sea field observations (Schultz et al., 2020), for existing piles found that stronger stratification (2° C, significantly less than the 10° C found in this study) are less impacted and recovered faster than weaker stratification corroborating impact finding of this study. Under a weak stratification of 0.5° C the impacts reached 450 m downstream but recovered after, whereas under the strong 2° C stratification no impacts were seen after 200 m downstream. It is apparent given the preceding calculations, corroborated by the field observations that the mixing energy provided by piles is too little to cause more than localized and transient impacts that are significantly smaller than natural mixing factors.

The assessment of the tidal regime and stratification was made based on observations from the SouthCoast Wind metocean data set. Observations and modeling showed that the thermal stratification is strongly affected under weak stratification with a surface to bottom temperature difference of 0.5° C or less. Under stronger stratification, surface to bottom temperature differences of greater than 1.5° C the impacts are less pronounced and temperature anomalies could be masked by other mixing mechanisms or variability. Greater temperature differences decrease the range of influence of the wake downstream. Stratified summer conditions off the coast of southern New England, including Nantucket Shoals, build to $>10^{\circ}$ C, roughly 10 times the stratification strength of the modeled conditions. This implies that the force needed for stratification breakdown would similarly be on the order of a magnitude greater as well.

Based on the forgoing analyses, it appears that there are no circumstances or combinations of hydrodynamics, wind wake, or tidal mixing that produce enough turbulent energy input to the water column from the turbine towers to mix and collapse the stratification before the annual collapse begins in October.

A literature-based WTG wind wake effect study (Xie and Archer, 2015) showed that the downwind speed deficit recovered its original profile in approximately 20 times the rotor diameter which for the two WTG configurations specified (at $D=220$ m and $D=280$ m) equates to 4,400 m and 5,600 m downwind. With a WTG spacing of 1,852 (1 nm) the wind speed deficit wake at hub height would reach several WTGs downwind if they were aligned. Recent LES and analytical modeling, analysis and measurements in the field have shown however, that the greatest wind speed deficits are experienced at hub height and that the sea surface speed deficits are significantly lower. Newer models use an anisotropic Gaussian wind speed distribution (Xie and Archer, 2015) rather than the earlier systems that used a “top hat”, flat form of the distribution (Jensen, 1983).

Wind along the surface of the water during the stratified months, mixes the surface water without breaking the thermocline. Atmospheric heating mixed into the surface waters affects the strength of the stratification in terms of temperature difference, thickness of the warmer surface layer, and the depth and thickness of the transition zone between the surface and bottom layers. Surface wind mixing also facilitates thermocline breakdown in the fall. It is important to note that there is a clear signature of thermocline disturbance from passing storms even at depths on the order of 50 m. The results from this study suggest that wind wake impacts to mixing in the water column are likely within the local variability, difficult to detect, and difficult to distinguish from natural variability.

An analysis of the wind wake effect was performed using a new analytical model (Xie and Archer, 2015), to determine the downwind speed deficit profiles with a focus on the sea surface wind speed deficits for the specific WTG specifications of the proposed SouthCoast Wind Project. The analysis found that the sea surface wind speed deficits were predominantly less than 10% and returned to less than 5% after 4 rotor diameters distance downstream. For the $D=220$ m and $H = 128$ m configuration WTGs the overall areal coverage of a wind speed deficit of 10% or greater was 6.6 % of the wind farm area. For a speed deficit of 5 % or greater the coverage was 43 % of the wind farm area. In contrast for the $D=280$ m and $H=184$ m WTG configuration the overall coverage of



a wind speed deficit of >10 % was significantly smaller at 0.1 % of the wind farm area but the >5 % deficit area coverage was larger, at 55 %. Though the areas look large, to put this in perspective, at the 50th percentile wind speed of 6.14 m/s and the average >5 % deficit the actual speed deficit is 0.46 m/s. This value is well within the variability of the hourly wind speed at the site and matches findings from other more detailed studies of the WTG sea surface impacts in the region as does the TKE deficit estimate of 13 % (Golbazi et al., 2022). The overall impacts of the wind wake effect of the planned large WTGs on the sea surface are relatively small, within the natural variability in the area and likely to be difficult to measure, which other researchers have also found, (Golbazi et al., 2022).

Calanus will be affected by regional population means and changes in the habitat at source locations. Sources in Georges Bank and the Bay of Funday are susceptible to climate change and changing current patterns. The presence of aggregations of Calanus dense enough to allow effective North Atlantic right whale feeding is susceptible to all these parameters. Ross et al., (2023) points out the necessity of not only identifying where whales are feeding, but predicting which areas may become or have the potential to become important feeding ground as conservation efforts struggle to keep up with the unpredictable behaviors observed since 2010. Information on Nantucket Shoals is sparse. Depth specific zooplankton sampling, whale feeding observation and concurrent zooplankton sampling, continuous oceanographic measurements, for example transects similar to the Nantucket Shoals flux experiment (Wright, 1983) but closer to and over the Shoals themselves, including ADCP stations and surface and bottom CTDs and CTD profiles at the ADCP stations, would aide in predicting the dynamics and the use of this region by North Atlantic right whales.

This study sought to address some of the concerns raised by European studies of the presently larger offshore wind farm buildout in the North Sea. In overview, some of the issues they are experiencing or predicting may not be manifested in the U.S. experience for the fact that the WTGs size and layout in the European Union is significantly smaller on both accounts. The WTGs in the European Union are shorter than those planned for the SouthCoast Wind Lease Area and are laid out considerably closer. Part of the findings of this study was that the wake effect of smaller WTG hub heights create greater impacts than the larger hub heights, despite larger rotor diameters. In addition, two wind farms studied in the North Sea (Carpenter et al., 2016) have WTGs 733 m – 866 m apart in comparison to the 1852 m (1 nm) separation of the SouthCoast Wind WTGs, and a WTG density of 6.4 and 4.6 times that of the SouthCoast Wind Project, which affect many of the impacts as the forgoing calculations have shown.

This study considered whether the aggregations of Calanus that draw North Atlantic right whales to Nantucket shoals would be prevented by changes to the local hydrodynamics due to the offshore wind farm. The distance between WTGs supports non-cumulative effects. The strong stratification of the region make it more resilient to thermocline collapse than case studies in the United Kingdom. Evaluation of the near and far field atmospheric wake effects and tidal mixing for the larger U.S. WTGs do not appear to produce enough turbulent energy to collapse the thermocline therefore preserving that important Calanus habitat feature. In addition, there is no indication that SouthCoast Wind Project will affect the advection of Calanus from source populations to Nantucket Shoals based on the large-scale regional circulations. The specifications of the SouthCoast Wind offshore wind farm and the conducted studies therefore suggest that the planned installation as it is currently configured will not substantially impact the mechanisms governing the movement and concentration of Calanus prey, nor the foraging behavior of the North Atlantic right whale for these prey.

7 REFERENCES

- Bastankhah M, Porté-Agel F. A new analytical model for wind-turbine wakes. *Renewable Energy* 2014; 70: 116–123.
- Baumgartner, M.F., 2003. Right whale ecology in the northwest Atlantic Ocean. Oregon State University.
- Baumgartner, M.F., and B.R. Mate. 2003. Summertime foraging ecology of North Atlantic right whales. *Marine Ecology Progress Series* 264: 123-135.
- Baumgartner, M.F., F.W. Wenzel, N.S.J. Lysiak, and M.R. Patrician. 2017. North Atlantic right whale foraging ecology and its role in human-caused mortality. *Marine Ecology Progress Series* 581: 165-181.
- Beardsley, R. C., B. Butman, W. R. Geyer, and P. Smith. 1997. Physical oceanography of the gulf of maine: an update, in *Proceedings of the Gulf of Maine Ecosystem Dynamics Scientific Symposium and Workshop*, pp. 39:52, 1997.
- Beardsley, R.C., Chapman, D.C., Brink, K.H., Ramp, S.R. and Schlitz, R. 1985. The Nantucket Shoals Flux Experiment (NSFE 79). Part 1: A basic description of the current and temperature variability. *Journal of Physical Oceanography*, Volume 15, p. 713-748.
- Belkin, I.M., Cornillon, P.C. and Sherman, K. 2009. Fronts in large marine ecosystems. *Progress in Oceanography*, 81(1-4), pp.223-236.
- van Berkel, J., H. Burchard, A. Christensen, L.O. Mortensen, O. Svenstrup Petersen, and F. Thomsen. 2020. The Effects of Offshore Wind Farms on Hydrodynamics and Implications for Fishes. *Oceanography | Vol.33, No.4*, pp 108.
- Boon, A.R., S. Caires, I.L. Wijnant, R. Verzijlbergh, F. Zijl, J.J. Schouten, S. Muis, T. van Kessel dr. L. van Duren, T. van Kooten (WMR), 2018. Assessment of system effects of large-scale implementation of offshore wind in the southern North Sea. Project 11202792-002, Attribute 11202792-002-ZKS-0006, Deltares, Delft.
- Brooks, D.A. 1992. A brief overview of the physical oceanography of the Gulf of Maine. In: Wiggin, J. and Mooers, C.N.K. (Eds.), *Proceedings of the Gulf of Maine Scientific Workshop*, Woods Hole, Massachusetts, 8-10 January, 1991. Published December, 1992, Urban Harbors Institute, University of Massachusetts at Boston, p. 51-74.
- Butman, B., R. C. Beardsley, B. Magnell, D. Frye, J. A. Vermersch, R. S. R. Limeburner, W. R. Wright, and M. A. Noble, Recent observations of the mean circulation on Georges Bank, *Journal of Physical Oceanography*, 12, 569-591, 1982.
- Carey, D.A. 1983. Particle resuspension in the benthic boundary layer induced by flow around polychaete tubes. *Canadian Journal of Fisheries and Aquatic Sciences*. 40 (Suppl. I): 301-308.
- Carpenter, J.R., L. Merckelbach, U. Callies, S. Clark, L. Gaslikova, and B. Baschek. 2016. Potential impacts of offshore wind farms on North Sea stratification. *PLoS ONE* 11(8):e0160830, <https://doi.org/10.1371/journal.pone.0160830>.
- Chamorro LP, Porté-Agel F., 2010. Effects of thermal stability and incoming boundary-layer flow characteristics on wind-turbine wakes: a wind-tunnel study. *Boundary-Layer Meteorology* 2010; 136: 515–533.



- Chapman, D. C., and R. C. Beardsley, On the origin of shelf water in the Middle Atlantic Bight, *Journal of Physical Oceanography*, v19, 384-391, 1989.
- Chen, C, R. C. Beardsley, J. Qi and H. Lin, 2016. Use of Finite-Volume Modeling and the Northeast Coastal Ocean Forecast System in Offshore Wind Energy Resource Planning. Final Report to the U.S. Department of the Interior, Bureau of Ocean Energy Management, Office of Renewable Energy Programs. BOEM 2016-050. 131pp.
- Christiansen, M.B., and C.B. Hasager. 2005. Wake effects of large offshore wind farms identified from satellite SAR. *Remote Sensing of Environment* 98:251–268, <https://doi.org/10.1016/j.rse.2005.07.009>.
- Codiga, D.L., and Ullman, D.S. 2010. Characterizing the physical oceanography of coastal waters off Rhode Island: Part 1: Literature review, available observations, and a representative model simulation. Final Report for Rhode Island Ocean Special Area Management Plan. Coastal Resources Management Council, Wakefield, RI.
- Davies KTA, Ross T, Taggart CT (2013) Tidal and subtidal currents affect deep aggregations of right whale prey, *Calanus spp.*, along a shelf-basin margin. *Mar Ecol Prog Ser* 479:263-282. <https://doi.org/10.3354/meps10189>
- Dorrell RM, Lloyd CJ, Lincoln BJ, Rippeth TP, Taylor JR, Caulfield CCP, Sharples J, Polton JA, Scannell BD, Greaves DM, Hall RA and Simpson JH, 2022. Anthropogenic Mixing in Seasonally Stratified Shelf Seas by Offshore Wind Farm Infrastructure. *Front. Mar. Sci.* 9:830927. doi: 10.3389/fmars.2022.830927
- Floeter, J., J.E. van Beusekom, D. Auch, U. Callies, J. Carpenter, T. Dudeck, S. Eberle, A. Eckhardt, D. Gloe, K. Hänselmann, and others. 2017. Pelagic effects of offshore wind farm foundations in the stratified North Sea. *Progress in Oceanography* 156:154–173, <https://doi.org/10.1016/j.pocean.2017.07.003>
- Frandsen S, Barthelmie R, Pryor S, Rathmann O, Larsen S, Høstrup J, Thøgersen M. Analytical modelling of wind speed deficit in large offshore wind farms. *Wind Energy* 2006; 9: 39–53.
- Ganju, N.K., S.J. Lentz, A.R. Kirincich, and J.T. Farrar. 2011. Complex mean circulation over the inner shelf south of Martha’s Vineyard revealed by observations and a high-resolution model. *Journal of Geophysical Research* 116: C10036. doi: 10.1029/2011JC007035
- Garrett, C., Keeley, J., and Greenberg, D. (1978). Tidal mixing versus thermal stratification in the bay of fundy and gulf of maine. *Atmosphere Ocean* 16, 403–423. doi: 10.1080/07055900.1978.9649046
- Golbazi, M., C.L. Archer and S. Alessandrini, 2022. Surface impacts of large offshore wind farms. *Environ. Res. Lett.* 17 064021
- Grashorn, S., and E.V. Stanev. 2016. Kármán vortex and turbulent wake generation by wind park piles. *Ocean Dynamics* 66:1,543–1,557, <https://doi.org/10.1007/s10236-016-0995-2>.
- Hare, J. (2021) EcoMon plankton counts (100-m³) from Bongo tows, including MARMAP data multiple cruises in the Northeast Continental Shelf of the United States from 1977-2015 (EcoMon Zooplankton project). Biological and Chemical Oceanography Data Management Office (BCO-DMO). (Version 3.1) Version Date 2018-01-02. doi:10.26008/1912/bco-dmo.3328.3.1 [2023/09/10]



- Hayes S.H., Josephson E., Maze-Foley K., Rosel, P.E., Wallace, J. (2022). U.S. Atlantic and Gulf of Mexico Marine Mammal Stock Assessments 2021. <https://doi.org/10.25923/6tt7-kc16>
- He, Ruoying and John L. Wilkin, 2006. Barotropic Tides on the Southeast New England Shelf: A View From a Hybrid Data Assimilative Modeling Approach. *Journal of Geophysical Research*, Vol. 111, C08002, Doi:10.1029/2005jc003254, 2006
- Jensen, N. O., 1983. A note on wind generator interaction, Tech Rep Risø-M-2411, Risø National Laboratory, Denmark, 16 pp., https://orbit.dtu.dk/files/55857682/ris_m_2411.pdf
- Johnson TL, van Berkel JJ, Mortensen LO, Bell MA, Tiong I, Hernandez, B, Snyder, DB, Thomsen, F, Svenstrup Petersen, O: 2021. Hydrodynamic modeling, particle tracking and agent-based modeling of larvae in the U.S. mid-Atlantic bight. Lakewood (CO): US Department of the Interior, Bureau of Ocean Energy Management. OCS Study BOEM 2021-049. 232 p.
- Kowalik, Z. and T.S. Murty, 1993. Numerical Modeling of Ocean Dynamics. Advanced Series on Ocean Engineering – Volume 5. Ed. P.L.F Liu. World Scientific Publishing Co. Pte. Ltd., River Edge, NJ 07661.
- Lass, H.U., V. Mohrholz, M. Knoll, and H. Prandke. 2008. Enhanced mixing downstream of a pile in an estuarine flow. *Journal of Marine Systems* 74:505–527, <https://doi.org/10.1016/j.jmarsys.2008.04.003>.
- Lentz, Steven J., 2008. Observations and a Model of The Mean Circulation Over the Middle Atlantic Bight Continental Shelf. *Journal of Physical Oceanography*, V38, June 2008. American Meteorological Society.
- Li, Y, PS Fratantoni, C Chen, JA Hare, Y Sun, RC Beardsley, and R Ji, 2015. Spatio-temporal patterns of stratification on the Northwest Atlantic shelf, *Progress in Oceanography* 134 (2015) 123–137.
- Lienhard, J. H., 1966. Synopsis of Lift, Drag and Vortex Frequency Data for Rigid Circular Cylinders. Bulletin 300. College of Engineering, Research Division. Published by Technical Extension Services, Washington State University, Pullman, Washington.
- Loder, J. W., and Greenberg, D. A. (1986). Predicted positions of tidal fronts in the gulf of maine region. *Cont. Shelf Res.* 6, 397–414. doi: 10.1016/0278-4343(86)90080-4.
- Mayo, C.A., Letcher, B.H. and Scott, S., 2020. Zooplankton filtering efficiency of the baleen of a North Atlantic right whale, *Eubalaena glacialis*. *J. Cetacean Res. Manage.*, pp.225-229.
- Mayo, C.A., and Marx, M.K.. 1990. Surface foraging behaviour of the North Atlantic right whale, *Eubalaena glacialis*, and associated zooplankton characteristics. *Canadian Journal of Zoology*. 68(10): 2214-2220. <https://doi.org/10.1139/z90-308>
- Mendelsohn, D.L. and J.C. Swanson, 2022. Hydrodynamic and Sediment Transport Modeling for the Brayton Point Export Cable Burial Assessment. Mayflower Wind Energy LLC | USA. 01 March 2022 - Final Report.
- Meyer-Gutbrod EL, Greene CH, Sullivan PJ, Pershing AJ (2015) Climate-associated changes in prey availability drive reproductive dynamics of the North Atlantic right whale population. *Mar Ecol Prog Ser* 535:243-258. <https://doi.org/10.3354/meps11372>
- Paskyabi, M B, 2015. Offshore Wind Farm Wake Effect on Stratification and Coastal Upwelling. 12th Deep Sea Offshore Wind R&D Conference, EERA DeepWind'2015.

- Poppe, L.J., Schlee, J.S., Butman, B., and Lane, C.M., 1989, The distribution of surficial sediment texture on Georges Bank and in the Gulf of Maine, U.S. Atlantic Continental Margin: U.S. Geological Survey Miscellaneous Investigations Series Map I-1986-A, 1 sheet, scale 1:1,000,000.
- Provincetown Center for Coastal Studies (PCCS), 2005. Toward an Ocean Vision for the Nantucket Shelf Region: Part I. Review of the Environmental Characteristics of the Nantucket Shelf Region; Part II. Management Options for Resource Protection and Sustainable Uses. Provincetown Center for Coastal Studies, Provincetown, Massachusetts. January 2005.
- Rennau, H., S. Schimmels, and H. Burchard. 2012. On the effect of structure-induced resistance and mixing on inflows into the Baltic Sea: A numerical model study. *Coastal Engineering* 60:53–68, <https://doi.org/10.1016/j.coastaleng.2011.08.002>.
- Rivier, A, A C Bennis, G Pinon, V Magar, M Gross, 2016. Parameterization of wind turbine impacts on hydrodynamics and sediment transport. *Ocean Dynamics* (2016) 66:1285–1299. DOI 10.1007/s10236-016-0983-6, Springer-Verlag, Berlin Heidelberg. 14 September 2016.
- Roberts, J.J., B.D. Best, L. Mannocci, E. Fujioka, P.N. Halpin, D.L. Palka, L.P. Garrison, K.D. Mullin, T.V.N. Cole, C.B. Khan, W.A. McLellan, D.A. Pabst, and G.G. Lockhart. 2016. Habitat-based cetacean density models for the U.S. Atlantic and Gulf of Mexico. *Scientific Reports* 6: 22615.
- Ross CH, Runge JA, Roberts JJ, Brady DC, Tupper B, Record NR (2023) Estimating North Atlantic right whale prey based on *Calanus finmarchicus* thresholds. *Mar Ecol Prog Ser* 703:1-16. <https://doi.org/10.3354/meps14204>
- Schlee, J. 1973. Atlantic Continental Shelf and Slope of the United States sediment texture of the northeastern part: U.S. Geological Survey Professional Paper 529-L, 64 p.
- Schultze, L. K. P., Merckelbach, L. M., Horstmann, J., Raasch, S., & Carpenter, J. R. (2020). Increased mixing and turbulence in the wake of offshore wind farm foundations. *Journal of Geophysical Research: Oceans*, 125, e2019JC015858. <https://doi.org/10.1029/2019JC015858>
- Segtnan, O. H. and K. Christakos, 2015: Effect of Offshore Wind farm Design on the Vertical Motion of the Ocean, 12th Deep Sea Offshore Wind R&D Conference, EERA DeepWind'2015, Energy Procedia, 80, 213 – 222.
- Siedersleben, SK , JK Lundquist, A Platis, J Bange, K Bärffuss, A Lampert, B Cañadillas, T Neumann and S Emeis, 2018. Micrometeorological impacts of offshore wind farms as seen in observations and simulations. *Environ. Res. Lett.* 13 (2018) 124012, <https://doi.org/10.1088/1748-9326/aaea0b>
- Simpson, J. H., and J. R. Hunter (1974), Fronts in the Irish Sea, *Nature*, 250, 404–406.
- Simpson, J. and J. Sharples, 2012. Chapter 8 - Tidal mixing fronts: their location, dynamics and biological significance. In: *Introduction to the Physical and Biological Oceanography of Shelf Seas* , pp. 233 - 265. DOI: <https://doi.org/10.1017/CBO9781139034098.011>. Publisher: Cambridge University Press, 2012
- Sorochan, K.A., S. Ploudre, M.F. Baumgartner, and C.L. Johnson. 2021. Availability, supply, and aggregation of prey (*Calanus* spp.) in foraging areas of the North Atlantic right whale (*Eubalaena glacialis*). *ICES Journal of Marine Science* 78(10): 3498-3520. <https://doi.org/10.1093/icesjms/fsab200>



- SouthCoast Wind, 2022. SouthCoast Wind Construction and Operations Plan (COP). Submitted To: Bureau of Ocean Energy Management, Office of Renewable Energy Programs. Submitted By: Mayflower Wind Energy, LLC, 101 Federal Street, Suite 1900 Boston, MA 02110. March 2022. Available: https://www.boem.gov/sites/default/files/documents/renewable-energy/state-activities/SouthCoast%20COP_Volume%20I_Rev_F.pdf
- Twichell, D.C., Butman, B., and Lewis, R.S. 1987. Shallow structure, surficial geology, and the processes currently shaping the Bank. In: Backus, R.H. and Bourne, D.W. (Eds.), Georges Bank. The MIT Press, Cambridge, Massachusetts, p.31-37.
- White, T. P., and R. R. Veit. 2020. Spatial ecology of long-tailed ducks and white-winged scoters wintering on Nantucket Shoals. *Ecosphere* 11(1):e03002. 10.1002/ecs2.3002
- Wishner, K., E. Durbin, A. Durbin, M. Macaulay, H. Winn and R.D. Kenney. 1988. Copepod patches and right whales in the Great South Channel off New England. *Bulletin of Marine Science* 43(3): 825–844.
- Wright, W. Redwood, 1983. Nantucket Shoals flux experiment. Data report I, Hydrography. Northeast Fisheries Center (U.S.), NOAA technical memorandum NMFS-F/NEC ; 23. URL : <https://repository.library.noaa.gov/view/noaa/5535>
- Wu S., Archer C.L., Mirocha J.D., 2023. New insights on wind turbine wakes from large-eddy simulation: Wake contraction, dual nature, and temperature effects. *Wind Energy*. 2023;1-22. doi:10.1002/we.2827
- Xie S, Archer C. Self-similarity and turbulence characteristics of wind turbine wakes via large-eddy simulation. *Wind Energy*. 2015;18(10):1815-1838.